Single-cell and spatial multi-omics highlight effects of anti-integrin therapy across cellular compartments in ulcerative colitis

Running Title: anti-integrin therapy affects multiple subsets in UC

Elvira Mennillo[1], Yang Joon Kim[2], Gyehyun Lee[1], Iulia Rusu[1], Ravi K. Patel[1,3], Leah C. Dorman[2], Emily Flynn[3], Stephanie Li[1], Jared L. Bain[1], Christopher Andersen[1,3], Arjun Rao[1,3], Stanley Tamaki[3], Jessica Tsui[1,3,4], Alan Shen[1,3,4], Madison L. Lotstein[1,3], Maha Rahim[5], Mohammad Naser[6], Faviola Bernard-Vazquez[1], Walter Eckalbar[3], Soo-jin Cho[4], Kendall Beck[1], Najwa El-Nachef[1], Sara Lewin[1], Daniel R Selvig[1], Jonathan P Terdiman[1], Uma Mahadevan[1], David Y. Oh[1,7], Gabriela K. Fragiadakis[1,3], Angela Pisco[2], Alexis J. Combes[1,3,4], Michael G. Kattah[1#]

1. Department of Medicine, University of California San Francisco, San Francisco, CA, USA
2. Chan Zuckerberg Biohub, San Francisco, CA, USA
3. CoLabs, University of California San Francisco, San Francisco, CA, USA
4. Department of Pathology, University of California San Francisco, San Francisco, CA 94143, USA
5. Helen Diller Family Comprehensive Cancer Center, University of California San Francisco, San Francisco, CA 94143, USA.
6. Biological Imaging Development CoLab, University of California San Francisco, San Francisco, CA, USA
7. Division of Hematology/Oncology, Department of Medicine, University of California San Francisco, San Francisco, CA, USA

To whom correspondence should be addressed:

Michael G. Kattah, 513 Parnassus Ave, S-357G Medical Science Building, San Francisco, CA 94143-0451.

Phone: 415-502-5717 Email: michael.kattah@ucsf.edu

ABSTRACT

Ulcerative colitis (UC) is driven by immune and stromal subsets, culminating in epithelial injury. Vedolizumab (VDZ) is an anti-integrin antibody that is effective for treating UC. VDZ is known to inhibit lymphocyte trafficking to the intestine, but its broader effects on other cell subsets are less defined. To identify the inflammatory cells that contribute to colitis and are affected by VDZ, we performed single-cell transcriptomic and proteomic analyses of peripheral blood and colonic biopsies in healthy controls and patients with UC on VDZ or other therapies. Here we show that VDZ treatment is associated with alterations in circulating and tissue mononuclear phagocyte (MNP) subsets, along with modest shifts in lymphocytes. Spatial multi-omics of formalin-fixed biopsies demonstrates trends towards increased abundance and proximity of MNP and fibroblast subsets in active colitis. Spatial transcriptomics of archived specimens pre-treatment identifies epithelial-, MNP-, and fibroblast-enriched genes related to VDZ responsiveness, highlighting important roles for these subsets in UC.

INTRODUCTION

Ulcerative colitis (UC) is a chronic inflammatory disorder of the intestine characterized by abnormal immune, stromal, and epithelial responses to microbial stimuli in genetically susceptible individuals, culminating in mucosal inflammation and epithelial injury. Vedolizumab (VDZ) is a monoclonal antibody against $\alpha_4\beta_7$ integrin that prevents binding to gut endothelial mucosal addressin-cell adhesion molecule 1 (MAdCAM-1), blocking the trafficking of leukocytes to the intestine. The cellular and genetic factors that mediate VDZ response and non-response are incompletely characterized[1–3]. There are conflicting data regarding which inflammatory intestinal cell subsets are the most affected[4]. Many studies emphasize the effects of VDZ on B and T lymphocytes and regulatory T cells (Tregs)[3–9], while others suggest an impact on innate immune myeloid populations[10,11]. Understanding the peripheral and tissue effects of VDZ is critical to stratify patients as potential responders or non-responders prior to treatment, and for identifying alternative treatment strategies for non-responders.

Tissue multi-omics studies in inflammatory bowel disease (IBD) have revealed important roles for stromal, epithelial, and immune compartments in driving disease and mediating treatment response and non-response[12–17]. To generate an unbiased, global assessment of the effects of colitis within the context of VDZ treatment, we performed a comprehensive single-cell multi-omics analysis that included single-cell RNA sequencing (scRNA-seq), cellular indexing of transcriptomes and epitopes by sequencing (CITE-seq, a modality that includes single-cell RNA-seq in addition to a DNA-barcoded antibody-based proteomic panel), and mass cytometry (CyTOF) of peripheral leukocytes and colonic biopsies in healthy controls (HC) and patients with UC on aminosalicylates (UC) or VDZ (UC-VDZ). To further investigate the spatial heterogeneity and proximity of intestinal tissue subsets, we performed multiplex ion beam imaging (MIBI), co-detection by indexing (CODEX), and highly multiplexed RNA *in situ hybridization* (RNA-ISH, CosMx) on formalin-fixed, paraffin-embedded (FFPE) colonic biopsies, using both unsupervised and supervised analytic methods. In separate groups of patients, we validated our findings with additional CyTOF analyses, and applied 1000-plex spatial transcriptomics to archived clinical FFPE specimens before and after VDZ treatment.

RESULTS

scRNA-seq of cryopreserved intestinal biopsies has high fidelity to fresh processing

To characterize the effects of VDZ in the peripheral blood and colon of UC patients, we first employed a cross-sectional, case-control study design consisting of healthy controls without IBD (HC, n=4), patients with UC on 5-aminosalicylates (5-ASA) (UC, n=4), and patients with UC on VDZ (UC-VDZ, n=4) (**Fig. 1a, Supplementary Table 1**). To improve internal validity and cross-validate multi-omics signatures in a small number of patients, we analyzed the same patient samples using a variety of single-cell and spatial transcriptomic and proteomic methods, including scRNA-seq, CITE-seq[18], cytometry by time of flight (CyTOF), multiplex RNA-ISH, MIBI[19], and CODEX[20] (**Fig. 1a, Supplementary Table 2**). Recent methods for cryopreserving undigested, intact intestinal mucosal biopsies have revolutionized tissue multi-omics pipelines by facilitating batch processing[16]. Batch processing of samples for scRNA-seq reduces cost and improves inter-sample comparison by minimizing batch effects[21]. To compare the performance of cryopreserved and non-frozen intestinal biopsies in scRNA-seq, we compared scRNA-seq of biopsies from two donors that were frozen briefly in cryopreservation media (Cryopreserved) to samples that were stored briefly on ice (Fresh) (**Fig. 1b**). Fresh and Cryopreserved colon biopsies yielded similar coarse cell clusters (**Fig. 1c,d**), with no statistically significant differences in immune, epithelial, and stromal cell subset frequencies (**Fig. 1e**). Cryopreservation reduces or eliminates granulocytes, and mast cells were decreased with cryopreservation (**Fig 1e**), though not statistically significant. Differentially expressed (DE) gene analysis identified up-regulation of heat-shock proteins (*HSPA1A, HSPA1B, HSP90AA1,* and *HSPD1*) in Fresh biopsies as well as up-regulation of *JUN* and *FOSB* in Cryopreserved biopsies (**Fig. 1f**). Reasonable concordance between freshly processed and cryopreserved intestinal biopsies, combined with the logistic, financial, and batch processing benefits of cryopreserved biopsies, favors cryopreservation.

VDZ is associated with modest transcriptional changes in peripheral leukocyte subsets

We hypothesized that patients on VDZ would exhibit increased circulating inflammatory lymphocytes due to inhibition of intestinal trafficking. To test this, we performed scRNA-seq on peripheral blood leukocytes (PBLs) from HC, UC, and UC-VDZ patients (**Fig. 2a**). Cryopreserved PBLs were thawed, pooled, run in a single batch, and deconvoluted with freemuxlet/demuxlet[21], minimizing batch effects. The anticipated coarse

(**Supplementary Fig. 1a**) and fine leukocyte subsets (**Fig. 2b**) were identified based on landmark genes expressed for each cluster (**Supplementary Fig. 1b-e**), in agreement with previously described gene sets[22,23]. Granulocytes were not observed, likely due to poor viability after freezing and thawing. Cells from each patient were mostly distributed across coarse and fine clusters (**Fig. 2c**), as well as disease and treatment status (**Fig. 2d**). HS12 had an expanded circulating cytotoxic lymphocyte population, but this was not observed in other UC-VDZ patients (**Fig. 2b,c).** When we compared the cell frequency for each fine leukocyte cell subset across conditions, we did not observe any statistically significant differences among patients (**Fig. 2d,e**). scRNA-seq DE gene analysis revealed up-regulation of *IFITM3* in UC patients compared to HC, and down-regulation of *IFITM2* in UC-VDZ patients compared to UC patients (**Fig. 2f**). DE gene analysis of individual leukocyte subsets identified a small number of differences in lymphocyte and monocyte subsets (**Fig 2g, Supplementary Fig. 2a,b**). VDZ was associated with an increase in *ITGB1* in CD8 T cells (**Supplementary Fig. 2b**). VDZ was also associated with increases in *TMEM176A* and *TMEM176B* in circulating $CD14^+$ monocytes (**Supplementary Fig. 2b**). *TMEM176B* has been suggested to inhibit the inflammasome and dendritic cell maturation[24–26]. To further identify pathways that were potentially pathogenic in UC, and targeted or reversed by VDZ, we then filtered for DE genes that were up-regulated in UC vs HC, and reciprocally down-regulated in UC-VDZ vs UC, and vice versa (**Fig. 2h**). This analysis highlighted up-regulation of *CCL4L2* in CD8 T cells, as well as up-regulation of *CD52 and HLA-DQB1* in $CD14^+$ monocytes in UC as compared to HC, all with reciprocal down-regulation in UC-VDZ patients**.** Although scRNA-seq identified some global and cell subset specific transcriptomic associations with UC and VDZ therapy, in general circulating leukocyte subset frequencies were relatively stable with modest transcriptional differences.

Tissue CITE-seq identifies shifts in multiple mucosal cell subsets associated with VDZ

To examine the alterations in cell subset abundance and expression programs associated with UC and VDZ therapy, we performed scRNA-seq and CITE-seq on colonic mucosal biopsies from the same patients (**Fig. 3a, Supplementary Table 2**). Cryopreserved biopsies were thawed, digested, pooled, run in a single batch, and deconvoluted with freemuxlet/demuxlet[21], minimizing batch effects. The anticipated coarse (**Supplementary Fig. 3a**) and fine colonic mucosal subsets (**Fig. 3b**) were identified using landmark genes

associated with each cluster (**Supplementary Fig. 3b** and **Supplementary Fig. 4,5**). The subsets identified using cryopreserved biopsies were similar to those previously described for fresh biopsies[12,13,15,27]. The CITE-seq panel provided a human intestinal cell surface proteome in HC, UC, and UC-VDZ patients, and for example, highlighted CD103 (αE integrin) expression by CD8 tissue resident memory T cells (Trm) (**Fig. 3c**, **Supplementary Fig. 4h**). CITE-seq identified sets of surface proteins associated with each intestinal cell subset (**Supplementary Fig. 3-5**). Cells from each patient were distributed across intestinal cell clusters (**Fig. 3d**). Biopsies were categorized as HC (gray), mild endoscopic disease activity (UC 0-1, purple), or moderate-to-severe endoscopic disease activity (UC 2-3, orange), or as coming from HC (gray), UC (blue), or UC-VDZ (red) patients (**Fig. 3e-h, Supplementary Fig. 6**). After correcting for multiple comparisons, there were significant increases in Tregs, S2 fibroblasts, pericytes, and endothelial cell subsets, with reductions in innate lymphoid cells (ILCs) and activated and memory $CD4^+$ T cells in more severely inflamed segments (**Fig. 3g**, **Supplementary Fig. 6a,b**). The relative frequencies of activated and memory $CD4^+$ and $CD8^+$ T lymphocyte subsets vary among studies depending on inflammatory status and disease activity[15,28], but increases in Tregs have been consistently reported[29–33]. Alterations in ILC3s have also been previously described in IBD scRNA-seq[34]. The relative increase in goblet cells we observed was likely due to a relative reduction in absorptive colonocytes and intestinal stem cells (ISCs) (**Supplementary Fig. 6a,b**), and variations in goblet cell abundances and maturation have been reported in other IBD transcriptomic studies[35,36]. We observed a global expansion of both venous and arterial endothelial cells in more severely inflamed UC biopsies (**Fig. 3g, Supplementary Fig. 6a,b**). Previous studies have characterized stromal cell subsets in IBD[12], and here CITE-seq highlighted a general shift from S1/3/4 stromal fibroblasts to increased S2 and activated fibroblasts in more severely inflamed UC biopsies. The activated fibroblasts identified in our dataset expressed high levels of *TIMP1, MMP1, MMP3, AREG, TMEM158, TNFRSF11B,* and surface CD10, while the S2 fibroblasts expressed high levels of *F3*, *POSTN, CXCL14, ENHO, PDGRFA, SOX6*, and surface CD10, CD146, and CD49a (**Supplementary Fig. 5c,d**), sharing some features with the *IL13RA2*$^+$*IL11*$^+$*TNFRSF11B*$^+$ inflammatory fibroblasts associated with anti-TNF resistance[15]. Interestingly, VDZ was not associated with significant reductions in lymphocyte subsets compared to UC biopsies. However, VDZ was associated with a statistically significant reduction in myeloid dendritic cells (mDCs), which were high in *CD1C* gene expression, as well as surface CD1c, CD11c, and FcεR1α (**Fig. 3h**, **Supplementary Fig. 4j**). VDZ correlated

with trends toward fewer activated fibroblasts, monocytes, macrophages, and mast cells (**Fig 3h, Supplementary Fig. 6d**). In the epithelial compartment, VDZ was associated with a statistically significant increase in epithelial cells generally, with a trend toward fewer deep crypt secretory (DCS) cells (**Fig. 3h**), which could be consistent with a mucosal healing effect. Although VDZ did not appear to significantly alter lymphocyte populations in colonic biopsies by CITE-seq, subsets of inflammatory MNPs and stromal cells trended lower in UC-VDZ patients, with a concomitant expansion of some epithelial subsets.

Analysis of gene expression in tissue CITE-seq revealed significant transcriptomic changes associated with HC, UC, and UC-VDZ patients. scRNA-seq DE gene analysis for all cells revealed an increase of *TIMP1* and *CD74* in UC as compared to UC-VDZ (**Supplementary Fig. 7a**). Both *TIMP1* and *CD74* were increased in a meta-analysis of UC colonic biopsy bulk gene-expression[37], and these genes were expressed at high levels in endothelial, stromal, and MNP subsets in our dataset. More DE genes were observed in biopsy cell subsets compared to peripheral blood. Stromal fibroblasts and endothelial cells exhibited the highest number of DE genes among the study subjects, as well as MNPs, mast cells, and cycling cells (**Supplementary Fig. 7b**). Although VDZ is frequently discussed in terms of its effect on lymphocyte trafficking, non-lymphoid subsets generally exhibited more dynamic DE genes than lymphocyte subsets (**Supplementary Fig. 7,8**). MNPs from UC patients expressed higher levels of *TIMP1*, *SOD2*, *TYMP*, *C15orf48,* and *CD63* compared to HC, all of which were reciprocally decreased in UC-VDZ patients (**Supplementary Fig. 7c, 8a,b**). Mast cells expressed multiple inflammatory genes at higher levels in UC-derived as compared to HC-derived biopsies, but VDZ did not appear to antagonize these signatures (**Supplementary Fig. 7c and 8a,b**). Stromal fibroblasts in UC patients exhibited elevated levels of *MMP3, TIMP1, TMEM158*, *COL6A3,* all of which were previously reported to be increased in bulk UC biopsies[37] (**Supplementary Fig. 5c; Supplementary Fig. 7c**). This activated signature was reciprocally downregulated by VDZ (**Supplementary Fig. 8b**). Endothelial cells expressed higher levels of *TIMP1*, *MGP, S100A6*, *TPM4, TM4SF1, CD59, PRKCDBP*, and lower levels of *TXNIP* and *FABP5* in UC vs HC samples (**Supplementary Fig. 7c and 8b**). These endothelial cell DE genes were consistent with trends observed in bulk UC biopsies[37], and all were reversed by VDZ (**Supplementary Fig. 8a,b**). Epithelial cells from UC patients expressed increased levels of *LCN2* and lower *FABP1*, correlating with a relative reduction of absorptive colonocytes in UC compared to HC and reversed by VDZ,

consistent with recovery of absorptive colonocytes (**Supplementary Fig. 5a and 7c, 8b**). Taken together, DE gene analysis identified relatively few transcriptional differences in lymphocyte subsets among HC, UC, and UC-VDZ patients, with more dynamic transcriptional changes in MNPs, stromal fibroblasts, and endothelial cells. The scRNA-seq and CITE-seq data from colonic mucosal biopsies indicates that VDZ may play a role in attenuating MNP trafficking and activation, diminishing activation of inflammatory fibroblasts and endothelial cells, thus facilitating the recovery of intestinal epithelial cells.

Unsupervised and supervised CyTOF analysis confirms VDZ association with changes in innate immune and epithelial compartments

To further explore the effects of VDZ on various cell populations, and to validate scRNA-seq and CITE-seq data with an orthogonal multi-omics technique, we performed CyTOF on paired PBLs and colon biopsies collected and processed in parallel from HC, UC, and UC-VDZ patients (**Fig. 4a, Supplementary Table 2**). This complementary multi-omic assay was carried out on the same initial cell preparations as CITE-seq, with the exception that CyTOF biopsy samples did not undergo Annexin-V-based dead cell depletion, and right (R) and left (L) colon biopsies were combined for each patient to increase cell yield. We performed an initial unsupervised analysis using UMAP visualization and clustering[38]. Based on marker intensity, we annotated 21 unsupervised clusters in PBLs (**Supplementary Fig. 9a-e**) and colon biopsies (**Fig 4b, Supplementary Fig. 9f-i**), and clusters with highly similar phenotypes were combined. For unsupervised analysis of PBL CyTOF data, all patients were represented in each cell cluster (**Supplementary Fig. 9c,d**). CyTOF identified granulocytes in PBLs, representing less than 2% of the total cells after freezing and thawing. After adjusting for multiple comparisons, there were no statistically significant alterations in circulating PBL subsets among the groups (**Supplementary Fig. 9e**). In the unsupervised analysis of colon biopsy CyTOF data, patient samples were distributed across cell clusters (**Supplementary Fig. 9g**), with some clusters enriched for HC, UC, or UC-VDZ derived cells (**Fig 4c**). The fraction of epithelial cells was higher in CyTOF than CITE-seq, likely because dead cell depletion was not needed prior to the CyTOF analysis. Multiple epithelial subsets emerged from the unsupervised clustering, including epithelial clusters 2/3_EpCAM^{+}CD15^{hi}, 5/6/8_EpCAM^{+}ICOS^{hi}, and 9/12_EpCAM^{+}HLA-DR^{+} (**Supplementary Fig. 9h,i**), in addition to the expected non-epithelial clusters. Cross-referencing the complementary CITE-seq data suggested that CD15^{hi} epithelial

cells are enriched in secretory and transit amplifying epithelial subsets (**Supplementary Fig. 5b**). $CD15^{hi}$ epithelial cells were significantly reduced in UC compared to HC and increased in UC-VDZ biopsies in the unsupervised analysis (**Supplementary Fig. 9i**). Unsupervised CyTOF analysis was informative in guiding the supervised analysis and identifying distinct epithelial subsets.

Following unsupervised clustering and analysis, we then performed a supervised gating strategy including the unique epithelial subsets (**Supplementary Fig. 10, 11**). Supervised analysis did not reveal any statistically significant changes in circulating PBLs by CyTOF (**Supplementary Fig. 11a**). In contrast, supervised analysis of biopsy CyTOF data demonstrated a borderline significant increase in HLA-DR^+ IECs in UC and UC-VDZ samples compared to HC, and a trend toward reduced $CD15^{hi}$ IECs in UC, with expansion in VDZ-treated patients (**Fig. 4d-f**). IECs expansion in UC-VDZ compared to UC approached statistical significance, consistent with CITE-seq data (**Fig. 3f)**. In agreement with the unsupervised CyTOF analysis and CITE-seq data, MNP subsets exhibited a trend toward reduction in UC-VDZ patients, including mDCs (cDC1, cDC2, cDC2b), classical monocytes, and macrophages (**Fig. 4g-i, Supplementary Fig. 11b**). Since VDZ selectively binds to the integrin $\alpha_4\beta_7$, blocking its interaction with MAdCAM-1, we then looked at the ratio of $\alpha_4\beta_7^+$ cells in the biopsies relative to the blood for each subset, and found that VDZ significantly decreased $\alpha_4\beta_7^+$ cells in colon biopsies in the majority (21 of 23) cell subsets to varying extents (**Fig 4j-l, Supplementary Fig. 11c**). This pattern was prominent in a hierarchically clustered heatmap, showing unsupervised clustering of UC-VDZ patients HS9-12 based on a lower abundance for all the defined $\alpha_4\beta_7^+$ cell populations in biopsies relative to blood (**Fig. 4j**). Therefore, VDZ does broadly interfere to some extent with intestinal trafficking for many cell types, even if frequencies of MNP subsets were more significantly affected than $CD4^+$ T lymphocyte subsets. To understand this process further, we evaluated the percent of each $\alpha_4\beta_7^+$ subset in the peripheral blood and tissue samples (**Fig. 4k,l**). mDCs, including cDC1, cDC2, and cDC2b, exhibited the largest percent increase in circulating $\alpha_4\beta_7^+$ cells in VDZ-treated patients (**Fig. 4k**). $\alpha_4\beta_7^+$ naïve and central memory CD8+ T cells and γδ T cells were reduced in UC-VDZ biopsies as compared to HC and UC patient biopsies (**Fig. 4l**), and reciprocally increased in the circulation (**Fig. 4k**), but there was no overall reduction in the frequency of these T cell subsets in UC-VDZ patient biopsies (**Supplementary Fig. 11b**).

To further validate these findings, we performed a replicate CyTOF experiment on a second group of patients in endoscopic remission, or near endoscopic remission, on stable maintenance therapy with VDZ, anti-TNF, or 5-ASA therapy (**Supplementary Table 1**). In VDZ-treated patients, mDCs again exhibited the most pronounced increase in the circulating $\alpha_4\beta_7^+$ fraction (**Supplementary Fig. 12a**). There were no differences in the overall PBL cell subset frequencies (**Supplementary Fig. 12b**). These results confirmed that the higher levels of circulating $\alpha_4\beta_7^+$ mDCs observed in VDZ-treated patients persisted during stable maintenance therapy, and when compared against anti-TNF agents. CyTOF of mucosal biopsies did not reveal a significant reduction in mucosal mDCs of VDZ-treated patients compared to HC or UC patients on other therapies, which could be explained by the later timepoint and endoscopic remission of this group (**Supplementary Fig. 12c,d**). There was an apparent reduction in total naïve $CD4^+$ and $CD8^+$ T cells in VDZ-treated UC patients compared to other therapies, although the results did not reach statistical significance (**Supplementary Fig. 12d**). Lastly, when we looked at the ratio of $\alpha_4\beta_7^+$ cells in the biopsies relative to the blood for each subset, we confirmed that VDZ significantly reduced $\alpha_4\beta_7^+$ cells in colon biopsies for 18 of 23 cell subsets (**Supplementary Fig. 12e,f**). Overall, CyTOF experiments confirmed that VDZ is associated with a shift of $\alpha_4\beta_7^+$ cells from tissue to peripheral blood across most subsets in either active or inactive UC. Notably impacted were the circulating $\alpha_4\beta_7^+$ mDCs, followed by CD8+ T, NK, γδ T, B, and plasma cells.

Spatial analysis of MNP and fibroblast subsets in FFPE samples from VDZ-treated patients

We used a variety of spatial transcriptomic and proteomic methods with single-cell resolution to evaluate the colonic tissue micro-environment across disease and treatment status in FFPE samples. 12-plex RNA-ISH exhibited sufficient sensitivity and specificity for some high-expressing cell lineage markers, but struggled to adequately measure genes expressed at lower levels, including *ITGA4, ITGB7*, *MADCAM1,* and *FLT3* (**Supplementary Fig 13a,b, Supplementary Table 3**). 39-plex MIBI on the same tissue microarray (TMA) identified 20 phenotypes with high signal-to-noise ratio (SNR), but the need to balance resolution and field-of-view (FOV) dimensions with longer acquisition times ultimately yielded fewer cells than RNA-ISH (**Fig. 5a-c, Supplementary Table 3,4)**. Despite limited cell counts with MIBI, there was a trend indicating a reduction in fibroblasts in UC-VDZ compared to UC biopsies (**Fig. 5d; Supplementary Fig. 13c**). We then performed 28-plex CODEX and unsupervised clustering, visualization, and annotation, mirroring the CyTOF analysis (**Fig.**

5e-j; **Supplementary Fig. 13d**; **Supplementary Tables 3,4**). Unsupervised analysis generated 24 clusters, and highly similar clusters were subsequently grouped to yield 11 clusters (**Fig. 5f**). The UMAP, similarity matrix heatmap, along with visual inspection of each channel, identified specific and nonspecific markers for the final supervised cell phenotype analysis of 18 subsets (**Fig. 5g,h**; **Supplementary Fig. 13d, Supplementary Table 4**). Memory $CD8^+$ T cells exhibited a statistically significant increase in UC compared to HC, but this was not significantly reduced in VDZ-treated patients (**Supplementary Fig. 13d**). While the CODEX panel lacked the specificity to accurately quantify mDCs, it could reliably detect and quantify both macrophages and $CD44^+PDPN^+$ activated/inflammatory fibroblasts. While not statistically significant, both subsets showed a trend toward increase in UC and reduction with VDZ (**Fig. 5i,j**), similar to the pattern observed with CITE-seq. In both MIBI and CODEX datasets, MNP and fibroblast subsets exhibited trends toward increased proximity by nearest neighbor (NN) analysis in UC compared to HC, with inhibition VDZ (**Fig. 6a,b)**. To further evaluate the colonic tissue microenvironment in this setting, we then performed 960-plex RNA-ISH (CosMx from Nanostring) on our FFPE TMA at subcellular resolution, as recently described[39,40] (**Fig. 6c**). After cell segmentation and mapping of transcript location (**Fig. 6d**; **Supplementary Fig 13e-g**), UMAP and corresponding spatial scatter plots (**Fig 6e,f**) were used to manually annotate cell types. Landmark genes for each subset correlated well with biopsy scRNA-seq (**Supplementary Fig. 13g**). Activated fibroblasts (*TIMP1, IL1R1, CXCL14*, *CD44*) and activated inflammatory MNPs (*S100A4, TIMP1, S100A9, CD80, ITGAX, LYZ, IL1B*) containing a mixture of inflammatory monocytes, macrophages, and mDCs, trended toward increased spatial proximity in UC biopsies as compared to HC, but not in UC-VDZ patients (**Fig. 6g,h**).

Spatial transcriptomics of archived FFPE biopsies identifies pre-treatment signatures associated with VDZ response and non-response

To examine tissue level differences between VDZ responders (VDZ-R) and non-responders (VDZ-NR), we retrieved longitudinal archived FFPE biopsies before and after therapy and performed 1000-plex CosMx spatial transcriptomics (**Fig 7a, Supplementary Tables 1,3**). The data quality using retrospectively identified, clinical archived FFPE samples underperformed prospectively collected FFPE samples, likely reflecting sample age and storage. Approximately 20% of cells were not annotated after filtering, and additional stromal

and lymphocyte subsets could not be confidently assigned due to lower levels of landmark gene expression and ambiguous cell identity. Importantly, the myeloid, stromal, and epithelial subsets of interest expressed landmark genes at higher levels. Unsupervised hierarchical clustering based on the abundance of these subsets distinguished HC from UC patient samples (**Supplementary Fig 14a**). We observed an increase in activated MNPs in UC compared to controls before VDZ treatment, with a decrease in responders and an increase in non-responders post-treatment (**Fig 7b**). IECs expressing high levels of MHCII were similarly elevated in active colitis compared to controls before VDZ treatment, with an apparent reduction in responders post-treatment (**Fig 7c**). Again, neighborhood enrichment analysis revealed trends toward increased proximity of activated fibroblast and activated MNP subsets in active colitis, and reduction after treatment, although this was not statistically significant and not clearly associated with response or non-response to VDZ (**Fig 7d**). Pre-treatment differences are the most relevant for developing precision medicine algorithms. Therefore, we performed pseudobulk DE gene analysis of pre-treatment FFPE biopsies from non-responders versus responders, to identify distinguishing baseline features (**Supplementary Table 7, Supplementary Fig 14b**). Genes specific to the IEC crypt base including *REG1A, OLFM4, AGR2, SPINK1,* and *LYZ* were associated with response to VDZ, while fibroblast and MNP-enriched genes including *MMP1, MMP2,* and *THBS1* were relatively higher in VDZ non-responders (**Fig 7e**). IgA plasma cell-associated genes were also higher in responders (**Fig 7e**). Spatial scatter plots of cell subsets and transcripts suggested that a robust IEC crypt base was associated with response to VDZ, while the abundance and activation of fibroblasts and MNPs were more linked to non-response prior to VDZ treatment (**Fig 7f-i**).

To further validate the association of MNP, stromal, and IEC genes with VDZ response and non-response, we performed gene set enrichment analysis (GSEA)[41,42] of a longitudinal, publicly available[1], bulk transcriptomic dataset of UC patients using landmark genes from our multi-omics analysis (**Supplementary Table 5**). Neutrophils were not present in our biopsy CITE-seq data, but a gene set signature was generated from canonical landmark genes. Not surprisingly, VDZ responders (n=9) exhibited broad reductions in immune and activated stromal Normalized Enrichment Scores (NES), with epithelial gene set enrichment post-treatment, consistent with reduced inflammation and mucosal healing (**Fig. 8a**). In contrast, VDZ non-responders (n=5) exhibited a high initial pre-treatment cytotoxic lymphocyte signature, and persistent

activated and S2 fibroblast gene signatures post-treatment, without significant epithelial enrichment post-treatment, consistent with a model where high initial cytotoxic lymphocyte injury and persistent stromal tissue inflammation prevents mucosal healing (**Fig. 8a**). Interestingly, the reduction in immune subsets in VDZ non-responders was smaller and not statistically significant compared to VDZ responders. VDZ non-responders (n=9) were differentiated from responders (n=11) by pre-treatment enrichment for endothelial, activated fibroblast, neutrophil, macrophage, and monocyte signatures (**Fig. 8b**). Gene signatures investigated were clearly distinguished by leading edge analysis (**Fig. 8c**). Additionally, GSEA using VDZ response and non-response signatures identified from our longitudinal spatial transcriptomics analysis of FFPE biopsies were validated in this external bulk transcriptomic dataset (**Fig. 8d,e; Supplementary Table 5).** Interestingly, the VDZ non-response signature was also significantly enriched in Infliximab non responders prior to treatment (pre-IFX), categorizing these genes as markers of non-response to both treatments (**Fig. 8f**,**g**). This is expected as all of the VDZ-treated patients in that study had previously been exposed to anti-TNF therapy[1], similar to our VDZ non-responders (**Supplementary Table 1**). In contrast, the pre-VDZ-response signature was specific to VDZ, and not associated with response to IFX (**Fig. 8f,g**). These data suggest that VDZ non-responders have higher pre-treatment tissue innate immune and activated stromal subset inflammation, and that these cell subsets likely drive inflammatory cell trafficking via $\alpha_4\beta_7$-independent pathways. Conversely, a robust IEC crypt base signature pre-treatment is linked to response to VDZ and mucosal healing.

DISCUSSION

To identify and validate the transcriptomic, proteomic, and cellular signatures associated with UC and VDZ treatment, we optimized a multi-omics pipeline that included batch processing of cryopreserved biopsies for simultaneous multiplexed CITE-seq and CyTOF, coupled with spatial analysis of FFPE biopsies. VDZ was associated with small shifts in peripheral leukocytes by scRNA-seq, while colonic tissue profiling demonstrated a significant reduction in MNPs, expansion of some epithelial subsets, and a trend toward fewer activated fibroblasts by CITE-seq. Among immune subsets analyzed by CyTOF, mDCs exhibited the largest increase in circulating $\alpha_4\beta_7^+$ cells in VDZ-treated patients. Spatial proteomics and transcriptomics of FFPE colonic biopsies using MIBI, CODEX, and highly multiplexed RNA-ISH demonstrated trends toward increased density and proximity of MNP and fibroblast subsets in UC as compared to HC. Spatial transcriptomics of archived clinical FFPE samples before treatment identified MNP, fibroblast, and epithelial

gene signatures linked to VDZ response and non-response, and these signatures were confirmed using an external, publicly available bulk transcriptomic dataset.

There are conflicting data regarding the primary cell subsets targeted by VDZ. VDZ has been reported to bind to CD4 T, CD8 T, B, NK, and granulocytes in the peripheral blood[43,44]. Here we confirm that VDZ shifts $\alpha_4\beta_7^+$ cells from the colon to the circulation for most cell types, but this results in a small net change in tissue cell frequency for most cell subsets. Multiple studies have investigated the effect of VDZ on T cell subsets, in general supporting models where pathogenic effector T cell subsets are excluded more efficiently than regulatory T cell subsets[6–8,45]. Our data do not exclude any of these observations, but rather add that VDZ is correlated with alterations in the abundance and expression of circulating and intestinal MNP subsets, which likely contributes to a reduction in tissue inflammation. One recent study demonstrated that VDZ did not consistently alter the phenotype, activation, or repertoire of lamina propria T cells by flow cytometry and TCR sequencing, but bulk transcriptomic data was consistent with a shift in MNP gene signatures[11], aligning with our analysis. Nonetheless, the impact of VDZ on intestinal MNP populations likely affects the recruitment and activation of both adaptive and innate immune subsets.

This study has important therapeutic implications. Our CyTOF analysis demonstrated that mDCs are highly dependent on $\alpha_4\beta_7$ for intestinal trafficking, consistent with MAdCAM-1-deficient and β7 integrin-deficient mice[10]. Our data suggest that T cells may be better able to exploit $\alpha_4\beta_7$-independent intestinal trafficking pathways than mDCs. These pathways could include $\alpha_4\beta_1$:VCAM1, GPR15:C10ORF99, CXCR4:CXCL12, or CCR6:CCL20[46]. Interestingly, *GPR15* and *CCR6* are expressed by lymphocytes, but not mDCs or monocytes, which could partially explain the impact of VDZ on tissue MNPs. Refractory IBD patients may benefit from additional combination therapies that target lymphocytes or activated stromal cell subsets, as is done sometimes in clinical practice[47]. Recently, inflammatory fibroblasts have been reported to secrete neutrophil-tropic CXCR1 and CXCR2 ligands in response to IL-1β[48]. Granulocytes are greatly diminished by cryopreservation, so our study was not optimized to analyze neutrophils, but we do show that VDZ non-responders exhibit increased activated fibroblast signatures at baseline and after therapy. The observation

that inflammatory MNPs and fibroblasts share similar cellular neighborhoods further supports a rationale for neutralization of IL-1 family members in refractory colitis.

A secondary objective of this study was to evaluate various multi-omics platforms on cryopreserved biopsies and FFPE tissue. CyTOF quantitated the most cells per patient, MIBI the fewest, while CITE-seq, CODEX, and CosMx methods yielded comparable numbers of cells per patient (**Supplementary Fig 14c**). Comparing across tissue compartments, CITE-seq over-sampled the immune compartment and under-sampled the epithelial compartment, when compared to other multi-omics methods (**Supplementary Fig 14d, Supplementary Table 6**). Given the ubiquity of FFPE tissue, preservation of spatial relationships, and more accurate representation of *in situ* cell frequencies and gene expression, FFPE-compatible spatial multi-omic technologies provide a powerful complementary method for analyzing patient-derived biospecimens.

There are several important limitations of this study. No functional investigations were performed, therefore alterations in cell abundance or gene expression could be directly or indirectly related to VDZ. Additional limitations include a small sample size and case-control approach for the primary analysis. We chose to perform in-depth multi-omic analysis in the same patients to maximize paired phenotypic data from each patient. In the future, prospective longitudinal single-cell and spatial multi-omic data from more patients on diverse therapies could permit detection of more subtle changes in differential gene and protein expression across various medication classes. Of note, the VDZ-non-responders in our study and the publicly available dataset were both previously exposed to anti-TNF, likely explaining why our VDZ non-response signature was associated with both VDZ and IFX non-response. While we found that archived clinical FFPE samples are suitable for spatial transcriptomics, the data are noisier, with smaller fold changes than sequencing methods, and some variability in probe performance and specimen integrity. Finally, this study focused exclusively on host factors, but microbial determinants and metabolomics have also been shown to contribute to therapeutic response in IBD[49,50]. Incorporating additional multi-omic modalities in future studies could enhance our understanding of treatment response and non-response in UC.

In summary, we performed comprehensive single-cell and spatial transcriptomic and proteomic phenotyping to establish MNPs as an important cell type impacted by anti-integrin therapy in UC, with associated changes in stromal and epithelial populations. This study highlights important cellular networks involving MNPs and fibroblasts in colitis. The combination of CITE-seq and CyTOF on identical sets of biopsies establish a surface protein cell atlas for the colon in health, disease, and during treatment. We also describe a spatial atlas for colitis with single-cell resolution using MIBI, CODEX, and CosMx on FFPE samples, allowing comprehensive analysis of cell subset frequency, differential gene expression, and cellular proximity. Ultimately, precision medicine implies approaching each patient as an n-of-1, and here we show that multiple orthogonal multi-omics analyses enhance internal validity for immunophenotyping, even with small sample sizes. Implementing single-cell and spatial multi-omics methods simultaneously in individual patients will provide deep immunophenotyping and lead to more precise treatment algorithms.

METHODS

Study approval

The study was conducted according to Declaration of Helsinki principles and was approved by the Institutional Review Board of the University of California, San Francisco (19-27302). Written informed consent was received from participants prior to inclusion in the study.

Study participants and biospecimen collection

For prospective sample collection, patients undergoing colonoscopy or sigmoidoscopy for standard of care indications were screened for study eligibility. Eligible patients were recruited consecutively to minimize self-selection bias. Patients were compensated $50 for each sample collection event. All participating patients gave written informed consent and approval. Peripheral blood and cold forceps biopsy samples were obtained from patients with UC, and individuals without IBD, referred to as healthy controls (HC). For retrospective archived FFPE sample retrieval, study subjects were identified by querying the electronic medical records of patients previously seen by UCSF Gastroenterology, followed by written informed consent and approval. Baseline demographic and clinical data for the study participants are provided in **Supplementary Table 1**. We have consent to publish de-identified patient demographics including age at the time of sample collection, sex, diagnosis, and medical center. Demographic options were defined by the investigators and participants chose their classifications. HC patients were patients without known or

suspected IBD undergoing elective colonoscopy or sigmoidoscopy for various indications (e.g., colorectal cancer screening). Biopsy samples were categorized as coming from an area that was endoscopically non-inflamed (score=0), mildly inflamed (score=1), moderately inflamed (score=2), or severely inflamed (score=3). Samples were assigned unique identifiers before biobanking.

Sample collection and storage

Colon biopsies were obtained with standard cold endoscopic biopsy forceps from two different regions of the colon (R=right/proximal and L=left/distal) with separate vials for different downstream applications. Two biopsies were collected in 10% formalin in 5 mL tubes for 24h, then washed with PBS twice and stored in 70% ethanol for paraffin embedding; two biopsies were collected in 4mL RNAlater in 5 mL tubes stored overnight at 4°C for, then the solution was aspirated, and biopsies were stored at -70°C until further analysis. Six biopsies were collected in a conical tube with Basal Media (Advanced DMEM/F12 with NEAA and Sodium Pyruvate, Thermo cat. No. 12634-010; 2mM Glutamax, Thermo cat. No. 35050061; 10 mM HEPES (Corning); Penicillin-Streptomycin-Neomycin (PSN) Antibiotic Mixture, Thermo cat. No. 15640055; Normocin 100 µg/mL, Invivogen cat. No. ant-nr-2; 1 mM N-acetylcysteine, Sigma-Aldrich, A9165) with 10 µM Y-27632 (MedChem Express) at 4°C. Samples were immediately placed on ice and transported to the laboratory for processing as previously described[51]. Biopsies were transferred into cryovials containing freezing media (90% (v/v) FCS, 10% (v/v) DMSO and 10 µM Y-27632) and immediately placed into a freezing container (Mr. Frosty or Coolcell) and stored at -70°C for up to 4 weeks before transferring to liquid nitrogen cryostorage until further processing. A PAXgene RNA tube (Qiagen) for peripheral blood was collected, stored, and processed according to the manufacturer's instruction. For peripheral blood leukocyte (PBL) isolation, peripheral blood was collected into EDTA tubes (BD, 366643). 2 mL aliquots of peripheral blood were treated with 30mL of RBC lysis buffer (Roche) for 5-8 minutes at room temperature with gentle mixing. Cells were re-suspended in CryoStor CS10 (at 4°C) freezing medium, aliquoted in cryovials, transferred to a freezing container (Mr. Frosty or Coolcell), and stored at -70°C for up to 4 weeks before transferring to liquid nitrogen cryostorage until further processing.

Preparation of colon and peripheral blood single-cell suspensions

Colon biopsies were thawed for 2min with gentle agitation in a 37°C water bath, transferred to a gentleMACS C Tube (Miltenyi Biotec), washed twice with basal media containing 10 µM Y-27632, and then incubated in 5

mL digestion buffer (basal media, 10 μM Y-27632, 600 U/mL Collagenase IV (Worthington cat. No. LS004189), 0.1 mg/mL DNAse I (Sigma-Aldrich, D4513) and digested for 20 min at 37°C in a shaking incubator set at 225 rpm. Subsequently, samples were placed in the gentleMACS Dissociator, processed with the gentleMACS program m_intestine_01, followed by 15 min incubation at 37°C in a shaking incubator set at 225 rpm. The suspension was then strained through a 100 μm strainer (Miltenyi) and centrifuged at 450g for 5 min at RT. Two additional washes were performed in Hanks' Balanced Salt Solution (HBSS) (Corning), containing 0.1 mg/mL DNAse I (Sigma-Aldrich, D4513). $1x10^6$ total cells were set aside for CyTOF. For the remaining cells, dead cells were removed with the Dead Cell Removal Kit (Miltenyi) according to the manufacturer's instructions. Cell suspensions were counted using a TC20 Automated Cell Counter (Bio-Rad) with 0.4% Trypan Blue Solution (Thermo Fisher Scientific). Live-cell enriched colon single-cell suspensions were used for tissue scRNA-seq and CITE-seq, with a final pooled viability >75%. PBLs were thawed for 2min with gentle agitation in a 37°C water bath and then washed twice with complete DMEM (Thermo Fisher) supplemented with nonessential amino acids (Thermo Fisher Scientific), sodium pyruvate (Thermo Fisher Scientific), HEPES (10 mM; Corning), Glutamax (2 mM; Thermo Fisher Scientific), Normocin (100 μg/mL; Invivogen, ant-nr-2), penicillin-streptomycin (Thermo Fisher Scientific) and 10% Fetal Bovine Serum (VWR). Cells were incubated with ACK lysis buffer (Quality Biological) for 5min at room-temperature, washed twice with complete DMEM, treated with HBSS (Corning) containing 0.1 mg/mL DNAse I (Sigma-Aldrich, D4513) for 5 min, and then strained through a 20um pre-separation filter (Miltenyi). Cells were counted using a TC20 Automated Cell Counter (Bio-Rad) with 0.4% Trypan Blue Solution (Thermo Fisher Scientific). Peripheral blood leukocytes (PBLs) from each donor were used for scRNA-seq and CyTOF, with a final pooled viability of >85%.

Bulk RNA-seq sample and computational processing

RNA was extracted from blood or biopsies following manufacturer's protocol using the PAXgene kit and Qiagen Rneasy Mini kit (Qiagen), respectively. RNA quality and integrity were measured with the Agilent RNA 6000 Nano Kit on the Agilent 2100 Bioanalyzer, according to manufacturer's instructions. Ribosomal and hemoglobin depleted total RNA-sequencing libraries were created using FastSelect (Qiagen cat#: 335377) and Tecan Universal Plus mRNA-Seq (0520-A01) with adaptations for automation of a Beckmen BioMek FXp system. Libraries were subsequently normalized and pooled for Illumina sequencing using a

Labcyte Echo 525 system available at the Center for Advanced Technology at UCSF. The pooled libraries were sequenced on an Illumina NovaSeq S4 flow cell lane with paired end 150bp reads. Computation processing for genotyping was performed as previously described[23,52]. Briefly, sequencing reads were aligned to the human reference genome and Ensembl annotation (GRCh38 genome build, Ensembl annotation version 95) using STAR v2.7.5c (PMID: 23104886) with the following parameter— --outFilterType BySJout –outFilterMismatchNoverLmax 0.04 – outFilterMismatchNmax 999 –alignSJDBoverhangMin 1 –outFilterMultimapNmax 1 – alignIntronMin 20 –alignIntronMax 1000000 –alignMatesGapMax 1000000. Duplicate reads were removed and read groups were assigned by individual for variant calling using Picard Tools v2.23.3 (https://broadinstitute.github.io/picard/). Nucleotide variants were identified from the resulting bam files using the Genome Analysis Tool Kit (GATK, v4.0.11.0) following the best practices for RNA-seq variant calling[53]. This includes splitting spliced reads, calling variants with HaplotypeCaller (added parameters: --don't-use-soft-clipped-bases -standcall-conf 20.0), and filtering variants with VariantFiltration (added parameters: -window 35 – cluster 3 –filter-name FS -filter FS > 30.0 –filter-name QD -filter QD < 2.0). Variants were further filtered to include a list of high quality SNPs for identification of the subject of origin of individual cells by removing all novel variants, maintaining only biallelic variants with MAF greater than 5%, a mix missing of one individual with a missing variant call at a specific site and requiring a minimum depth of two (parameters: --max-missing 1.0 –min-alleles 2 –max-alleles 2 –removeindels –snps snp.list.txt –min-meanDP 2 –maf 0.05 –recode –recode-INFO-all –out).

scRNA-seq and CITE-seq sample loading and sequencing

PBL or colon single-cell suspensions from each patient were pooled with equivalent number of live cells and resuspended at 1-2.5x10^3 cells/µl in 0.04%BSA/PBS, with the addition of 10 µM Y-27632 (MedChem Express) for colon samples. Samples from unique individuals were pooled, and samples from the proximal (Right,R) or distal (Left,L) colon of the same individual were placed in separate pools, so each sample could later be uniquely identified using demuxlet[21]. For the primary biopsy UC and VDZ analysis, the two pools were loaded into four wells each of a Chromium Single Cell 3′ v2 Reagent Kit (10X Genomics), with a total of 8 wells (**Supplementary Table 2**). 1x10^6 cells of both single-cell colon suspension pools were stained with a custom TotalSeq-A panel, (BioLegend) (**Supplementary Table 3**) according to the manufacturer's instructions and loaded into two wells. For all experiments, 60,000 cells were loaded per well and processed

for single-cell encapsulation and cDNA library generation using the Chromium Single Cell 3′ v2 Reagent Kits (10X Genomics). TotalSeq-A library generation was performed according to manufacturer's instructions (BioLegend). Libraries were sequenced on an Illumina NovaSeq6000 to obtain 25,000 reads per cell for the gene expression libraries and 10,000 reads per cell for the TotalSeq libraries.

scRNA-seq and CITE-seq data pre-processing, inter-sample doublet detection, and demuxlet

10x Genomics Chromium scRNA-seq data were processed as previously described[23,52]. Briefly, sequencer-obtained bcl files were demultiplexed into individual library fastq trios using the mkfastq program from the Cellranger 3.0.2 suite of tools (https://support.10xgenomics.com). Feature-barcode matrices were obtained for each sample by aligning the raw fastqs to GRCh38 reference genome (annotated with Ensembl v85) using the Cellranger count. Raw feature-barcode matrices were loaded into Seurat 3.1.5[54] and low-quality cells (with fewer than 100 features), and features in 3 or fewer cells were dropped from the dataset. The remaining events were assessed for inter-sample doublet detection (generated due to libraries containing samples pooled prior to loading) using Freemuxlet (https://github.com/statgen/popscle), the genotype-free version of Demuxlet[21]. Clusters of cells belonging to the same patient were identified via SNP concordance to a truth set generated by bulk RNASeq. Briefly, the aligned reads from Cellranger were filtered to retain reads overlapping a high-quality list of SNPs obtained from the 1000 Genomes Consortium (1KG)[55]. Freemuxlet was run on this filtered bam using the 1KG vcf file as a reference, the input number of samples/pool as a guideline for clustering groups of cells by SNP concordance, and all other default parameters. Cells are classified as singlets (arising from a single library), doublets (arising from two or more libraries), or as ambiguous (cells that cannot be accurately assigned to any existing cluster due to a lack of sufficient genetic information). Clusters of cells belonging to a unique sample were mapped to patients using their individual Freemuxlet-generated genotype, and ground truth genotypes per patient identified via bulk RNA-seq. The pairwise discordance between inferred and ground-truth genotypes was assessed using the bcftools gtcheck command[56]. The feature-barcode Matrices were further filtered to remove cells with greater than 50% percent mitochondrial content or ribosomal content, and cells assigned as doublets or ambiguous by Freemuxlet. Visual outliers in the feature-vs-UMIs plots were filtered uniformly across all libraries. The cell cycle state of each cell was assessed using a published set of genes associated with various stages of human mitosis[57].

scRNA-seq and CITE-seq quality control, normalization, and intra-sample heterotypic doublet detection

The filtered count matrices were normalized, and variance stabilized using negative binomial regression via the scTransform method offered by Seurat[58]. The effects of mitochondrial content, ribosomal content, and cell cycle state were regressed out of the normalized data to prevent any confounding signal. The normalized matrices were reduced to a lower dimension using Principal Component Analyses (PCA) and the first 30 principal coordinates per sample were subjected to a non-linear dimensionality reduction using Uniform Manifold Approximation and Projection (UMAP). Clusters of cells sharing similar transcriptomic signals were initially identified using the Louvain algorithm, and clustering resolutions varied between 0. 6 and 1.2 based on the number and variety of cells obtained in the datasets. All libraries were further processed to identify intra-sample heterotypic doublets arising from the 10X sample loading. Processed and annotated Seurat objects were processed using the DoubletFinder package[59]. The prior doublet rate per library was approximated using the information provided in the 10x knowledgebase (https://kb.10xgenomics.com/hc/en-us/articles/360001378811) and this was corrected to account for inter-sample doublets identified by freemuxlet, and for homotypic doublets using the per-cluster numbers in each dataset. Heterotypic doublets were removed. The raw and log-normalized counts per library were then pruned to retain only genes shared by all libraries. Pruned counts matrices were merged into a single Seurat object and the batch (or library) of origin was stored in the metadata of the object. The log-normalized counts were reduced to a lower dimension using PCA and the individual libraries were aligned in the shared PCA space in a batch-aware manner (Each individual library was considered a batch) using the Harmony algorithm[60]. ADT counts were centered log-ratio (CLR) normalized. The resulting Harmony components were used to generate batch corrected UMAP visualizations and cell clustering.

scRNA-seq and CITE-seq cell annotation and differential expression

For both blood and biopsy scRNA-seq and CITE-seq, we generated h5ad files with the UMAP, Louvain clusters, and metadata. We then refined the “coarse” and “fine” cell-type annotations in a semi-supervised manner using exploratory CZ CELLxGENE (ExCellxGene) (https://pypi.org/project/excellxgene/), a restructured version of CZ CELLxGENE[61,62]. Expression of cell-type specific markers were used to assign identities to “coarse” and “fine” clusters, guided by previously described gene sets[12,13,15,27,63]. Cells that were

unable to be further categorized by fine annotations were labeled as the coarse parental population-not otherwise specified (NOS). The “Mito Hi immune” cluster, consisting of cells with high mitochondrial gene expression, were not considered in downstream analysis. scRNA-seq and CITE-seq data analysis and visualization were then performed in Jupyter notebooks using Scanpy==1.9.1[64]. To compute differentially express (DE) genes between two conditions, we first subsetted our datasets with a pair of conditions (HC vs UC, UC vs VDZ, and HC vs VDZ). Then, we used the MAST R package v1.20 which implements a negative-binomial model using the zlm method and corrects for differences in sequencing depth across samples[65]. Briefly, for a subsetted dataset of two conditions, we analyzed all cells in aggregate, and then subsetted again for each cell-type (coarse annotation for biopsies, and fine annotation for blood) to identify DE genes for each cell-type between the two conditions. We also corrected for the number of detected genes as a potential confounding variable[65]. When comparing paired cryopreserved versus fresh samples, patients were treated as a random effect. P-values were corrected using the Bonferroni correction. Platelets and erythrocytes were excluded from blood DE gene analysis.

Fresh versus cryopreserved biopsy scRNA-seq comparison

For the fresh versus cryopreserved comparison, twelve colon biopsies were divided into two vials, each containing six biopsies, for two donors. The fresh biopsies were stored in Basal Media on ice for 80 min, while the cryopreserved biopsies were transferred into cryovials containing freezing media (90% (v/v) FCS, 10% (v/v) DMSO and 10 μM Y-27632) and immediately placed into a freezing container (Mr Frosty or Coolcell) and stored at -70°C for 80min. The cryopreserved biopsies were then thawed, and both the fresh and cryopreserved biopsies were digested as above. Half of the fresh biopsies from each donor were labeled with TotalSeq-A0251 barcode sequence GTCAACTCTTTAGCG (Biolegend 394601), and the other half of the fresh biopsy sample was labeled with MULTI-seq lipid-tag barcode sequence CCTTGGCACCCGAGAATTCCAGGAGAAGA[66]. Half of the cryopreserved biopsies from each donor were labeled with TotalSeq-A0252 barcode sequence TGATGGCCTATTGGG (Biolegend 394603), and the other half of the cryopreserved biopsy sample was labeled with MULTI-seq lipid-tag barcode sequence CCTTGGCACCCGAGAATTCCACCACAATG[66]. The MULTI-seq labeled samples were combined into one pool, and the TotalSeq Hasthag samples were combined in a second pool. The two pools were loaded separately into one well each of a Chromium Single Cell 3′ v2 Reagent Kit (10X Genomics). 60,000 cells

were loaded per well and processed for single-cell encapsulation and cDNA library generation as described above. Representative UMAPs comparing cryopreserved and fresh biopsies and coarse cell subset annotations, as well as the scRNA-seq DE genes, were generated from the MULTI-seq labeled samples as described above. Quantitation of cell subset frequency was performed on both MULTI-seq and TotalSeq barcoded samples.

Mass Cytometry (CyTOF) sample staining and acquisition.

A 37-parameter CyTOF panel was designed (**Supplementary Table 3**). All mass cytometry antibodies were conjugated in-house to their corresponding metal isotope. Metals were conjugated according to the manufacturer's instructions (Fluidigm, South San Francisco, CA, USA). In brief, this process consisted of loading the metal to a polymer for 1h at RT. The unconjugated antibody is transferred into a 50 kDA Amicon Ultra 500 V-bottom filter (Fisher Scientific, Hampton, NH, USA) and reduced for 30 min at 37°C with 1:125 dilution of Tris (2-carboxyethyl) phosphine hydrochloride (TCEP) (ThermoFisher, Waltham, MA, USA). Subsequently, the column was washed twice with C-buffer (Fluidigm) and the metal-loaded polymer was suspended in 200 µL of C-buffer in the 3 kDA Amicon Ultra 500 mLV-bottom filter. The suspension was transferred to the 50 kDA filter containing the antibody and incubated for 1.5h at 37°C. After incubation, antibodies were washed three times with W-buffer (Fluidigm) and quantified for protein content using Nanodrop. Once the concentration was determined, the antibodies were resuspended at a concentration of 0.2 mg/mL with Antibody Stabilizer (Boca Scientific, Dedham, Ma, USA) and stored at 4°C. Optimal concentrations for all antibodies were determined by different rounds of titrations. The staining protocol was optimized to use each antibody in aliquots of 6 million cells as previously described[67].

CyTOF Panel Design, Staining, and Acquisition.

CyTOF was performed on paired peripheral blood and colon biopsies obtained from the primary case control study (n=12) and from the secondary remission case control study (n=17). Single-cell suspensions of colon biopsies from the right and left colon were pooled to ensure sufficient cell counts per donor for the primary case control study (n=12), or run in separate pools for the secondary remission case control study (n=17). Dead cells were labeled with Cisplatin (Fluidigm) according to the manufacturer's instructions, washed in wash buffer (PBS, 0.5% BSA, 5mM EDTA), fixed in 1.6% PFA for 10 min, washed in wash buffer and then resuspended in freezing medium (PBS, 0.5% BSA, 10% DMSO) and stored at -80°C until staining. Samples

were then thawed and washed with wash buffer. Prior to staining with the antibody panel (**Supplementary Table 3**), cells from each patient were barcoded using a unique set of metals, enabling sample identification as previously described[68,69]. The barcode staining was performed following the manufacturer's instructions (Fluidigm, South San Francisco, CA, USA). Briefly, each sample was incubated for 15 min at RT on a shaker (200rpm) with a barcoding solution containing 10 µL of barcode in 1x Perm Buffer solution (Fluidigm, Cat#201057) diluted in cell staining media (CSM, Fluidgim, Cat#201068). Samples were then washed, centrifuged, resuspended in CSM, and pooled. Subsequently, extracellular staining was performed for 30 min at 4°C. After incubation, the samples were washed with CSM and centrifuged before resuspending in 1x Permeabilization Buffer (eBioscience™ Permeabilization Buffer Cat# 00-8333-56) for 10min at 4°C. The samples were then washed and incubated with Ir-intercalator (Biolegend CNS, San Diego, CA, USA) diluted 1:500 in 4% fresh PFA for 20 min at RT. After incubation, samples were washed and kept at 4°C overnight in EQ™ bead solution (Fluidigm Cat#201078) diluted in MaxPar Water (Fluidigm Cat# 201069) at $1.2x10^6$ cells/mL. Samples were analyzed on the CyTOF®2 instrument (Fluidigm). Commercial Fluidigm CYTOF software was used for CyTOF data acquisition.

CyTOF data analysis

After acquisition, the .fcs files were concatenated, normalized to the EQ™ calibration beads, and de-barcoded using CyTOF software (Fluidigm). FlowJo v10 software was used for confirming the elimination of the EQ™ calibration beads, concatenating, and manually gating the files. Singlets were gated by Event Length and DNA. Live cells were identified as cisplatin-negative. The unsupervised analysis was performed on the case control study (n=12) using an R-based Cytometry Clustering Optimization aNd Evaluation (Cyclone) pipeline developed by the UCSF Data Science CoLab (https://github.com/UCSF-DSCOLAB/cyclone)[38]. Specifically, the data were preprocessed, arcsinh transformed (cofactor 5) and then clustered using FlowSOM 2.6.0[70]. We used default values for FlowSOM parameters except for the grid size. A grid size of 3x7 was chosen based on a local minimum of Davies-Bouldin Index (DBI). The clustering was visualized using UMAP, which was calculated using uwot package in R. The pre-cluster median expression levels of each of the 37 antibodies panel for each cluster were used to annotate clusters. This was plotted as a heatmap. In parallel, supervised analysis was performed on the same dataset and on the remission case control study (n=17) defining cell subsets based on canonical markers and followed the scheme illustrated in

Supplementary Fig. 10 and **Supplementary Table 4**. Additionally, the supervised analysis was used to further define cell subsets expressing $\alpha_4\beta_7$. Finally, specific populations and markers of the focused panel were manually gated to validate and extend the results from the unsupervised analysis.

Histology FFPE Tissue Microarray (TMA) construction

Colon biopsies from patients were fixed in 10% neutral-buffered formalin (Millipore Sigma) for 16-24 hours, washed in PBS three times, then placed in 70% ethanol and stored at RT until paraffin-embedding by the Biospecimen Resource Program (BIOS) at UCSF. Sectioning, hematoxylin and eosin (H&E), and high-resolution (40X) scanning were performed according to standard protocols. H&E histologic severity quantification was performed using the Geboes scoring system[71]. Tissue microarrays were constructed from prospectively collected FFPE blocks by UCSF BIOS or retrospectively retrieved, clinical archived FFPE blocks by Pantomics, with 1.1-2mm cores. The recipient TMA block was sectioned with a clearance angle of 10° and a thickness of 4 µm or 5 µm along the width of the block and used for H&E staining and multiplexed RNA-ISH. The TMA block was stored at -20 °C in order to reduce sample degradation and preserve RNA detection in the transcriptomic assays[72]. Freshly cut TMA sections were prepared before each experiment, according to the type of spatial assay performed.

CODEX multiplexed tissue staining, imaging, and data analysis

Colon biopsies from the FFPE TMA block were mounted on coverslips provided by Akoya Biosciences and prepared according to the CODEX® User Manual. Briefly, FFPE TMAs were sectioned onto poly-L-lysine-coated coverslips with a thickness of 5 µm. TMA coverslips were stored individually at 4 °C to avoid tissue damage until the experiment run. Conjugation of DNA oligonucleotides to purified antibodies, antibody validation and titration, and CODEX multicycle reactions were optimized and performed by Akoya Biosciences according to the protocol previously described[73]. CODEX samples were stained and imaged by Akoya. Briefly, TMA coverslips were pretreated on a hot plate at 55°C with tissue facing up for 20-25 minutes, then positioned on a rack at RT for 5min to allow the tissues to cool down. Subsequently, deparaffinization and hydration steps were performed. Next, the TMA coverslips were submerged in a beaker containing antigen retrieval solution (1x Tris/EDTA buffer, pH 9) and placed in a pressure cooker for 20 min. After incubation, samples were cooled at RT for 10 min, washed in distilled water for 2 min (2x), incubated in a hydration buffer for 2 min (2x), and then equilibrated in a staining buffer for 20-30 min before antibody

staining. A customized CODEX panel of 28 antibodies was used and each CODEX®-tagged antibody had a barcode that was complementary to a specific reporter; all related details are summarized in **Supplementary Table 3**. A single staining step with the antibody cocktail solution containing blocking buffer and the panel of antibodies was performed on the tissues for 3 hours at RT in a humidity chamber. After incubation, the TMA coverslips were washed with the staining buffer for 2 min (2x) then the coverslips were incubated with post staining fixing solution (2% PFA) for 10 min at RT. Subsequently, TMA coverslips were washed in 1x PBS (3x), placed in ice-cold methanol for 5 min and transferred rapidly in 1x PBS for three consecutive washes. After the washing steps, TMA coverslips were placed on a tray and tissues were incubated with a final fixative solution for 20 min in a humidity chamber. After incubation, TMA coverslips were rinsed with 1x PBS (3x) and were ready for the CODEX® multicycle experiment. Images were collected using a Keyence BZ-X800 Fluorescent microscope configured with fluorescent channels (ATTO550, Cy5, AF647, and AF750) and equipped with a cooled CCD camera. The resolution was 0.25 μm per pixel. Images for the 28 DNA-conjugated antibodies were acquired over 13 cycles of staining. In each cycle, the reporters revealed up to three markers of interest (and DAPI) simultaneously. After each cycle of imaging, the reporters were removed from the tissue by a gentle isothermal wash. Each core was imaged with a 20x objective. Images were processed, stitched with background subtraction and deconvolution, and aligned into a 28-color overlay figure for the selected markers for analysis at UCSF. Cell segmentation was performed using HALO 3.4 image analysis software (Indica Labs), DAPI was used as the reference nuclear dye. Nuclear contrast threshold, minimum nuclear intensity, and nuclear size were determined using the pre-trained Nuclear Segmentation algorithm (AI default) and kept constant for the entire analysis. Membrane segmentation was done considering a cytoplasm radius of 6μm based on average cell sizes determined using reference H&E images. After cell segmentation, comma-separated value (.csv) files containing signal intensity at single-cell level were generated from each core and used for unsupervised analysis. Data were imported into R and the unsupervised analysis was performed using the Cyclone pipeline as described above[74]. The number of clusters was defined using the FlowSOM clustering (grid size 4x6) and then visualized using UMAPs. The median level of expression of each of the 28 antibodies panel for each cluster was used to annotate the clusters. This was plotted as a Heatmap. Subsequently, based on the unsupervised clusters, a supervised analysis in HALO was performed defining 18 phenotypes based on positive and/or negative channel selection

criteria using the HiPlex FL v 4.1.3 module. Cell frequency for each phenotype was exported as a percentage of positive cells over the total number of cells defined. To define cell interactions, spatial plots were generated for each core using the Spatial Analysis module in HALO. Nearest Neighbor Analysis was conducted on the object data from each suitable core to determine the average distance between two cells or object populations. For this experiment, a total of 20 cores were imaged and 15 of them were selected for further analysis based on the quality of the core. Low-quality cores were excluded if they were grossly damaged or detached during processing, or if they had poor nuclei staining that precluded cell segmentation. For Nearest Neighbor Analysis 12 cores were considered, all the cores containing less than 5 unique cells per phenotypes of interest were excluded from the analysis.

MIBI staining, data acquisition, and analysis

Slide preparation, staining, antibody optimization, and imaging were performed by the MIBI Core at UCSF. Antibodies were conjugated to metal-loaded MIBItags (Ionpath) according to the manufacturer's instructions. Initial imaging QC was performed on the conjugated antibodies and compared to already established positive controls of FFPE spleen and tonsil tissue. The final 39-plex antibody panel for MIBI-TOF is reported in **Supplementary Table 3**. TMA slides containing 20 cores of colon tissues were sectioned (5 µm section thickness) from paraffin tissue blocks on gold and tantalum-sputtered microscope slides. Slides were baked at 70°C overnight, followed by deparaffinization and rehydration with washes in xylene (3x), 100% ethanol (2x), 95% ethanol (2x), 80% ethanol (1x), 70% ethanol (1x) and distilled water (1x). Next, tissues underwent antigen retrieval by submerging the slides in 1X Target Retrieval Solution (pH 9, DAKO Agilent) and incubating at 97 °C for 40 min in a Lab Vision PT Module (Thermo Fisher Scientific). After cooling to RT for 30 min, slides were washed in 1X TBS-T pH7.6 (IONpath). Subsequently, all tissues underwent two rounds of blocking, the first to block endogenous biotin and avidin with an Avidin/Biotin Blocking Kit (BioLegend). Tissues were then washed with wash buffer and blocked for 11 hours at RT with 1X TBS with 5% (v/v) normal donkey serum (Sigma-Aldrich). The first antibody cocktail was prepared in 1X TBS-T 5% (v/v) normal donkey serum (Sigma-Aldrich) and filtered through a 0.1µm centrifugal filter (Millipore) prior to incubation with tissue overnight at 4 °C in a humidity chamber. Following the overnight incubation, slides were washed twice for 5 min in 1X TBS-T pH7.6. The second day, an antibody cocktail was prepared as described and incubated with the tissues for 1h at 4 °C in a humidity chamber. Following staining, slides were washed twice for 5 min

in wash buffer and fixed in a solution of 2% glutaraldehyde (Electron Microscopy Sciences) solution in low-barium PBS for 5 min. Slides were washed in PBS (1x), 0.1 M Tris at pH 8.5 (3x) and distilled water (2x) and then dehydrated by washing in 70% ethanol (1x), 80% ethanol (1x), 95% ethanol (2x) and 100% ethanol (2x). Slides were dried under vacuum prior to imaging. Imaging was performed using a MIBIscope (IonPath) with a Hyperion ion source. Xe+ primary ions were used to sequentially sputter pixels for a given field of view (FOV). The following imaging parameters were used: acquisition setting, 80 kHz; field size, 400 µm x 400 µm at 1,024 ×1,024 pixels; dwell time, 24 ms; median gun current on tissue, 1.45 nA Xe+; ion dose, and 3.75 nAmp h per mm2 (450 µm2 FOVs). Mass correction was done using MIBI/O (IONpath) with their standard JSON file. FOV images were analyzed using the HALO software and the HiPlex FL v 4.1.3 module was used. Cellular segmentation was performed using the Histone H3 nuclear DNA marker as the reference nuclear dye. Nuclear contrast threshold, minimum nuclear intensity, and nuclear size were determined using the traditional segmentation method and kept constant throughout the entire image analysis. Membrane segmentation was done using EpCAM as the reference dye, and a cytoplasm radius of 6 µm was set based on average cell sizes determined using reference H&E images. 20 phenotypes each corresponding to a major cell type were created based on positive and/or negative channel selection criteria. To define cell interactions, spatial plots were generated for each suitable FOV using the Spatial Analysis module. Nearest Neighbor Analysis was conducted on the object data to determine the average distance between two cells or object populations. A total of 37 FOV images were acquired and 32 of them were used for phenotype identification and quantification. FOVs that contained exclusively lymphoid aggregates, with no mucosal or submucosal cellular compartments, were excluded. Among the 32 FOVs analyzed, 29 were selected for Nearest Neighbor Analysis based on the number of cells per phenotype. FOVs containing less than 5 unique cells per phenotype of interest were excluded from the analysis.

Multiplexed (12-plex) RNA *In Situ* Hybridization (RNA-ISH)

FFPE TMA slides containing colon biopsies from our study cohort were used for multiplexed RNA-ISH. The assay was performed following the manufacturer's instructions (HiPlex RNAscope, ACDBio). Briefly, FFPE TMA slides were deparaffinized sequentially with xylene (2x, 5 min) and 100% ethanol (2x, 2 min). After deparaffinization, a retrieval step of 15 min at 99°C was performed. Slides were permeabilized with Protease III for 30 min at 40°C. The 12 probes were hybridized for 2 hours at 40°C and amplified (3 amplification

steps, 30 min each at 40 °C) using the HybEZ hybridization system. Probes were chosen from high-abundance landmark genes from the scRNA-seq data and additional genes of interest. Probes are listed in **Supplementary Table 3**. After probe hybridization and amplification steps, slides were hybridized with the first round of fluorophores for 15 min at 40°C then washed, counterstained with DAPI, and mounted with ProLong Gold Antifade Mountant. The first round of imaging was performed by scanning each full core using the automated Zeiss Axioscanner Z1 with a 20X objective on Orca Flash 4.0 v2 (Hamamatsu) camera in fluorescence channels (DAPI, FITC/GFP, Cy3/Atto550, and Cy5). The image scanner was controlled using ZEN 3.1 software. After each round of imaging, the coverslip was removed by soaking in 4x SSC buffer for 30 min and fluorophores were cleaved using manufacturer cleaving solution. Then the slides were washed and prepared for the second round of fluorophore hybridization and imaging, these last steps were repeated for a total of four rounds. All images were acquired at the UCSF HDFCCC Histology and Biomarker Core. A total of 21 core images were obtained and 19 of them were used for further analysis. Low-quality cores were excluded if they were grossly damaged or detached during processing. Images obtained from the four rounds of staining were then registered, fused, and analyzed using HALO 3.1 image analysis software (Indica Labs). For this analysis, we used the following modules: TMA and FISH v3.1.3. Cell detection was based on Nuclei staining (DAPI) with traditional nuclei segmentation type, nuclear contrast threshold was set at 0.5 with an intensity of 0.015 and aggressiveness of 0.6. The nuclear size was ranging from 5 to 150 (μm^2), the minimum roundness of segmentation was set at 0.05 and the cytoplasm radius was set at 1.5μm. For the analysis, the FISH score was set at 2+ minimum copies/cell, and phenotypes were defined by exclusive channels and according to the round of imaging. Data were expressed as the percentage of positive cells among the total number of cells detected.

<u>Highly multiplexed CosMx spatial transcriptomics tissue processing, staining, imaging, and analysis</u>

FFPE TMA processing, staining, imaging, and cell segmentation were performed as previously described by Nanostring and data were analyzed at UCSF[39]. Briefly, 4-5μm sections of an FFPE TMA block were sectioned on the back of a VWR Superfrost Plus Micro Slide (Cat# 48311-703) using a microtome, placed in a heated water bath, and adhered. Slides were then dried at 37 °C overnight, vacuum sealed, and stored at 4 °C until analysis. Manual FFPE tissue preparation, ISH hybridization, coverslip application, and cyclic RNA readout on the SMI were performed as previously described[39]. After all cycles were completed, additional

visualization markers for morphology and cell segmentation were added including DAPI, pan-cytokeratin (PanCK), CD45, CD3, CD68, and/or CD298/B2M as indicated in AnnData objects (anndata==0.8.0). A 3D multichannel image stack was obtained at each FOV location. Registration, feature detection, localization, determination of the presence individual transcripts, and cell segmentation were performed as previously described[39]. The final segmentation mapped each transcript location in the registered image to the corresponding cell, as well as to the cell compartment (nuclei, cytoplasm, membrane), where the transcript is located. Other features/properties generated included shape (area, aspect ratio) and fluorescence intensity statistics (minimum, maximum, average) per cell. Single-cell spatial RNA-ISH results were analyzed using scanpy[64] and squidpy ==1.2.3[75]. Low-quality cores were excluded if they were extensively damaged or detached during processing, or if they had poor nuclei staining that precluded cell segmentation. For the primary CosMx experiment, 22 FOV were selected, five were ultimately eliminated due to poor tissue adherence or low gene count per cell. For the secondary longitudinal experiment of archived FFPE specimens, 73 out of 81 FOV passed quality control. Cells with <10 unique genes per cell or <50 counts per cell were filtered out, and genes expressed in fewer than 1 cell (1st batch) or 10 cells (2nd batch) were excluded. The data were further normalized, log-transformed, and scaled as previously described[76]. For cell type identification and annotation of CosMx results alone, principal components were computed using scanpy's tl.pca() function with default settings. UMAP plots and leiden clustering were calculated using tl.umap() and tl.leiden(). To annotate the computed clusters, we examined the top differentially expressed genes in each cluster using the tl.rank_genes_groups() function and compared with known marker genes for the various cell types. We then refined the "coarse" and "fine" cell-type annotations in a semi-supervised manner using exploratory CZ CELLxGENE (ExCellxGene==2.9.2)[61,62]. Neighborhood enrichment analysis was performed using squidpy's sq.gr.nhood_enrichment() function. CosMx pseudobulk DE genes were analyzed using DESeq2 to compare non-responders to responders pre-treatment[77].

Antibodies and reagents

Antibodies and reagents for all experiments are listed in **Supplementary Table 3.**

Gene Set Enrichment Analysis (GSEA) on a validation cohort

The bulk transcriptomic study (GSE73661)[1] performed on colonic biopsies obtained from UC patients before and after VDZ treatment was downloaded from GEO database and used for GSEA analysis[41]. Samples were

divided into pre- and post-VDZ treatment and responders (R, responding at week 52, n=9) or non-responders (NR, not responding at week 52). Three comparisons were made: 1-pre- vs post-VDZ treatment for responders, 2-pre- vs post-VDZ treatment for non-responders, and 3-responders (at either week 6,12 or 52) vs non-responders (at either week 12 or 52) pre-VDZ treatment (n=11 for R and n=9 for NR). Data were normalized and expressed as Z-scores before reading into the GSEA program (version 4.3.2). Based on our gene expression data we defined 14 cell type gene signatures with a minimum of 10 genes (**Supplementary Table 5)**. GSEA analysis was performed for each gene signature. The number of permutations was set at 1000, no collapse dataset, chip Affymetrix Human Gene 1.0 ST Array, t-test. For each analysis and gene set, a Normalized Enrichment Score (NES) was calculated and only NES with a p-value <0.05 and adjusted q-value (FDR) <0.1 were considered significant. A leading edge analysis was performed to display overlaps between all cell subsets and to elucidate key genes that contributed the most to the enrichment signal of specified gene sets. Based on our spatial transcriptomic data from the longitudinal experiment we defined pre-VDZ responder and non-responder signatures (**Supplementary Table 5)** and queried these genes in responders vs non-responders from pre-VDZ (R=11 and NR=9) and pre-IFX (R=8 and NR=15) dataset[1]. Additional leading edge analyses were performed on these GSEAs in order to define the genes that significantly contributed to the core enrichment for pre-VDZ and pre-IFX.

Statistics

Non-parametric comparisons were performed using one-way ANOVA Kruskal-Wallis test for multiple groups or Mann-Whitney test for two groups, followed by a two-stage linear step-up procedure of Benjamini, Krieger and Yekutieli to correct for multiple comparisons by controlling the false discovery rate (FDR). Parametric comparisons for multiple groups were performed using two-way ANOVA if comparing multiple variables per group or one-way ANOVA if comparing one variable per group, followed by FDR correction. The q-value is the FDR-adjusted p-value, and q<0.1 was used as the threshold for discovery, unless otherwise indicated. For biopsy CITE-seq cell subset frequency analysis, an additional nested one-way ANOVA test was performed on log transformed values treating biopsies as replicates, with unadjusted p<0.05 as an additional threshold for discovery. Categorical variables were analyzed by Chi-square test as indicated. For MAST DE gene analysis, p-values were corrected using Bonferroni correction, and corrected p-value of <0.05 was used as the threshold for statistical significance. For CosMx Deseq analysis, in addition to q<0.1 after FDR-

correction for all transcripts per FOV, DEseq comparisons were made treating FOVs or biopsies as replicates with unadjusted $p<0.05$ as an additional threshold for discovery (**Supplementary Table 7**). For all other analyses, biopsy values were averaged per patient. Additional analyses were performed using GraphPad PRISM 9. Hierarchically clustered heatmaps for cell subset abundance (Euclidean distance, average linkage) and marker similarity matrices (Pearson correlation) were generated with the Morpheus software (https://software.broadinstitute.org/morpheus/). The ComplexHeatmap R package was used to generate expression z-score heatmaps for DE genes.

Data availability

The raw sequencing data generated in this study have been deposited on the dbGaP database under accession code phs003502.v1.p1. The raw sequencing data are available under controlled access for privacy concerns; access can be requested through dbGaP. Processed data are deposited as a GEO Super Series under accession code GSE250498 and are publicly available. All additional data generated in this study are provided in the Supplementary Information/Source Data file and on Figshare. Processed and annotated objects are saved in AnnData (h5ad) format[78]. These AnnData objects are accessible in Figshare (fresh versus cryopreserved scRNA-seq 10.6084/m9.figshare.21936240; blood scRNA-seq 10.6084/m9.figshare.21900948; biopsy scRNA-seq 10.6084/m9.figshare.21919425; biopsy CITE-seq 10.6084/m9.figshare.21919356; PBL CyTOF 10.6084/m9.figshare.21977834; biopsy CyTOF 10.6084/m9.figshare.21977798; secondary CyTOF PBL and biopsy analysis 10.6084/m9.figshare.23902065; CosMx 960-plex RNA-ISH 1st run 10.6084/m9.figshare.21919338; CosMx 1000-plex RNA-ISH 2nd longitudinal analysis 10.6084/m9.figshare.23896959). Publicly available microarray data (GSE73661) were downloaded from the NCBI gene expression omnibus. GRCh38 was used as the reference genome. Source data are provided with this paper.

Code availability

All code used in this study including R markdowns,Jupyter notebooks, and conda environment .yaml files are available on the Ulcerative Colitis project GitHub repository (https://github.com/mkattah/UC_VDZ). R-based Cytometry Clustering Optimization aNd Evaluation (Cyclone) pipeline was developed by the UCSF Data Science CoLab (https://github.com/UCSF-DSCOLAB/cyclone).

REFERENCES

1. Arijs, I. *et al.* Effect of vedolizumab (anti-α4β7-integrin) therapy on histological healing and mucosal gene expression in patients with UC. *Gut* **67**, 43–52 (2018).
2. Verstockt, B. *et al.* Expression Levels of 4 Genes in Colon Tissue Might Be Used to Predict Which Patients Will Enter Endoscopic Remission After Vedolizumab Therapy for Inflammatory Bowel Diseases. *Clin. Gastroenterol. Hepatol.* **18**, 1142-1151.e10 (2020).
3. Feagan, B. G. *et al.* Vedolizumab as Induction and Maintenance Therapy for Ulcerative Colitis. *N. Engl. J. Med.* **369**, 699–710 (2013).
4. Luzentales-Simpson, M., Pang, Y. C. F., Zhang, A., Sousa, J. A. & Sly, L. M. Vedolizumab: Potential Mechanisms of Action for Reducing Pathological Inflammation in Inflammatory Bowel Diseases. *Front. Cell Dev. Biol.* **9**, 612830 (2021).
5. Soler, D. *et al.* The Binding Specificity and Selective Antagonism of Vedolizumab, an Anti-$\alpha_4\beta_7$ Integrin Therapeutic Antibody in Development for Inflammatory Bowel Diseases. *J. Pharmacol. Exp. Ther.* **330**, 864–875 (2009).
6. Abreu, M. T. *et al.* Transcriptional Behavior of Regulatory T Cells Predicts IBD Patient Responses to Vedolizumab Therapy. *Inflamm. Bowel Dis.* izac151 (2022) doi:10.1093/ibd/izac151.
7. Becker, E. *et al.* Residual homing of α4β7-expressing $\beta1^+$ $PI16^+$ regulatory T cells with potent suppressive activity correlates with exposure-efficacy of vedolizumab. *Gut* **71**, 1551–1566 (2022).
8. Rath, T. *et al.* Effects of Anti-Integrin Treatment With Vedolizumab on Immune Pathways and Cytokines in Inflammatory Bowel Diseases. *Front. Immunol.* **9**, 1700 (2018).
9. Canales-Herrerias, P. *et al. Gut-associated lymphoid tissue attrition associates with response to anti-α4β7 therapy in ulcerative colitis*. http://biorxiv.org/lookup/doi/10.1101/2023.01.19.524731 (2023) doi:10.1101/2023.01.19.524731.
10. Clahsen, T., Pabst, O., Tenbrock, K., Schippers, A. & Wagner, N. Localization of dendritic cells in the gut epithelium requires MAdCAM-1. *Clin. Immunol.* **156**, 74–84 (2015).
11. Zeissig, S. *et al.* Vedolizumab is associated with changes in innate rather than adaptive immunity in patients with inflammatory bowel disease. *Gut* **68**, 25–39 (2019).
12. Kinchen, J. *et al.* Structural Remodeling of the Human Colonic Mesenchyme in Inflammatory Bowel Disease. *Cell* **175**, 372-386.e17 (2018).

13. Parikh, K. *et al.* Colonic epithelial cell diversity in health and inflammatory bowel disease. *Nature* **567**, 49–55 (2019).
14. Boland, B. S. *et al.* Heterogeneity and clonal relationships of adaptive immune cells in ulcerative colitis revealed by single-cell analyses. *Sci. Immunol.* **5**, eabb4432 (2020).
15. Smillie, C. S. *et al.* Intra- and Inter-cellular Rewiring of the Human Colon during Ulcerative Colitis. *Cell* **178**, 714-730.e22 (2019).
16. Konnikova, L. *et al.* High-dimensional immune phenotyping and transcriptional analyses reveal robust recovery of viable human immune and epithelial cells from frozen gastrointestinal tissue. *Mucosal Immunol.* **11**, 1684–1693 (2018).
17. Mitsialis, V. *et al.* Single-Cell Analyses of Colon and Blood Reveal Distinct Immune Cell Signatures of Ulcerative Colitis and Crohn's Disease. *Gastroenterology* (2020) doi:10.1053/j.gastro.2020.04.074.
18. Stoeckius, M. *et al.* Simultaneous epitope and transcriptome measurement in single cells. *Nat. Methods* **14**, 865–868 (2017).
19. Kondo, A. *et al.* Highly Multiplexed Image Analysis of Intestinal Tissue Sections in Patients With Inflammatory Bowel Disease. *Gastroenterology* **161**, 1940–1952 (2021).
20. Mayer, A. T. *et al.* A tissue atlas of ulcerative colitis revealing evidence of sex-dependent differences in disease-driving inflammatory cell types and resistance to TNF inhibitor therapy. *Sci. Adv.* **9**, eadd1166 (2023).
21. Kang, H. M. *et al.* Multiplexed droplet single-cell RNA-sequencing using natural genetic variation. *Nat. Biotechnol.* **36**, 89–94 (2018).
22. Hao, Y. *et al.* Integrated analysis of multimodal single-cell data. *Cell* **184**, 3573-3587.e29 (2021).
23. Combes, A. J. *et al.* Global absence and targeting of protective immune states in severe COVID-19. *Nature* **591**, 124–130 (2021).
24. Picotto, G., Morse, L. R., Nguyen, N., Saltzman, J. & Battaglino, R. TMEM176A and TMEM176B Are Candidate Regulators of Inhibition of Dendritic Cell Maturation and Function after Chronic Spinal Cord Injury. *J. Neurotrauma* **37**, 528–533 (2020).
25. Mattiola, I., Mantovani, A. & Locati, M. The tetraspan MS4A family in homeostasis, immunity, and disease. *Trends Immunol.* **42**, 764–781 (2021).

26. Duhalde Vega, M. *et al.* PD-1/PD-L1 blockade abrogates a dysfunctional innate-adaptive immune axis in critical β-coronavirus disease. *Sci. Adv.* **8**, eabn6545 (2022).
27. Martin, J. C. *et al.* Single-Cell Analysis of Crohn's Disease Lesions Identifies a Pathogenic Cellular Module Associated with Resistance to Anti-TNF Therapy. *Cell* **178**, 1493-1508.e20 (2019).
28. Smids, C. *et al.* Intestinal T Cell Profiling in Inflammatory Bowel Disease: Linking T Cell Subsets to Disease Activity and Disease Course. *J. Crohns Colitis* **12**, 465–475 (2018).
29. Maul, J. *et al.* Peripheral and intestinal regulatory CD4+ CD25(high) T cells in inflammatory bowel disease. *Gastroenterology* **128**, 1868–1878 (2005).
30. Holmén, N. *et al.* Functional CD4+CD25high regulatory T cells are enriched in the colonic mucosa of patients with active ulcerative colitis and increase with disease activity. *Inflamm. Bowel Dis.* **12**, 447–456 (2006).
31. Yu, Q. T. *et al.* Expression and functional characterization of FOXP3+ CD4+ regulatory T cells in ulcerative colitis. *Inflamm. Bowel Dis.* **13**, 191–199 (2007).
32. Lord, J. D., Valliant-Saunders, K., Hahn, H., Thirlby, R. C. & Ziegler, S. F. Paradoxically increased FOXP3+ T cells in IBD do not preferentially express the isoform of FOXP3 lacking exon 2. *Dig. Dis. Sci.* **57**, 2846–2855 (2012).
33. Lord, J. D. Promises and paradoxes of regulatory T cells in inflammatory bowel disease. *World J. Gastroenterol.* **21**, 11236–11245 (2015).
34. Lyu, M. *et al.* ILC3s select microbiota-specific regulatory T cells to establish tolerance in the gut. *Nature* **610**, 744–751 (2022).
35. Elmentaite, R. *et al.* Single-Cell Sequencing of Developing Human Gut Reveals Transcriptional Links to Childhood Crohn's Disease. *Dev. Cell* **55**, 771-783.e5 (2020).
36. Kanke, M. *et al.* Single-Cell Analysis Reveals Unexpected Cellular Changes and Transposon Expression Signatures in the Colonic Epithelium of Treatment-Naïve Adult Crohn's Disease Patients. *Cell. Mol. Gastroenterol. Hepatol.* **13**, 1717–1740 (2022).
37. Linggi, B. *et al.* Meta-analysis of gene expression disease signatures in colonic biopsy tissue from patients with ulcerative colitis. *Sci. Rep.* **11**, 18243 (2021).

38. Patel, R. K. *et al.* Cyclone: an accessible pipeline to analyze, evaluate, and optimize multiparametric cytometry data. *Front. Immunol.* **14**, 1167241 (2023).
39. He, S. *et al.* High-plex imaging of RNA and proteins at subcellular resolution in fixed tissue by spatial molecular imaging. *Nat. Biotechnol.* (2022) doi:10.1038/s41587-022-01483-z.
40. Garrido-Trigo, A. *et al.* Macrophage and neutrophil heterogeneity at single-cell spatial resolution in human inflammatory bowel disease. *Nat. Commun.* **14**, 4506 (2023).
41. Subramanian, A. *et al.* Gene set enrichment analysis: A knowledge-based approach for interpreting genome-wide expression profiles. *Proc. Natl. Acad. Sci.* **102**, 15545–15550 (2005).
42. Mootha, V. K. *et al.* PGC-1α-responsive genes involved in oxidative phosphorylation are coordinately downregulated in human diabetes. *Nat. Genet.* **34**, 267–273 (2003).
43. Soler, D. *et al.* The Binding Specificity and Selective Antagonism of Vedolizumab, an Anti- 4 7 Integrin Therapeutic Antibody in Development for Inflammatory Bowel Diseases. *J. Pharmacol. Exp. Ther.* **330**, 864–875 (2009).
44. Becker, E. *et al.* Limited Dose-Dependent Effects of Vedolizumab on Various Leukocyte Subsets. *Clin. Transl. Gastroenterol.* **13**, e00494 (2022).
45. Lord, J. D. *et al.* Circulating integrin alpha4/beta7+ lymphocytes targeted by vedolizumab have a pro-inflammatory phenotype. *Clin. Immunol.* **193**, 24–32 (2018).
46. Habtezion, A., Nguyen, L. P., Hadeiba, H. & Butcher, E. C. Leukocyte Trafficking to the Small Intestine and Colon. *Gastroenterology* **150**, 340–354 (2016).
47. Alayo, Q. A. *et al.* Systematic Review With Meta-analysis: Safety and Effectiveness of Combining Biologics and Small Molecules in Inflammatory Bowel Disease. *Crohns Colitis 360* **4**, otac002 (2022).
48. Friedrich, M. *et al.* IL-1-driven stromal–neutrophil interactions define a subset of patients with inflammatory bowel disease that does not respond to therapies. *Nat. Med.* **27**, 1970–1981 (2021).
49. Ananthakrishnan, A. N. *et al.* Gut Microbiome Function Predicts Response to Anti-integrin Biologic Therapy in Inflammatory Bowel Diseases. *Cell Host Microbe* **21**, 603-610.e3 (2017).
50. Lee, J. W. J. *et al.* Multi-omics reveal microbial determinants impacting responses to biologic therapies in inflammatory bowel disease. *Cell Host Microbe* **29**, 1294-1304.e4 (2021).

51. Rusu, I. *et al.* Microbial signals, MyD88, and lymphotoxin drive TNF-independent intestinal epithelial tissue damage. *J. Clin. Invest.* **132**, e154993 (2022).
52. Combes, A. J. *et al.* Discovering dominant tumor immune archetypes in a pan-cancer census. *Cell* **185**, 184-203.e19 (2022).
53. Auwera, G. A. *et al.* From FastQ Data to High-Confidence Variant Calls: The Genome Analysis Toolkit Best Practices Pipeline. *Curr. Protoc. Bioinforma.* **43**, (2013).
54. Stuart, T. *et al.* Comprehensive Integration of Single-Cell Data. *Cell* **177**, 1888-1902.e21 (2019).
55. The 1000 Genomes Project Consortium *et al.* A global reference for human genetic variation. *Nature* **526**, 68–74 (2015).
56. Li, H. A statistical framework for SNP calling, mutation discovery, association mapping and population genetical parameter estimation from sequencing data. *Bioinformatics* **27**, 2987–2993 (2011).
57. Dominguez, D. *et al.* A high-resolution transcriptome map of cell cycle reveals novel connections between periodic genes and cancer. *Cell Res.* **26**, 946–962 (2016).
58. Hafemeister, C. & Satija, R. Normalization and variance stabilization of single-cell RNA-seq data using regularized negative binomial regression. *Genome Biol.* **20**, 296 (2019).
59. McGinnis, C. S., Murrow, L. M. & Gartner, Z. J. DoubletFinder: Doublet Detection in Single-Cell RNA Sequencing Data Using Artificial Nearest Neighbors. *Cell Syst.* **8**, 329-337.e4 (2019).
60. Korsunsky, I. *et al.* Fast, sensitive and accurate integration of single-cell data with Harmony. *Nat. Methods* **16**, 1289–1296 (2019).
61. The Tabula Sapiens Consortium & Quake, S. R. *The Tabula Sapiens: a multiple organ single cell transcriptomic atlas of humans*. http://biorxiv.org/lookup/doi/10.1101/2021.07.19.452956 (2021) doi:10.1101/2021.07.19.452956.
62. Kim, Y. J. *et al.* Tutorial: guidelines for manual cell type annotation of single-cell multi-omics datasets using interactive software. 2023.07.11.548639 Preprint at https://doi.org/10.1101/2023.07.11.548639 (2023).
63. Fawkner-Corbett, D. *et al.* Spatiotemporal analysis of human intestinal development at single-cell resolution. *Cell* (2021) doi:10.1016/j.cell.2020.12.016.

64. Wolf, F. A., Angerer, P. & Theis, F. J. SCANPY: large-scale single-cell gene expression data analysis. *Genome Biol.* **19**, 15 (2018).
65. Finak, G. *et al.* MAST: a flexible statistical framework for assessing transcriptional changes and characterizing heterogeneity in single-cell RNA sequencing data. *Genome Biol.* **16**, 278 (2015).
66. McGinnis, C. S. *et al.* MULTI-seq: sample multiplexing for single-cell RNA sequencing using lipid-tagged indices. *Nat. Methods* **16**, 619–626 (2019).
67. Ma, T. *et al.* HIV efficiently infects T cells from the endometrium and remodels them to promote systemic viral spread. *eLife* **9**, e55487 (2020).
68. Bodenmiller, B. *et al.* Multiplexed mass cytometry profiling of cellular states perturbed by small-molecule regulators. *Nat. Biotechnol.* **30**, 858–867 (2012).
69. Zunder, E. R. *et al.* Palladium-based mass tag cell barcoding with a doublet-filtering scheme and single-cell deconvolution algorithm. *Nat. Protoc.* **10**, 316–333 (2015).
70. Van Gassen, S. *et al.* FlowSOM: Using self-organizing maps for visualization and interpretation of cytometry data: FlowSOM. *Cytometry A* **87**, 636–645 (2015).
71. Geboes, K. A reproducible grading scale for histological assessment of inflammation in ulcerative colitis. *Gut* **47**, 404–409 (2000).
72. Baena-Del Valle, J. A. *et al.* Rapid Loss of RNA Detection by In Situ Hybridization in Stored Tissue Blocks and Preservation by Cold Storage of Unstained Slides. *Am. J. Clin. Pathol.* **148**, 398–415 (2017).
73. Black, S. *et al.* CODEX multiplexed tissue imaging with DNA-conjugated antibodies. *Nat. Protoc.* **16**, 3802–3835 (2021).
74. Patel, R. K. *et al.* Cyclone: an accessible pipeline to analyze, evaluate and optimize multiparametric cytometry data. 2023.03.08.531782 Preprint at https://doi.org/10.1101/2023.03.08.531782 (2023).
75. Palla, G. *et al.* Squidpy: a scalable framework for spatial omics analysis. *Nat. Methods* **19**, 171–178 (2022).
76. Liu, J. *et al.* Concordance of MERFISH Spatial Transcriptomics with Bulk and Single-cell RNA Sequencing. *bioRxiv* 2022.03.04.483068 (2022) doi:10.1101/2022.03.04.483068.
77. Love, M. I., Huber, W. & Anders, S. Moderated estimation of fold change and dispersion for RNA-seq data with DESeq2. *Genome Biol.* **15**, 550 (2014).

78. Virshup, I., Rybakov, S., Theis, F. J., Angerer, P. & Wolf, F. A. anndata: Annotated data. *bioRxiv* 2021.12.16.473007 (2021) doi:10.1101/2021.12.16.473007.

Acknowledgements

MGK was supported by a Career Development Award from the Crohn's and Colitis Foundation and NIH K08 DK123202. Michael George Kattah, M.D., Ph.D., holds a Career Award for Medical Scientists from the Burroughs Wellcome Fund. This work was also supported by funding from UCSF ImmunoX and the Kenneth Rainin Foundation. Schematics created with BioRender.com. This work was also supported by RRID:SCR_018206, DRC Center Grant NIH P30 DK063720, NIH S10 1S10OD018040-01 (CyTOF), and NIH S10 1S10OD025187-01 (MIBI). We would like to acknowledge Nanostring CosMx™ SMI Technology Access Program, Akoya Biosciences Spatial Tissue Exploration Program (STEP), ACDBio, Pantomics, and the Indica Labs HALO team. We thank James Lord for helpful discussion. We also acknowledge the Research Core of the UCSF Division of Hospital Medicine. We thank the study participants for contributing to this research.

Author Contributions Statement

Conceptualization: MGK; patient recruitment and sample collection: GL, S.Li, JLB, FBV, KB, NE, SL, DRS, JPT, UM, MGK; sample processing (scRNA-seq/CITE-seq, CyTOF): EM, GL, IR, JT, AS, WE, DYO, AJC, MGK; scRNA-seq/CITE-seq analysis: YJK, CA, AR, DYO, GKF, AP, MGK; CyTOF analysis: EM, GL, IR, RKP, JT, AS, GKF, AJC, MGK; MIBI and CODEX processing and analysis: EM, GL, IR, RKP, JLB, ST, MR, MN, SJC, GKF; 12-plex RNA-ISH: EM, IR, JLB, MN, SJC; CosMx: EM, YJK, GL, IR, LCD, JLB, MLL, EF, GKF, AP, AJC, MGK; data curation: EM, YJK, MLL, LCD, MGK; GSEA: EM; supervision: GKF, AP, AJC, MGK; funding acquisition: MGK; all authors contributed to manuscript preparation.

Competing Interests Statement

S. Lewin has received research support from Takeda. N. El-Nachef is a consultant for Ferring, Federation Bio Grant, and receives funding from Finch Therapeutics, Seres, Freenome, and Assembly Biosciences. U. Mahadevan serves as a consultant for Abbvie, BMS, Boeringher Ingelheim, Gilead, Janssen, Lilly, Pfizer, Prometheus biosciences, Protagonist, Rani Therapeutics, Surrozen, and Takeda. D. Oh has received research support from Merck, PACT Pharma, the Parker Institute for Cancer Immunotherapy, Poseida Therapeutics, TCR2 Therapeutics, Roche/Genentech, and Nutcracker Therapeutics, and

travel/accommodations from Roche/Genentech. The Combes lab has received research support from Eli Lilly and Genentech and A. Combes consults for Foundery Innovations. The Kattah lab receives research support from Eli Lilly. M. Kattah has consulted for Sonoma Biotherapeutics and Morphic Therapeutic.

Figure Legends

Figure 1. Schematic of study design and fidelity of cryopreserved compared to fresh biopsy processing for scRNA-seq. a, Schematic of study design. **b**, Schematic of Cryopreserved versus Fresh biopsy processing comparison. **c,d**, Representative UMAP visualization of 10,648 cells for two donors comparing (**c**) Cryopreserved versus Fresh biopsies and (**d**) coarse cell subset annotations. **e**, Cell frequency as a percent of total for coarse cell subsets for two donors comparing Cryopreserved versus Fresh biopsies (mean ± standard error of the mean (SEM); n=number of patients; each dot represents one patient sample; multiple Mann-Whitney tests with FDR correction; q<0.1 threshold for discovery, only significant differences are indicated). f, Heatmap of expression z-scores for differentially expressed (DE) genes with log_2 fold-change (log_2fc) >0.4 or <-0.4 and Bonferroni p-value <0.1 comparing Cryopreserved (Up/Down) relative to Fresh biopsies for two study subjects ID1 and ID2 identified by MAST analysis. Only significant differences are shown. MNP-mononuclear phagocyte: Treg-regulatory T cell; NK-natural killer; ILC-innate lymphoid cell.

Figure 2. scRNA-seq of peripheral blood leukocytes (PBLs) reveals correlation of VDZ with DE genes, but not circulating leukocyte subset frequency. a, Schematic of PBL scRNA-seq. **b-d**, UMAP visualization of pooled multiplex scRNA-seq for 20,130 PBLs from HC (n=4), UC (n=3), and UC-VDZ (n=4) patients highlighting (**b**) fine cell annotations, (**c**) patient identity, and (**d**) disease and treatment status. e, Cell frequency as a percent of total cells per study subject stratified by disease and treatment status (mean ± SEM; n=number of patients; each dot represents one patient sample; multiple one-way ANOVA Kruskal-Wallis test with FDR correction; q<0.1 threshold for discovery, only significant differences are indicated). f, Heatmap of expression z-scores for scRNA-seq DE genes for all PBLs with log_2fc >1 or <-1 and Bonferroni-corrected p-value<0.1 comparing UC (Up/Down) relative to HC, and UC-VDZ (Up/Down) relative to UC identified by MAST analysis. g, Number of scRNA-seq DE genes in the indicated PBL subsets with log_2fc >2 or <-2 in UC relative to HC and UC-VDZ relative to UC identified by MAST analysis. h, scRNA-seq DE genes in the indicated PBL subsets with log_2fc >1.5 or <-1 in UC versus HC, and an inverse log_2fc for UC-VDZ versus UC log_2fc <-0.5 or >0.5, respectively identified by MAST analysis. For panels f,h,; ribosomal and

mitochondrial genes are not displayed. NOS-not otherwise specified; mDC-myeloid dendritic cell; ASDC-AXL$^+$ SIGLEC6$^+$ myeloid DC; pDC-plasmacytoid DC; MAIT- mucosal-associated invariant T.

Figure 3. scRNA-seq and CITE-seq of mucosal biopsies highlighted multiple immune and non-immune subsets correlating with inflammatory severity, disease status, and VDZ treatment. a, Schematic of scRNA-seq and CITE-seq of mucosal biopsies. **b-f,** UMAP visualization of 93,900 cells from HC (n=4), UC (n=4), and UC-VDZ (n=4) patients highlighting (**b**) fine cell subset annotations (**c**) representative CITE-seq CD103 antibody-derived tag (ADT), (**d**) patient identity, (**e**) endoscopic severity scores, and (**f**) disease and treatment status. **g,h,** Cell frequency for the indicated fine cell subset, expressed as a percent of total cells per study subject, stratified by (**g**) endoscopic severity and (**h**) disease and treatment status (mean ± SEM; n=number of patients; each dot represents one biopsy location, up to two locations were biopsied per patient; multiple one-way ANOVA Kruskal-Wallis tests with FDR correction; q<0.1 threshold for discovery; select subsets are shown with exact p-value and q-value; individual inter-column q-values are displayed only for cell subsets with overall q<0.1, an additional nested one-way ANOVA test was performed treating biopsies as replicates, with unadjusted p<0.05 as an additional threshold for discovery). NOS-not otherwise specified.

Figure 4. Unsupervised and supervised CyTOF analysis identifies significant increase in circulating $\alpha_4\beta_7^+$ DCs in UC-VDZ patients. a, Schematic of CyTOF on blood and biopsy samples. **b-c,** UMAP visualization of the indicated samples (60,000 out of 684,249 live cell events displayed for biopsies) highlighting (**b**) annotated clusters, and (**c**) disease and treatment status. **d-i,** Cell frequency of the indicated supervised subset analysis among conditions in biopsies expressed as $\log_2$ (cell freq/median) (mean ± SEM; n=number of patients; each dot represents one patient sample; multiple one-way ANOVA Kruskal-Wallis test with FDR correction; q<0.1 threshold for discovery; individual inter-column q-values are displayed only for cell subsets with overall FDR corrected q<0.1); the legend for (**d-i**) is shown in (**i**). **j**, Heatmap of biopsy/blood ratio of $\alpha_4\beta_7^+$ cells for each cell subset by patient (hierarchically clustered by Euclidian distance, average linkage). **k,l,** Percentage of $\alpha_4\beta_7^+$ cells in each defined cell subset per condition for blood and biopsy samples, respectively (mean ± SEM; n=number of patients; each dot represents one patient sample; two-way ANOVA comparing HC vs UC-VDZ and UC vs UC-VDZ with FDR correction; q<0.1 threshold for discovery; *q<0.05; **q<0.01; ***q<0.001; and ****q<0.0001 (exact q-value are reported in Source Data); only significant

differences are indicated). Class mono-classical monocyte; Nonclass mono-nonclassical monocyte; mDC-cDC1,cDC2,cDC2b; N/A-Not Applicable.

Figure 5. MIBI and CODEX spatial proteomics using FFPE tissue identifies distinct phenotypes in mucosal biopsies of UC-VDZ patients. a, Schematic of MIBI workflow and customized antibody panel. **b,c,** MIBI images representative of 32 FOVs for (**b**) nuclear DNA, indicated major cell lineage markers, and 5 color overlay, and (**c**) 39-plex overlay, selected channels, and related spatial scatter plots for coarse annotation of the indicated cell subsets. **d,** Cell frequency as a percent of total cells detected by MIBI for the indicated cell subset. **e,** Schematic of CODEX workflow and antibody panel. **f,** UMAP visualization of 68,804 captured cells (50,000 cells displayed) highlighting annotated clusters. **g,** Marker similarity matrix among 23 selected markers (Pearson correlation). **h,** CODEX images representative of 15 cores, phenotype identification highlighting indicated markers and major phenotype colocalization. **i,j,** Cell frequency as a percent of total cells detected by CODEX for the indicated cell subsets. For panels (**d**),(**i**),(**j**), mean ± SEM; n=number of patients; each dot represents one FOV for MIBI or one core for CODEX; multiple one-way ANOVA Kruskal-Wallis test with FDR correction; q<0.1 threshold for discovery; ns-not significant.

Figure 6. MNP and fibroblast subsets trend toward spatial proximity in UC patients compared to HC. a,b, Spatial scatter plots of the indicated cell subsets and nearest-neighbor (NN) analysis for (**a**) MIBI (representative of 29 FOVs) and (**b**) CODEX (representative of 12 cores); n=number of patients; each dot represents one FOV for MIBI or one core for CODEX; one-way ANOVA Kruskal-Wallis tests with FDR correction; q<0.1 threshold for discovery)**. c,** Schematic of 960-plex RNA-ISH of FFPE TMA. **d,** CosMx images representative of 17 FOVs, cell segmentation and probe signal for the indicated cells and genes. **e,** UMAP visualization of 960-plex CosMx for 48,783 cells from HC (n=4), UC (n=3), and UC-VDZ (n=3) patients highlighting the indicated cell subsets. **f,g** Representative spatial scatter plots highlighting the indicated cell subsets (spatial scatter plots were representative of 17 FOVs); the legend for (**f**) is shown in (**e**). **h,** Z-score of activated fibroblast and activated MNP neighborhood enrichment (n=number of patients; each dot represents one FOV; one-way ANOVA Kruskal-Wallis tests with FDR correction; q<0.1 threshold for discovery; ns-not significant). For panels (**a,b**) and (**h**) box and whisker plots, the band indicates the median, the box indicates the first and third quartiles, and the whiskers indicate minimum and maximum, all points are shown.

Figure 7. CosMx spatial transcriptomics of archived FFPE specimens with single-cell resolution

identified tissue signatures of VDZ response and non-response prior to therapy in activated MNP, fibroblast, and IEC crypt base subsets. a, Schematic of retrospective, longitudinal analysis of archived FFPE specimens using 1000-plex CosMx spatial transcriptomics of 126,368 cells from 73 FOVs; n of schematic applies to left panels in (**b-d)**. **b,c** Cell frequencies of indicated subsets comparing (left) HC and pre-treatment samples (pre-VDZ) (Mann Whitney, two-tailed), as well as (middle, right) pre-VDZ and post-VDZ treatment for the indicated subsets for both responders (R) and non-responders (NR), only patients with matching biopsies pre- and post-VDZ are shown (Mann Whitney, two-tailed of Δ post VDZ - pre VDZ for R and NR). **d,** Z-score of activated fibroblast and activated MNP neighborhood enrichment comparing (left) HC and pre-VDZ (Mann Whitney, two-tailed) and (right) one-way ANOVA Kruskal-Wallis test with Dunn's multiple comparison test. **e,** Dot plot representation of a subset of genes from pseudobulk DE gene analysis for the indicated subsets. **f,h,** Representative spatial cell scatter plots highlighting the relevant cell subsets relatively increased in (**f**) VDZ R or (**h**) VDZ NR**. g,i,** Representative spatial transcript scatter plots highlighting a subset of genes relatively increased in (**g**) VDZ R and (**i**) VDZ NR. (**f-i**) Spatial scatter plots were representative of 73 FOVs. For panels (**b-d**), mean ± SEM; n=number of patients; each dot represents averaged FOV per patient. R-responder; NR-non-responder.

Figure 8. Gene set enrichment analysis (GSEA) of an external, publicly-available, bulk transcriptomic dataset (GSE73661) using cell subset and spatial transcriptomic signatures associated with response and non-response to VDZ. a,b, Normalized Enrichment Scores (NES) in bulk tissue transcriptomic data comparing (**a**) pre- and post-treatment samples for VDZ responders (R) and non-responders (NR), (**b**) pre-VDZ R vs NR (red bars FDR < 0.1, gray bars FDR > 0.1). **c,** Leading edge analysis of significantly enriched gene sets. **d-g,** GSEA of VDZ response and non-response spatial signatures in external cohort of patients (**d**) pre-VDZ and (**f**) pre-IFX. **e,g**, Subset of genes comprising the leading edge of the NES and FDR q-values in (**e**) pre-VDZ and (**g**) pre-IFX patients, respectively. IFX, infliximab.

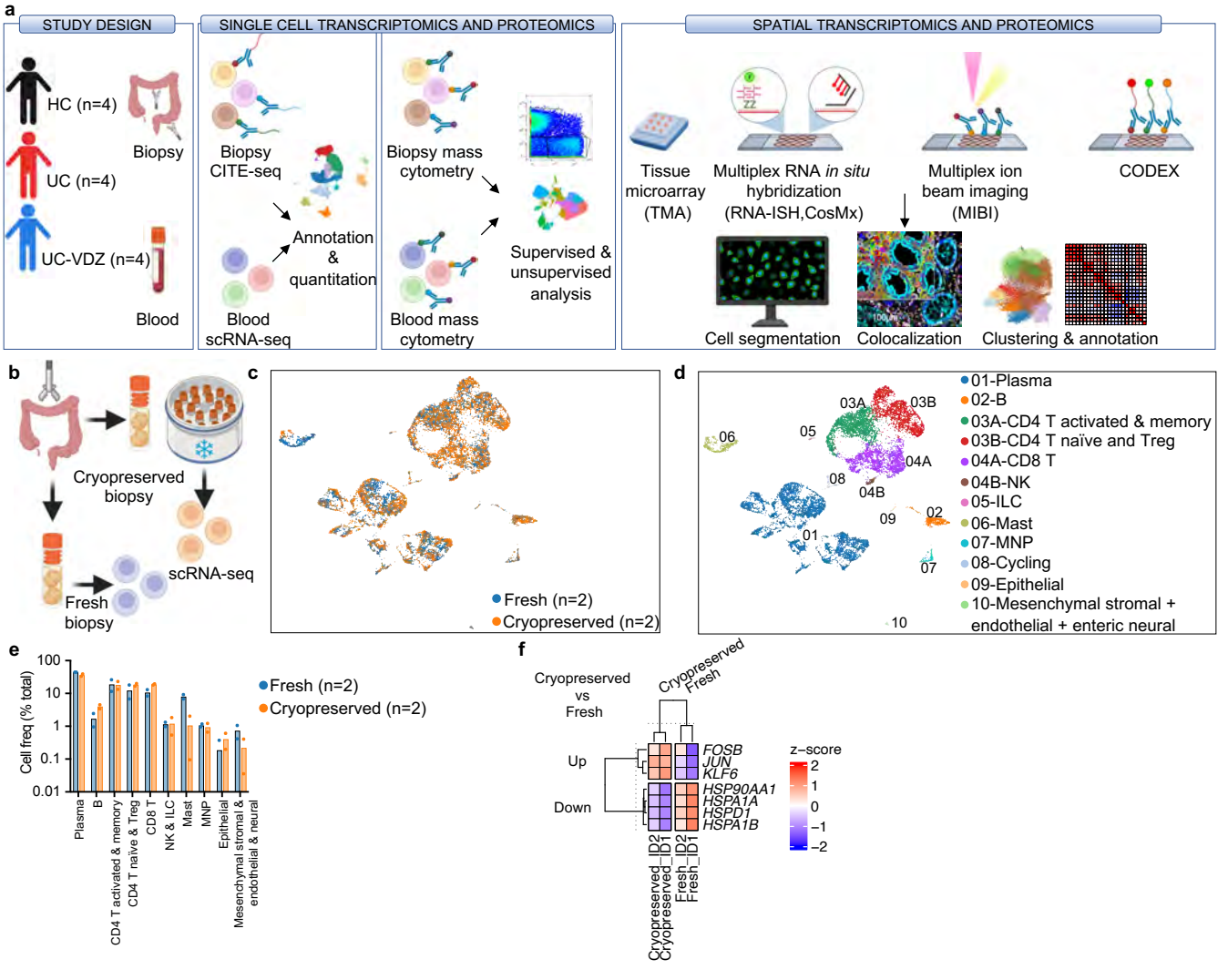
a
STUDY DESIGN
HC (n=4)
UC (n=4)
UC-VDZ (n=4)
Biopsy
Blood
SINGLE CELL TRANSCRIPTOMICS AND PROTEOMICS
Biopsy CITE-seq
Annotation & quantitation
Blood scRNA-seq
Biopsy mass cytometry
Blood mass cytometry
Supervised & unsupervised analysis
SPATIAL TRANSCRIPTOMICS AND PROTEOMICS
Tissue microarray (TMA)
Multiplex RNA in situ hybridization (RNA-ISH,CosMx)
Multiplex ion beam imaging (MIBI)
CODEX
Cell segmentation
Colocalization
Clustering & annotation
b
Cryopreserved biopsy
scRNA-seq
Fresh biopsy
c
Fresh (n=2)
Cryopreserved (n=2)
d
01-Plasma
02-B
03A-CD4 T activated & memory
03B-CD4 T naïve and Treg
04A-CD8 T
04B-NK
05-ILC
06-Mast
07-MNP
08-Cycling
09-Epithelial
10-Mesenchymal stromal + endothelial + enteric neural
e
Cell freq (% total)
Fresh (n=2)
Cryopreserved (n=2)
Plasma
B
CD4 T activated & memory
CD4 T naïve & Treg
CD8 T
NK & ILC
Mast
MNP
Epithelial
Mesenchymal stromal & endothelial & neural
f
Cryopreserved vs Fresh
Up
Down
FOSB
JUN
KLF6
HSP90AA1
HSPA1A
HSPD1
HSPA1B
z-score

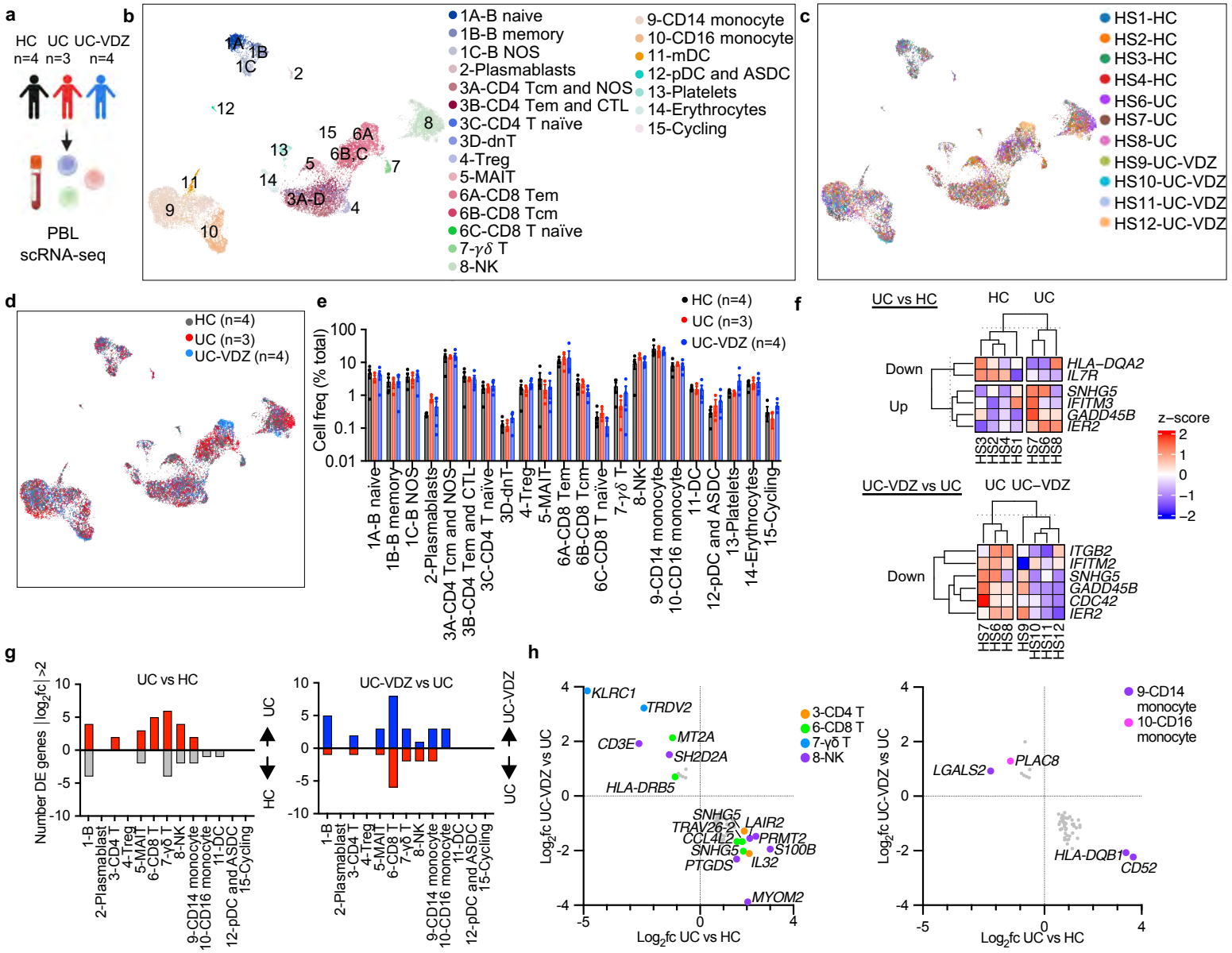
a
HC n=4
UC n=3
UC-VDZ n=4
PBL
scRNA-seq
b
1A-B naive
1B-B memory
1C-B NOS
2-Plasmablasts
3A-CD4 Tcm and NOS
3B-CD4 Tem and CTL
3C-CD4 T naïve
3D-dnT
4-Treg
5-MAIT
6A-CD8 Tem
6B-CD8 Tcm
6C-CD8 T naïve
7-γδ T
8-NK
9-CD14 monocyte
10-CD16 monocyte
11-mDC
12-pDC and ASDC
13-Platelets
14-Erythrocytes
15-Cycling
c
HS1-HC
HS2-HC
HS3-HC
HS4-HC
HS6-UC
HS7-UC
HS8-UC
HS9-UC-VDZ
HS10-UC-VDZ
HS11-UC-VDZ
HS12-UC-VDZ
d
HC (n=4)
UC (n=3)
UC-VDZ (n=4)
e
Cell freq (% total)
f
UC vs HC
Down
Up
HLA-DQA2
IL7R
SNHG5
IFITM3
GADD45B
IER2
z-score
UC-VDZ vs UC
ITGB2
IFITM2
SNHG5
GADD45B
CDC42
IER2
g
UC vs HC
UC-VDZ vs UC
Number DE genes |log2fc| >2
h
Log2fc UC-VDZ vs UC
Log2fc UC vs HC
KLRC1
TRDV2
CD3E
MT2A
SH2D2A
HLA-DRB5
SNHG5
TRAV26-2
LAIR2
CCL4L2
PRMT2
SNHG5
S100B
PTGDS
IL32
MYOM2
3-CD4 T
6-CD8 T
7-γδ T
8-NK
9-CD14 monocyte
10-CD16 monocyte
LGALS2
PLAC8
HLA-DQB1
CD52

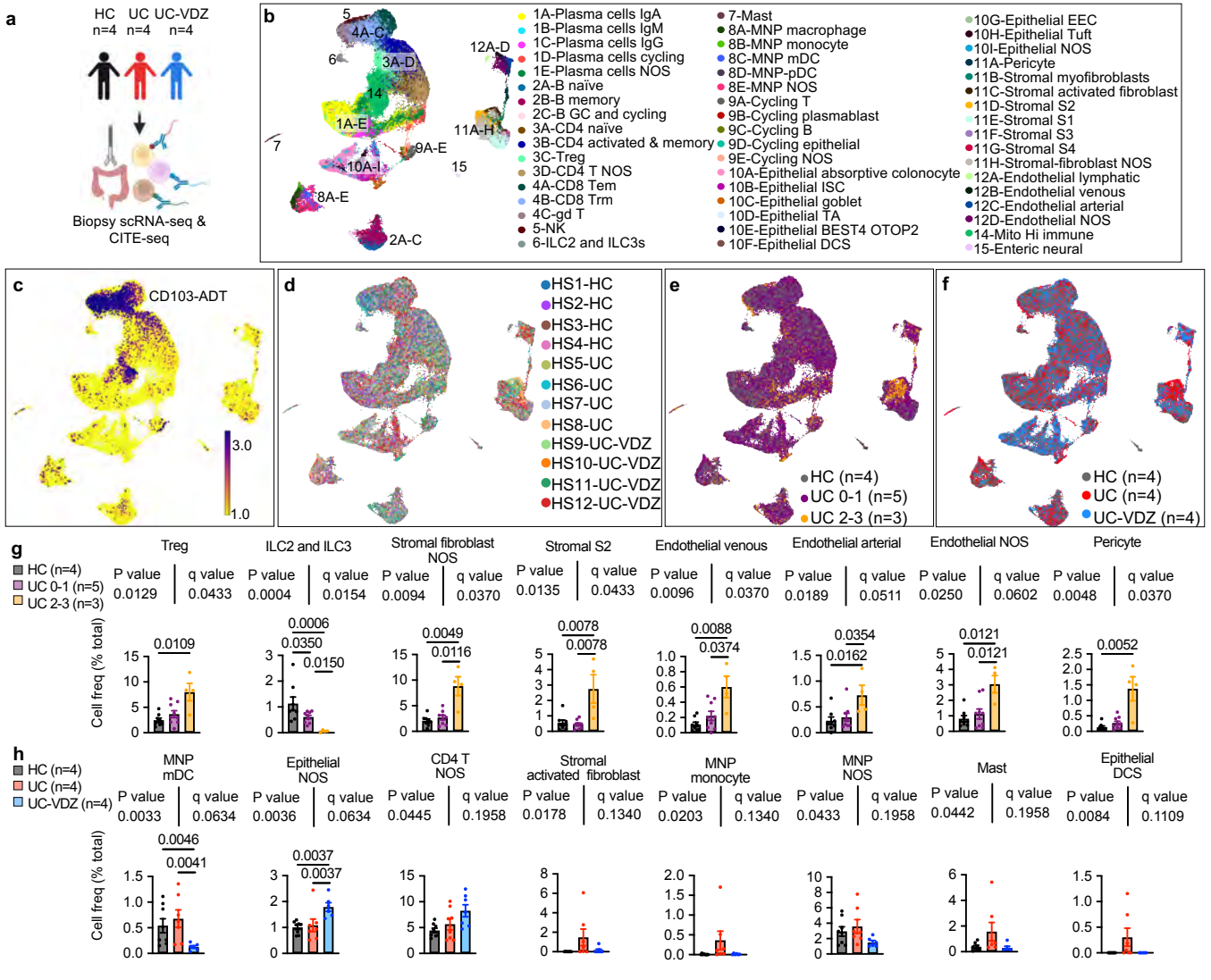
a
HC n=4
UC n=4
UC-VDZ n=4
Biopsy scRNA-seq & CITE-seq
b
1A-Plasma cells IgA
1B-Plasma cells IgM
1C-Plasma cells IgG
1D-Plasma cells cycling
1E-Plasma cells NOS
2A-B naïve
2B-B memory
2C-B GC and cycling
3A-CD4 naïve
3B-CD4 activated & memory
3C-Treg
3D-CD4 T NOS
4A-CD8 Tem
4B-CD8 Trm
4C-gd T
5-NK
6-ILC2 and ILC3s
7-Mast
8A-MNP macrophage
8B-MNP monocyte
8C-MNP mDC
8D-MNP-pDC
8E-MNP NOS
9A-Cycling T
9B-Cycling plasmablast
9C-Cycling B
9D-Cycling epithelial
9E-Cycling NOS
10A-Epithelial absorptive colonocyte
10B-Epithelial ISC
10C-Epithelial goblet
10D-Epithelial TA
10E-Epithelial BEST4 OTOP2
10F-Epithelial DCS
10G-Epithelial EEC
10H-Epithelial Tuft
10I-Epithelial NOS
11A-Pericyte
11B-Stromal myofibroblasts
11C-Stromal activated fibroblast
11D-Stromal S2
11E-Stromal S1
11F-Stromal S3
11G-Stromal S4
11H-Stromal-fibroblast NOS
12A-Endothelial lymphatic
12B-Endothelial venous
12C-Endothelial arterial
12D-Endothelial NOS
14-Mito Hi immune
15-Enteric neural
c
CD103-ADT
3.0
1.0
d
HS1-HC
HS2-HC
HS3-HC
HS4-HC
HS5-UC
HS6-UC
HS7-UC
HS8-UC
HS9-UC-VDZ
HS10-UC-VDZ
HS11-UC-VDZ
HS12-UC-VDZ
e
HC (n=4)
UC 0-1 (n=5)
UC 2-3 (n=3)
f
HC (n=4)
UC (n=4)
UC-VDZ (n=4)
g
HC (n=4)
UC 0-1 (n=5)
UC 2-3 (n=3)
Treg P value 0.0129 q value 0.0433
ILC2 and ILC3 P value 0.0004 q value 0.0154
Stromal fibroblast NOS P value 0.0094 q value 0.0370
Stromal S2 P value 0.0135 q value 0.0433
Endothelial venous P value 0.0096 q value 0.0370
Endothelial arterial P value 0.0189 q value 0.0511
Endothelial NOS P value 0.0250 q value 0.0602
Pericyte P value 0.0048 q value 0.0370
Cell freq (% total)
h
HC (n=4)
UC (n=4)
UC-VDZ (n=4)
MNP mDC P value 0.0033 q value 0.0634
Epithelial NOS P value 0.0036 q value 0.0634
CD4 T NOS P value 0.0445 q value 0.1958
Stromal activated fibroblast P value 0.0178 q value 0.1340
MNP monocyte P value 0.0203 q value 0.1340
MNP NOS P value 0.0433 q value 0.1958
Mast P value 0.0442 q value 0.1958
Epithelial DCS P value 0.0084 q value 0.1109
Cell freq (% total)

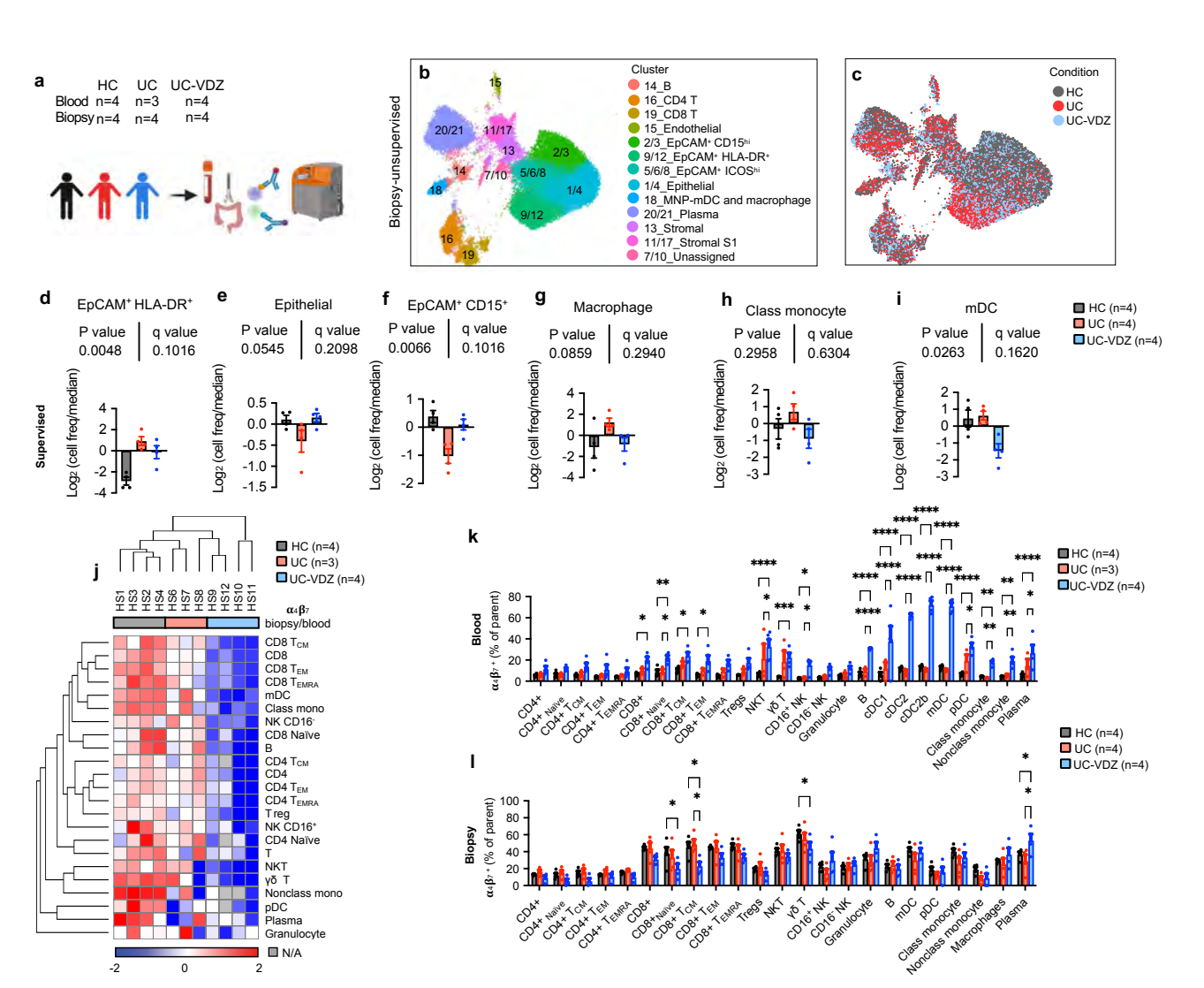
a
HC UC UC-VDZ
Blood n=4 n=3 n=4
Biopsy n=4 n=4 n=4
b
Biopsy-unsupervised
Cluster
14_B
16_CD4 T
19_CD8 T
15_Endothelial
2/3_EpCAM+ CD15hi
9/12_EpCAM+ HLA-DR+
5/6/8_EpCAM+ ICOShi
1/4_Epithelial
18_MNP-mDC and macrophage
20/21_Plasma
13_Stromal
11/17_Stromal S1
7/10_Unassigned
c
Condition
HC
UC
UC-VDZ
d
EpCAM+ HLA-DR+
P value 0.0048
q value 0.1016
e
Epithelial
P value 0.0545
q value 0.2098
f
EpCAM+ CD15+
P value 0.0066
q value 0.1016
g
Macrophage
P value 0.0859
q value 0.2940
h
Class monocyte
P value 0.2958
q value 0.6304
i
mDC
P value 0.0263
q value 0.1620
HC (n=4)
UC (n=4)
UC-VDZ (n=4)
Supervised
Log2 (cell freq/median)
j
HC (n=4)
UC (n=3)
UC-VDZ (n=4)
HS1 HS3 HS2 HS4 HS6 HS7 HS8 HS9 HS12 HS10 HS11
α4β7
biopsy/blood
CD8 TCM
CD8
CD8 TEM
CD8 TEMRA
mDC
Class mono
NK CD16-
CD8 Naïve
B
CD4 TCM
CD4
CD4 TEM
CD4 TEMRA
T reg
NK CD16+
CD4 Naïve
T
NKT
γδ T
Nonclass mono
pDC
Plasma
Granulocyte
N/A
-2 0 2
k
Blood
α4β7+ (% of parent)
HC (n=4)
UC (n=3)
UC-VDZ (n=4)
CD4+
CD4+ Naive
CD4+ TCM
CD4+ TEM
CD4+ TEMRA
CD8+
CD8+ Naive
CD8+ TCM
CD8+ TEM
CD8+ TEMRA
Tregs
NKT
γδ T
CD16+ NK
CD16- NK
Granulocyte
B
cDC1
cDC2
cDC2b
mDC
pDC
Class monocyte
Nonclass monocyte
Plasma
l
Biopsy
α4β7+ (% of parent)
HC (n=4)
UC (n=4)
UC-VDZ (n=4)
CD4+
CD4+ Naive
CD4+ TCM
CD4+ TEM
CD4+ TEMRA
CD8+
CD8+ Naive
CD8+ TCM
CD8+ TEM
CD8+ TEMRA
Tregs
NKT
γδ T
CD16+ NK
CD16- NK
Granulocyte
B
mDC
pDC
Class monocyte
Nonclass monocyte
Macrophages
Plasma

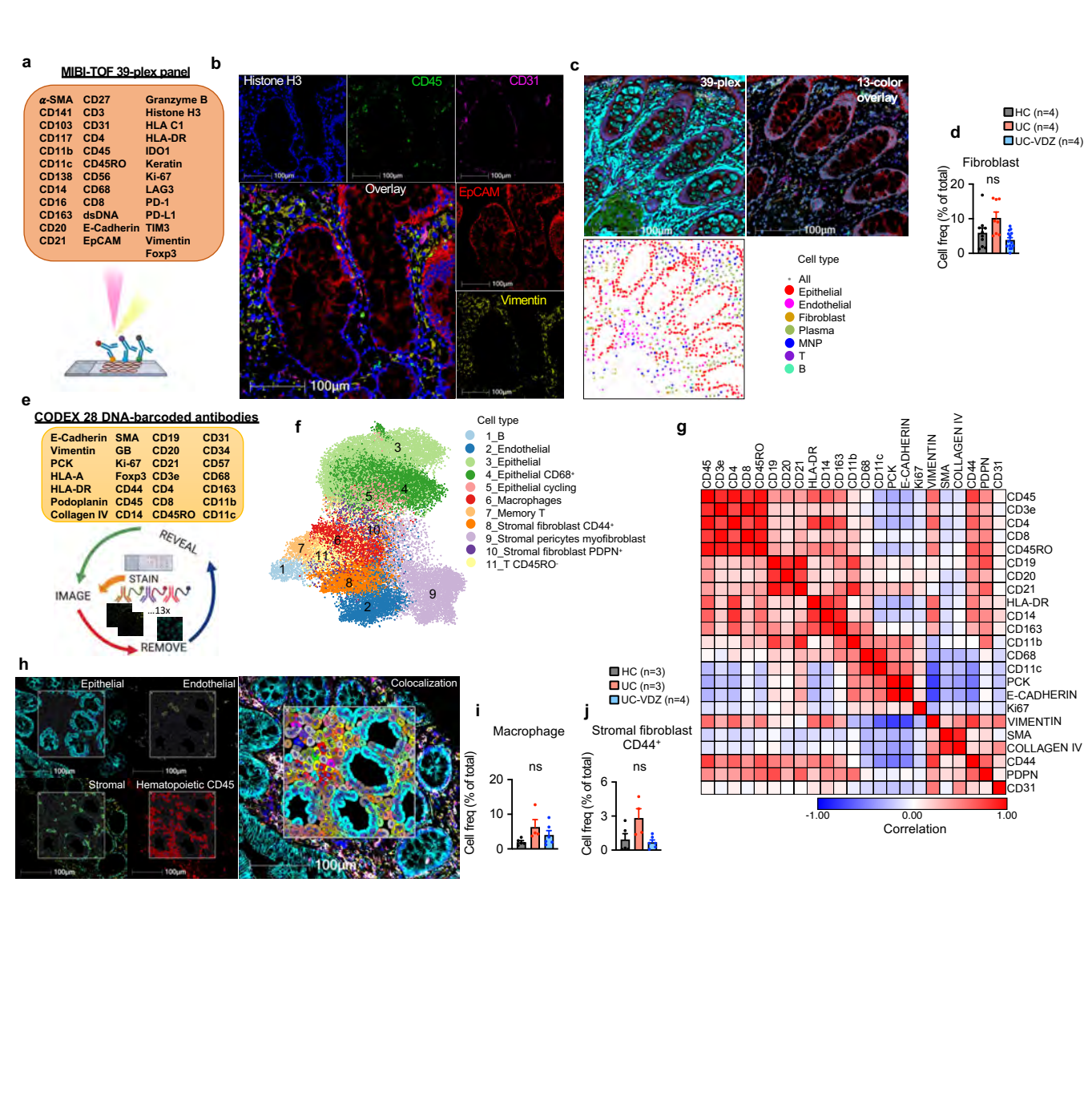
a
MIBI-TOF 39-plex panel
α-SMA CD27 Granzyme B
CD141 CD3 Histone H3
CD103 CD31 HLA C1
CD117 CD4 HLA-DR
CD11b CD45 IDO1
CD11c CD45RO Keratin
CD138 CD56 Ki-67
CD14 CD68 LAG3
CD16 CD8 PD-1
CD163 dsDNA PD-L1
CD20 E-Cadherin TIM3
CD21 EpCAM Vimentin
Foxp3
b
Histone H3
CD45
CD31
Overlay
EpCAM
Vimentin
100µm
c
39-plex
13-color overlay
Cell type
All
Epithelial
Endothelial
Fibroblast
Plasma
MNP
T
B
d
HC (n=4)
UC (n=4)
UC-VDZ (n=4)
Fibroblast
ns
Cell freq (% of total)
e
CODEX 28 DNA-barcoded antibodies
E-Cadherin SMA CD19 CD31
Vimentin GB CD20 CD34
PCK Ki-67 CD21 CD57
HLA-A Foxp3 CD3e CD68
HLA-DR CD44 CD4 CD163
Podoplanin CD45 CD8 CD11b
Collagen IV CD14 CD45RO CD11c
REVEAL
STAIN
IMAGE
...13x
REMOVE
f
Cell type
1_B
2_Endothelial
3_Epithelial
4_Epithelial CD68+
5_Epithelial cycling
6_Macrophages
7_Memory T
8_Stromal fibroblast CD44+
9_Stromal pericytes myofibroblast
10_Stromal fibroblast PDPN+
11_T CD45RO-
g
CD45 CD3e CD4 CD8 CD45RO CD19 CD20 CD21 HLA-DR CD14 CD163 CD11b CD68 CD11c PCK E-CADHERIN Ki67 VIMENTIN SMA COLLAGEN IV CD44 PDPN CD31
-1.00
0.00
1.00
Correlation
h
Epithelial
Endothelial
Stromal
Hematopoietic CD45
Colocalization
100µm
i
Macrophage
ns
Cell freq (% of total)
j
Stromal fibroblast CD44+
ns
Cell freq (% of total)
HC (n=3)
UC (n=3)
UC-VDZ (n=4)

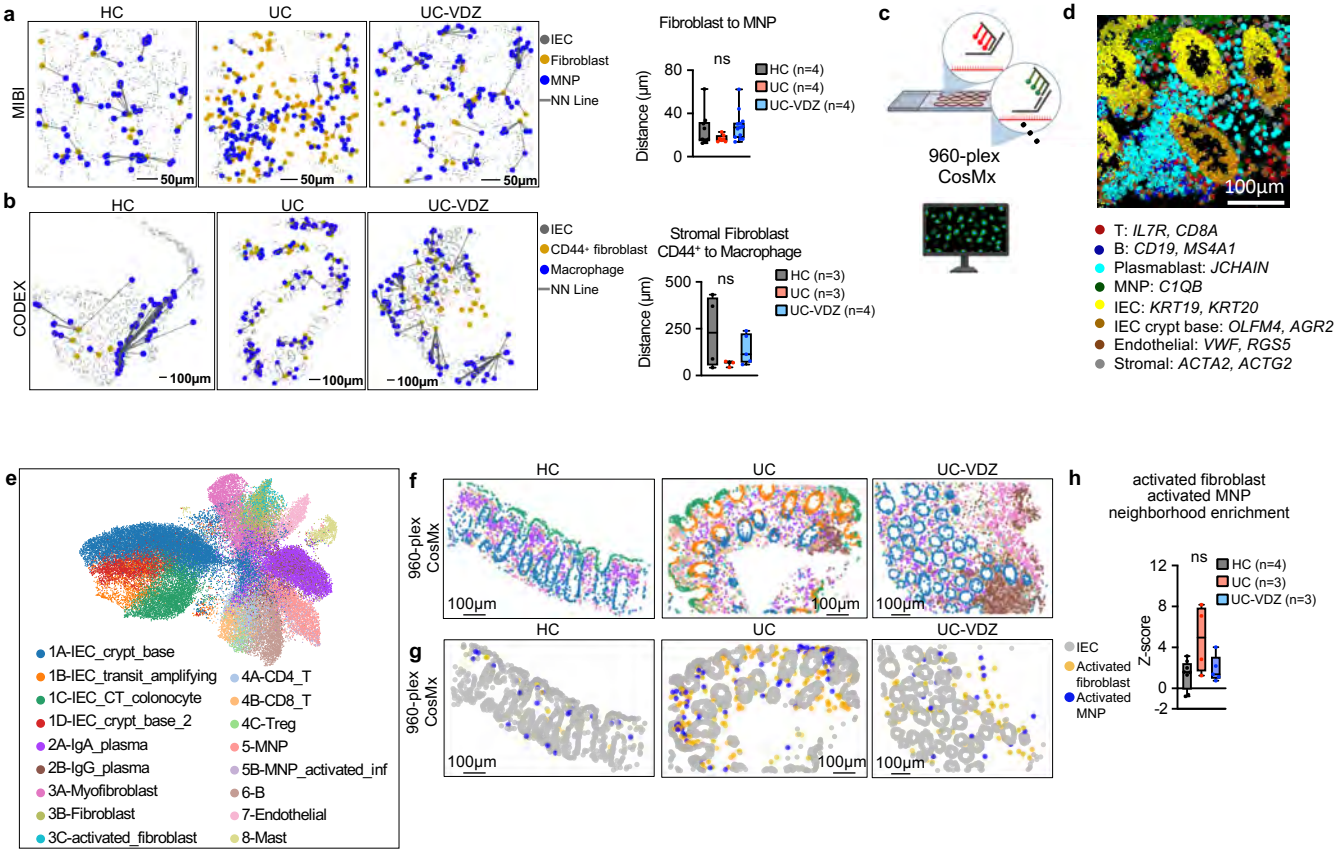
a
HC
UC
UC-VDZ
MIBI
50µm
IEC
Fibroblast
MNP
NN Line
Fibroblast to MNP
ns
Distance (µm)
80
40
0
HC (n=4)
UC (n=4)
UC-VDZ (n=4)
b
CODEX
100µm
CD44+ fibroblast
Macrophage
Stromal Fibroblast
CD44+ to Macrophage
500
250
HC (n=3)
UC (n=3)
UC-VDZ (n=4)
c
960-plex
CosMx
d
T: IL7R, CD8A
B: CD19, MS4A1
Plasmablast: JCHAIN
MNP: C1QB
IEC: KRT19, KRT20
IEC crypt base: OLFM4, AGR2
Endothelial: VWF, RGS5
Stromal: ACTA2, ACTG2
e
1A-IEC_crypt_base
1B-IEC_transit_amplifying
1C-IEC_CT_colonocyte
1D-IEC_crypt_base_2
2A-IgA_plasma
2B-IgG_plasma
3A-Myofibroblast
3B-Fibroblast
3C-activated_fibroblast
4A-CD4_T
4B-CD8_T
4C-Treg
5-MNP
5B-MNP_activated_inf
6-B
7-Endothelial
8-Mast
f
960-plex
CosMx
g
h
activated fibroblast
activated MNP
neighborhood enrichment
Z-score
12
8
4
0
-2
IEC
Activated fibroblast
Activated MNP

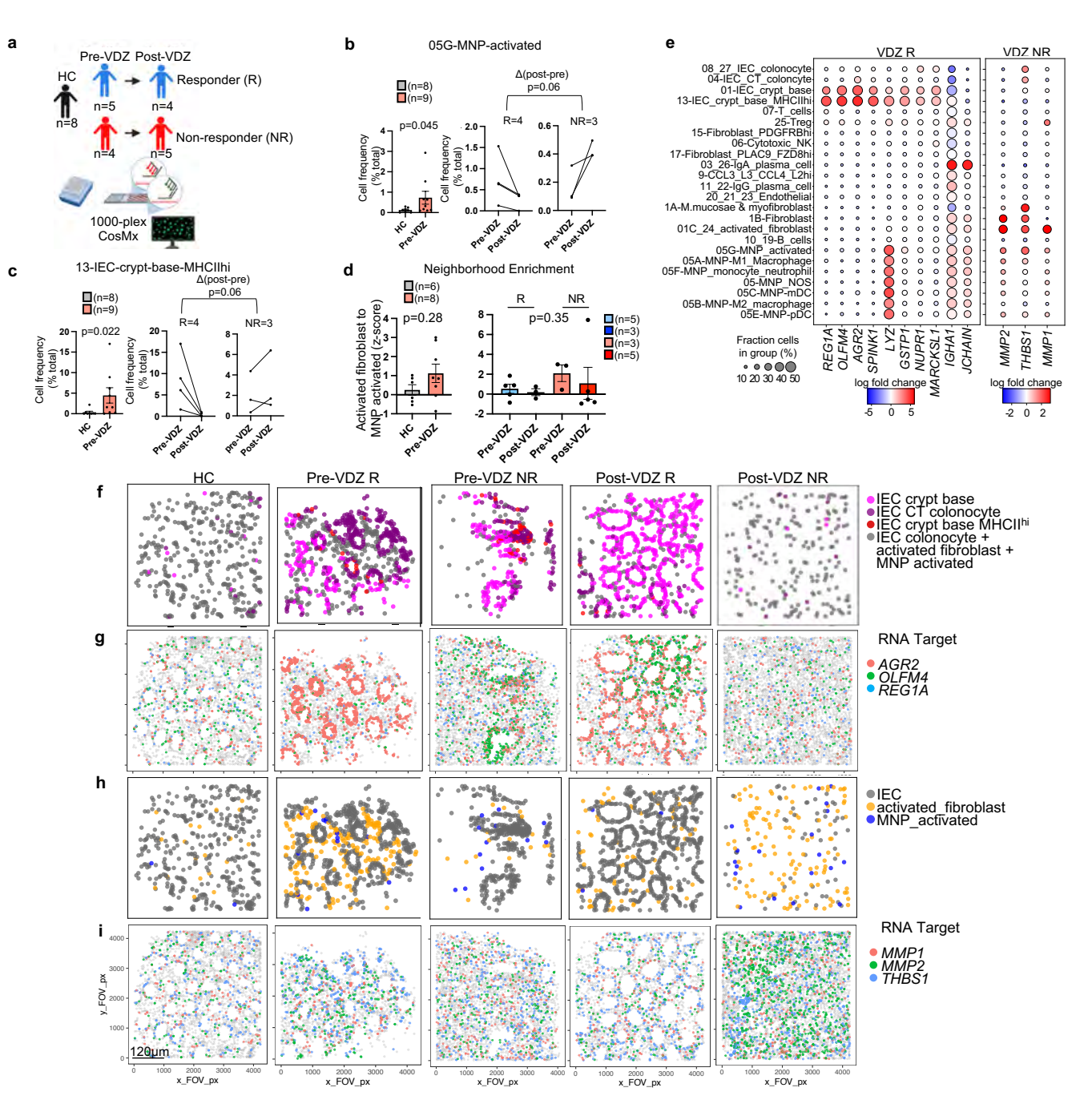
a
Pre-VDZ Post-VDZ
HC
Responder (R)
n=5
n=4
n=8
Non-responder (NR)
n=4
n=5
1000-plex
CosMx
b
05G-MNP-activated
(n=8)
(n=9)
p=0.045
Cell frequency (% total)
HC
Pre-VDZ
Δ(post-pre)
p=0.06
R=4
NR=3
Pre-VDZ
Post-VDZ
c
13-IEC-crypt-base-MHCIIhi
(n=8)
(n=9)
p=0.022
Cell frequency (% total)
HC
Pre-VDZ
Δ(post-pre)
p=0.06
R=4
NR=3
Pre-VDZ
Post-VDZ
d
Neighborhood Enrichment
(n=6)
(n=8)
p=0.28
Activated fibroblast to MNP activated (z-score)
HC
Pre-VDZ
R
NR
p=0.35
(n=5)
(n=3)
(n=3)
(n=5)
Pre-VDZ
Post-VDZ
e
VDZ R
VDZ NR
08_27_IEC_colonocyte
04-IEC_CT_colonocyte
01-IEC_crypt_base
13-IEC_crypt_base_MHCIIhi
07-T_cells
25-Treg
15-Fibroblast_PDGFRBhi
06-Cytotoxic_NK
17-Fibroblast_PLAC9_FZD8hi
03_26-IgA_plasma_cell
9-CCL3_L3_CCL4_L2hi
11_22-IgG_plasma_cell
20_21_23_Endothelial
1A-M.mucosae & myofibroblast
1B-Fibroblast
01C_24_activated_fibroblast
10_19-B_cells
05G-MNP_activated
05A-MNP-M1_Macrophage
05F-MNP_monocyte_neutrophil
05-MNP_NOS
05C-MNP-mDC
05B-MNP-M2_macrophage
05E-MNP-pDC
REG1A
OLFM4
AGR2
SPINK1
LYZ
GSTP1
NUPR1
MARCKSL1
IGHA1
JCHAIN
MMP2
THBS1
MMP1
Fraction cells in group (%)
10 20 30 40 50
log fold change
-5 0 5
log fold change
-2 0 2
f
HC
Pre-VDZ R
Pre-VDZ NR
Post-VDZ R
Post-VDZ NR
IEC crypt base
IEC CT colonocyte
IEC crypt base MHCIIhi
IEC colonocyte + activated fibroblast + MNP activated
g
RNA Target
AGR2
OLFM4
REG1A
h
IEC
activated_fibroblast
MNP_activated
i
RNA Target
MMP1
MMP2
THBS1
y_FOV_px
x_FOV_px
120µm

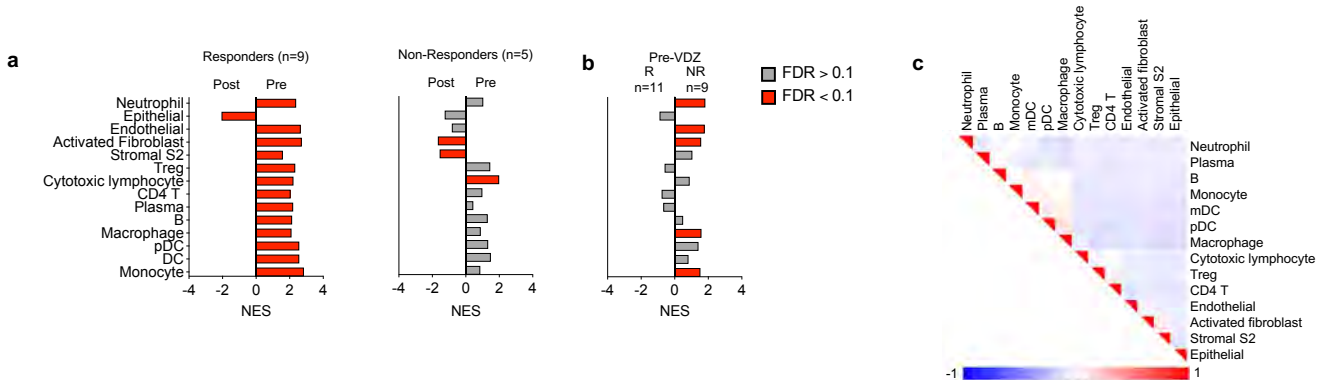

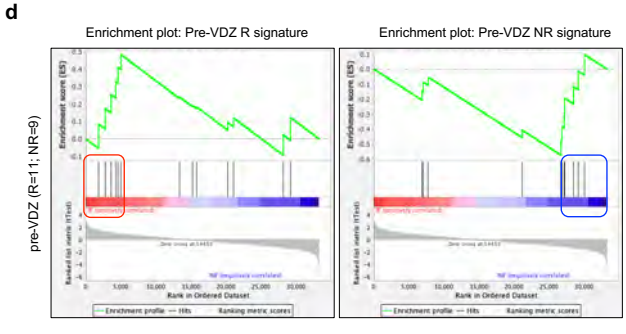

e

Leading edge genes in pre-VDZ R/NR

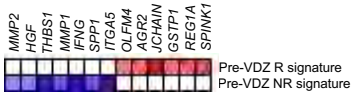

Gene Signature	NES	FDR q-value
Pre-VDZ R	1.42	0.09
Pre-VDZ NR	-1.49	0.06

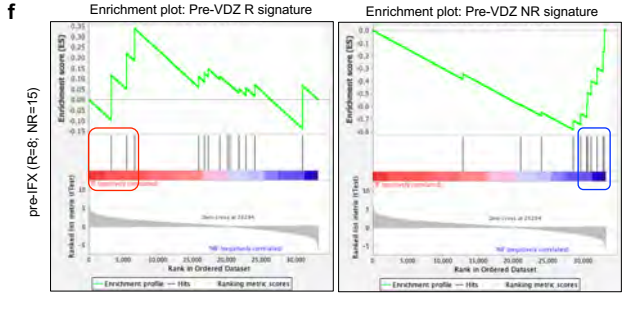

g

Leading edge genes in pre-IFX R/NR

Gene Signature	NES	FDR q-value
Pre-VDZ R	0.91	0.58
Pre-VDZ NR	-2.28	0

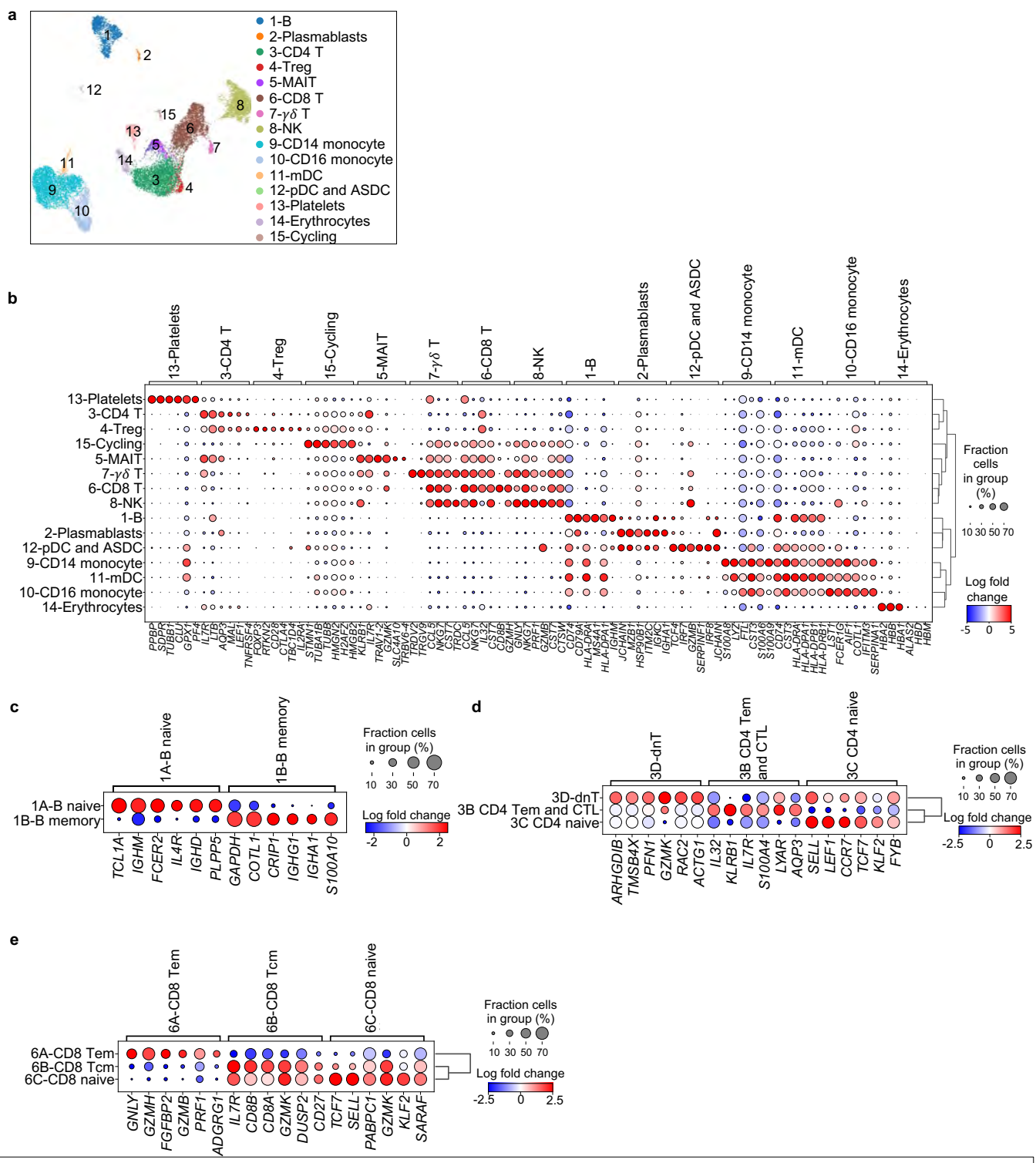

Supplementary Fig.1| Peripheral blood leukocyte (PBL) scRNA-seq coarse cell subset annotations and both coarse and fine cell subset landmark genes. a, UMAP visualization of pooled multiplex PBL scRNA-seq for 20,130 cells from HC (n=4), UC (n=3), and UC-VDZ (n=4) patients highlighting coarse cell subset annotations. **b-e,** Dot plot representation of landmark genes expressed by (**b**) coarse cell subsets and (**c-e**) fine PBL cell subsets. Genes ranked by Wilcoxon rank-sum. Cell subsets without landmark genes above selected minimum log fold change are not displayed.

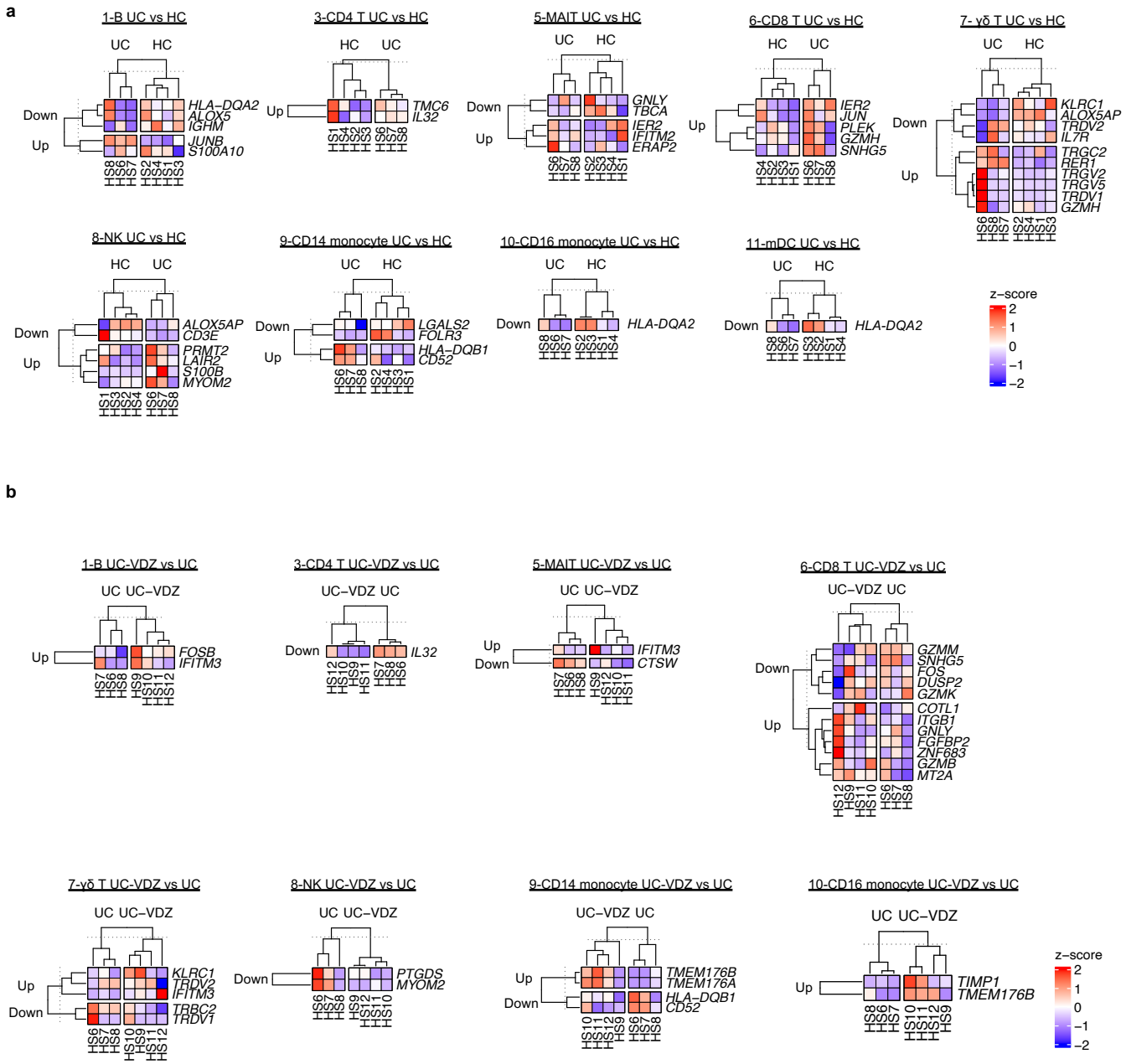

Supplementary Fig.2| PBL scRNA-seq DE gene analysis comparing UC versus HC and UC-VDZ versus UC. a,b, Heatmap of expression z-scores for scRNA-seq DE genes in the indicated PBL cell subsets with $\log_2$fc >2 or <-2 and and Bonferroni-corrected p-value<0.1 in (**a**) UC (Up/Down) relative to HC and (**b**) UC-VDZ (Up/Down) relative to UC identified by MAST analysis. Ribosomal and mitochondrial genes are not displayed; cell subsets without DE genes are not displayed.

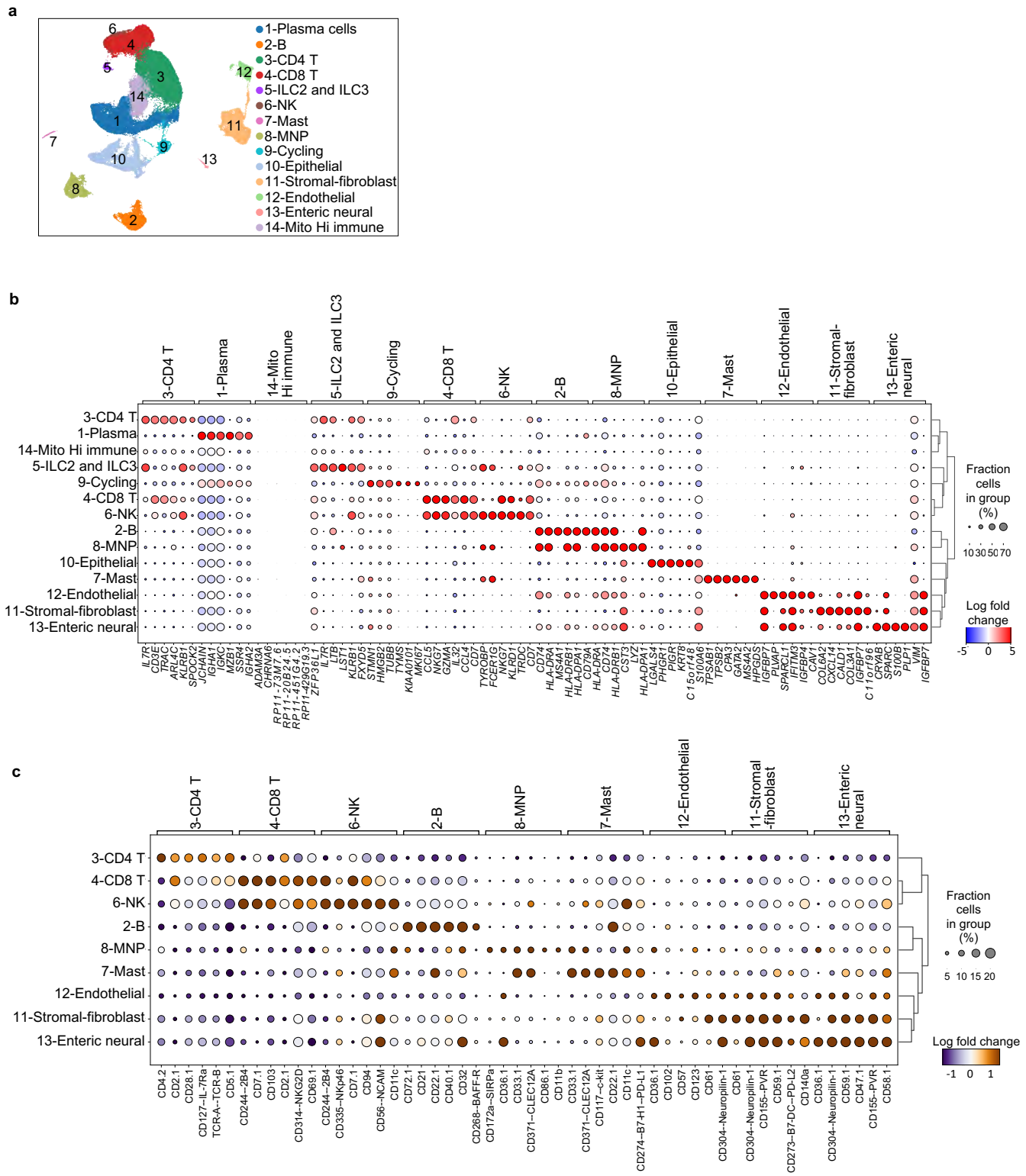

Supplementary Fig.3| Biopsy scRNA-seq and CITE-seq coarse cell subset annotations and landmark genes and proteins. a, UMAP visualization of scRNA-seq and CITE-seq for 93,900 cells from HC (n=4), UC (n=4), and UC-VDZ (n=4) patients highlighting coarse cell subset annotations. **b-c,** Dot plot representation of landmark (**b**) genes and (**c**) proteins expressed by indicated coarse cell subsets. Genes and proteins were ranked by Wilcoxon rank-sum. Cell subsets without landmark genes or proteins above selected minimum log fold change are not displayed.

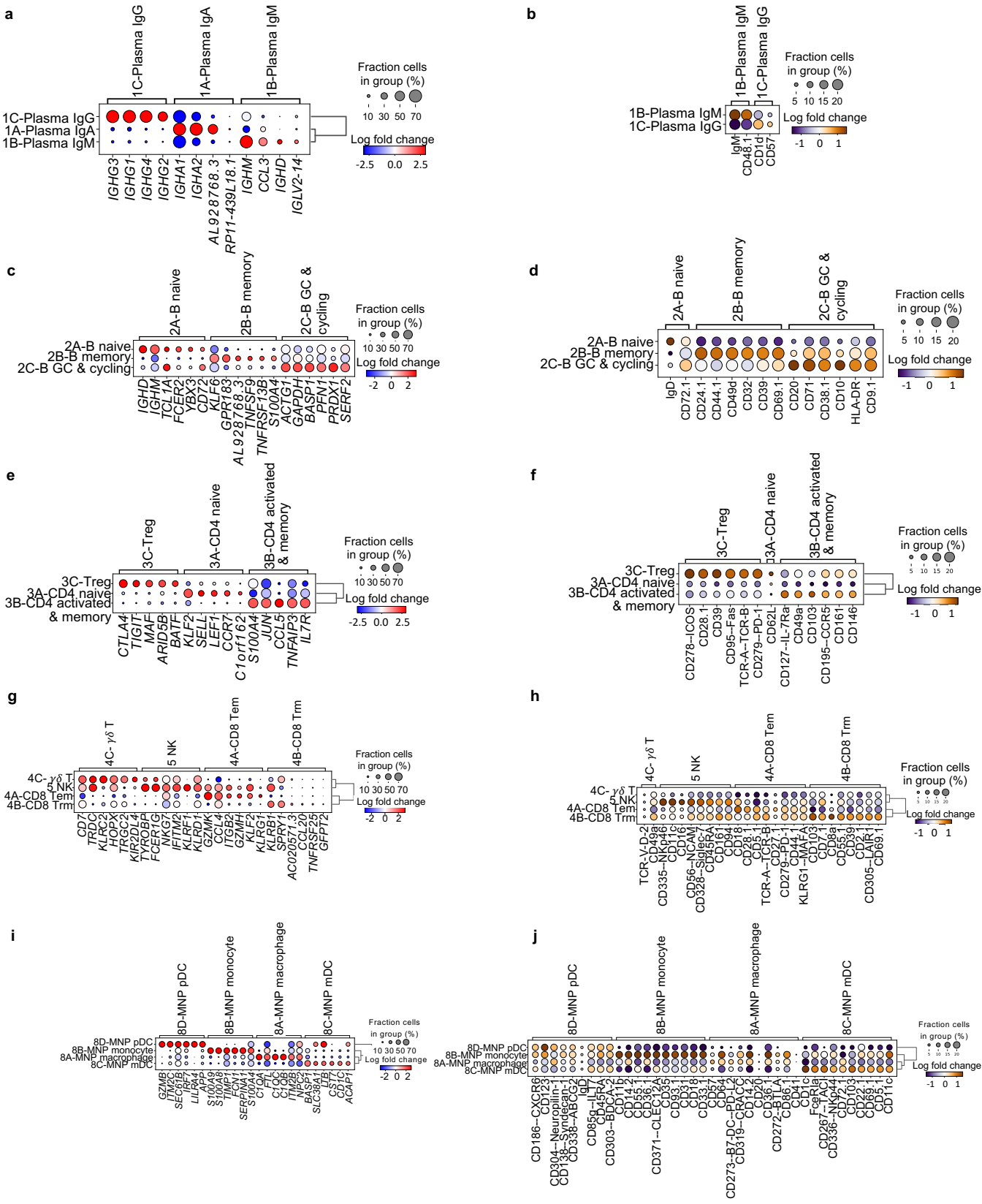

Supplementary Fig.4| Landmark genes and proteins associated with fine immune cell subsets in biopsy scRNA-seq and CITE-seq data. a-j, Dot plot representation of landmark (**a,c,e,g,i**) genes and (**b,d,f,h,j**) proteins expressed by indicated fine cell subsets. Genes and proteins were ranked by Wilcoxon rank-sum. Cell subsets without landmark genes or proteins above selected minimum log fold change are not displayed.

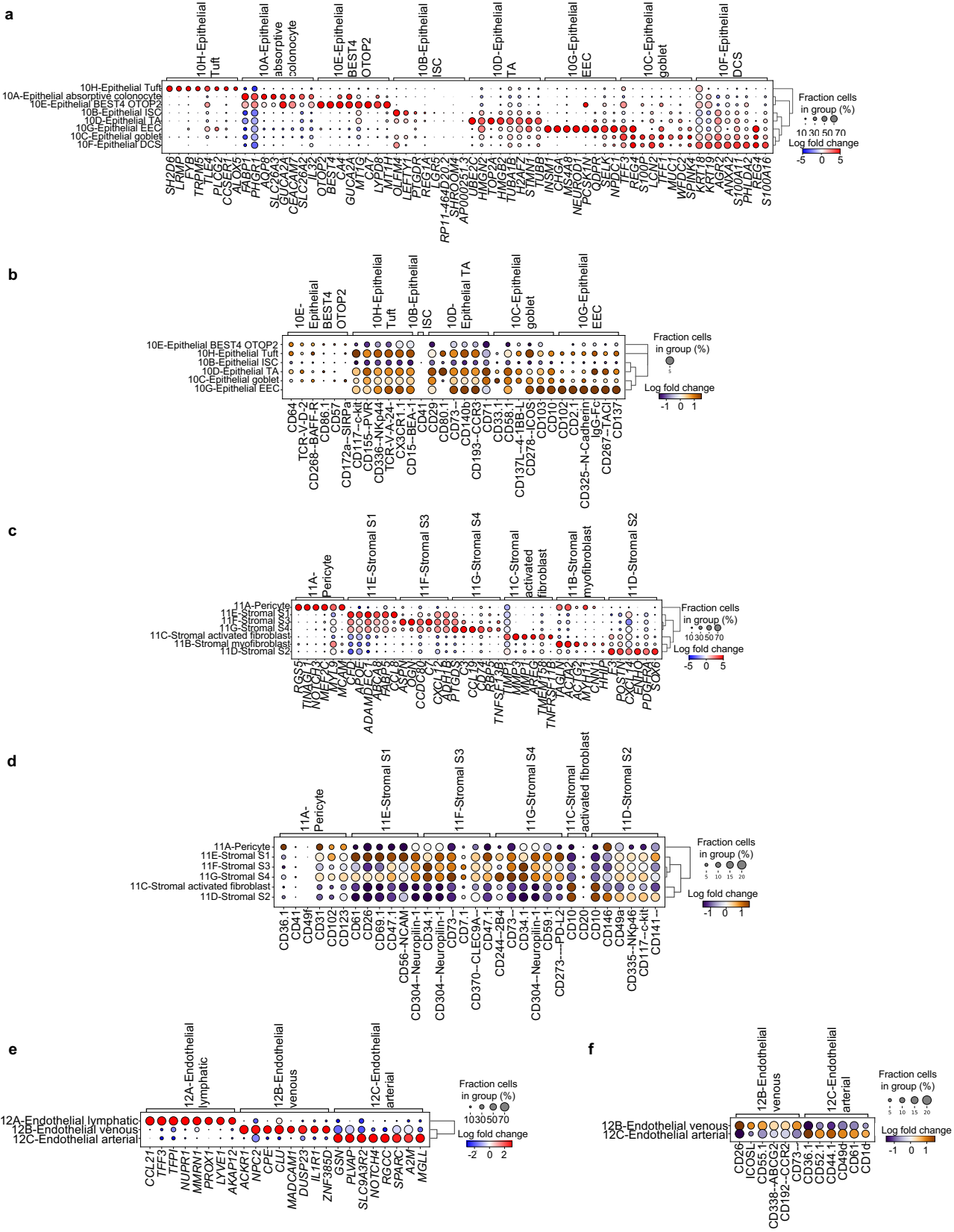

Supplementary Fig. 5| Landmark genes and proteins associated fine non-immune cell subsets in biopsy biopsy scRNA-seq and CITE-seq data. a-f, Dot plot representation of landmark (**a,c,e**) genes and (**b,d,f**) proteins expressed by indicated biopsy fine cell subsets. Genes and proteins were ranked by Wilcoxon rank-sum. Cell subsets without landmark genes or proteins above selected minimum log fold change are not displayed.

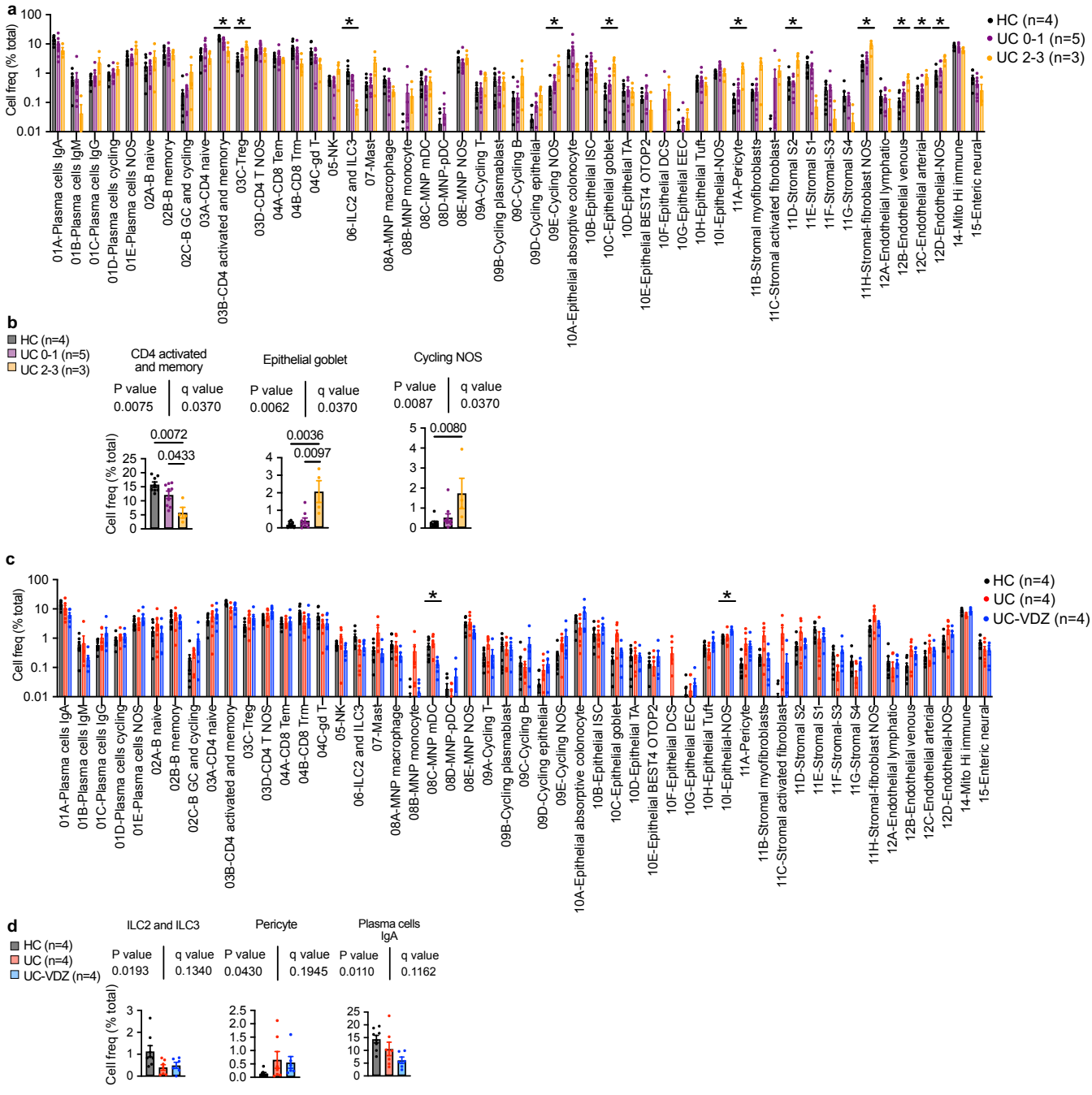

Supplementary Fig. 6| Biopsy CITE-seq cell subsets that correlated with inflammatory severity, disease status, and VDZ treatment. a-d, Cell frequency as a percent of total cells per study subject and fine cell annotation stratified by (**a,b**) endoscopic severity and (**c,d**) disease and treatment status (mean ± SEM; n=number of patients; each dot represents one patient sample). One-way ANOVA Kruskal-Wallis test was performed for each cell subset individually in (**a**, **c**), followed by global FDR correction of all p-values for all cell subsets, with q<0.1 threshold for discovery (*=q<0.1, only significant differences are indicated). A nested one-way ANOVA test was also performed on log transformed values treating biopsies as replicates with an unadjusted p<0.05 as an additional threshold for discovery (*). Select subsets are shown in (**b, d**) with exact p-value and q-value; NOS-"not otherwise specified".

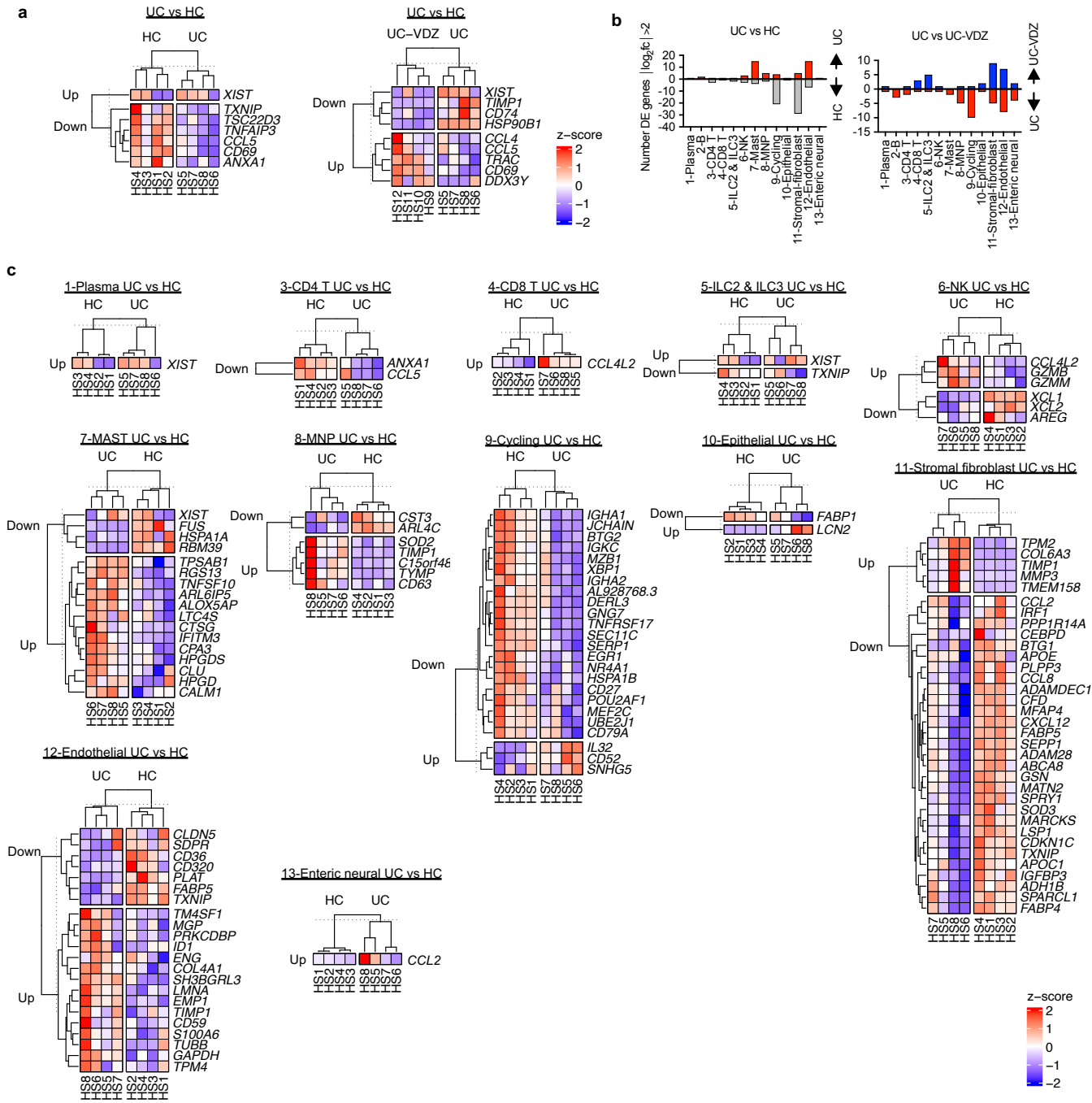

Supplementary Fig.7| Biopsy scRNA-seq DE genes in cell subsets comparing UC vs HC and UC-VDZ vs UC. a, Heatmap of expression z-scores for scRNA-seq DE genes for all biopsy cells, with $\log_2$fc >1 or <-1 and Bonferroni-corrected p-value<0.1, comparing UC (Up/Down) relative to HC and UC-VDZ (Up/Down) relative to UC identified by MAST analysis. **b,** Number of scRNA-seq DE genes in biopsy cell subsets with $\log_2$fc >2 or <-2 in UC versus HC and UC-VDZ versus UC identified by MAST analysis. **c,** Heatmap of expression z-scores for scRNA-seq DE genes for the indicated cell subsets with $\log_2$fc >2 or <-2 and Bonferroni-corrected p-value <0.1 in UC (Up/Down) relative to HC identified by MAST analysis. Ribosomal and mitochondrial genes are not displayed; cell subsets without DE genes are not displayed.

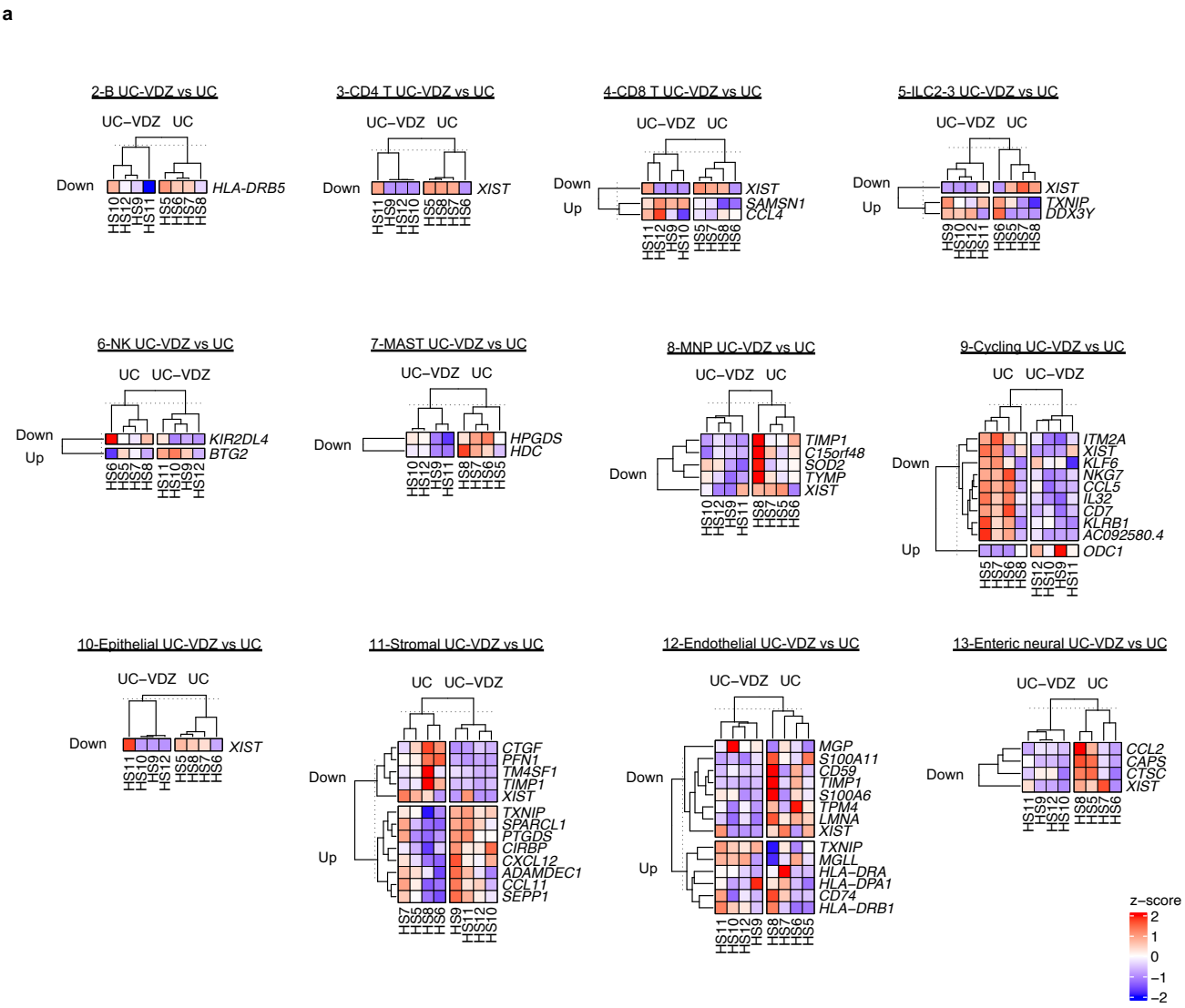

Supplementary Fig.8| Biopsy scRNA-seq DE genes in cell subsets comparing UC-VDZ vs UC and reciprocal expression analysis. a, Heatmap of expression z-scores for scRNA-seq DE genes for the indicated cell subsets with log_2fc >2 or <-2 and Bonferroni-corrected p-value <0.1 in UC-VDZ (Up/Down) relative to UC identified by MAST analysis. **b,** scRNA-seq DE genes in biopsy coarse cell annotation subsets with log_2fc >2 or <-2 in UC versus HC and an inverse log_2fc for UC-VDZ versus UC with log_2fc <-0.5 or >0.5 identified by MAST analysis, respectively. Ribosomal and mitochondrial genes are not displayed; cell subsets without DE genes are not displayed.

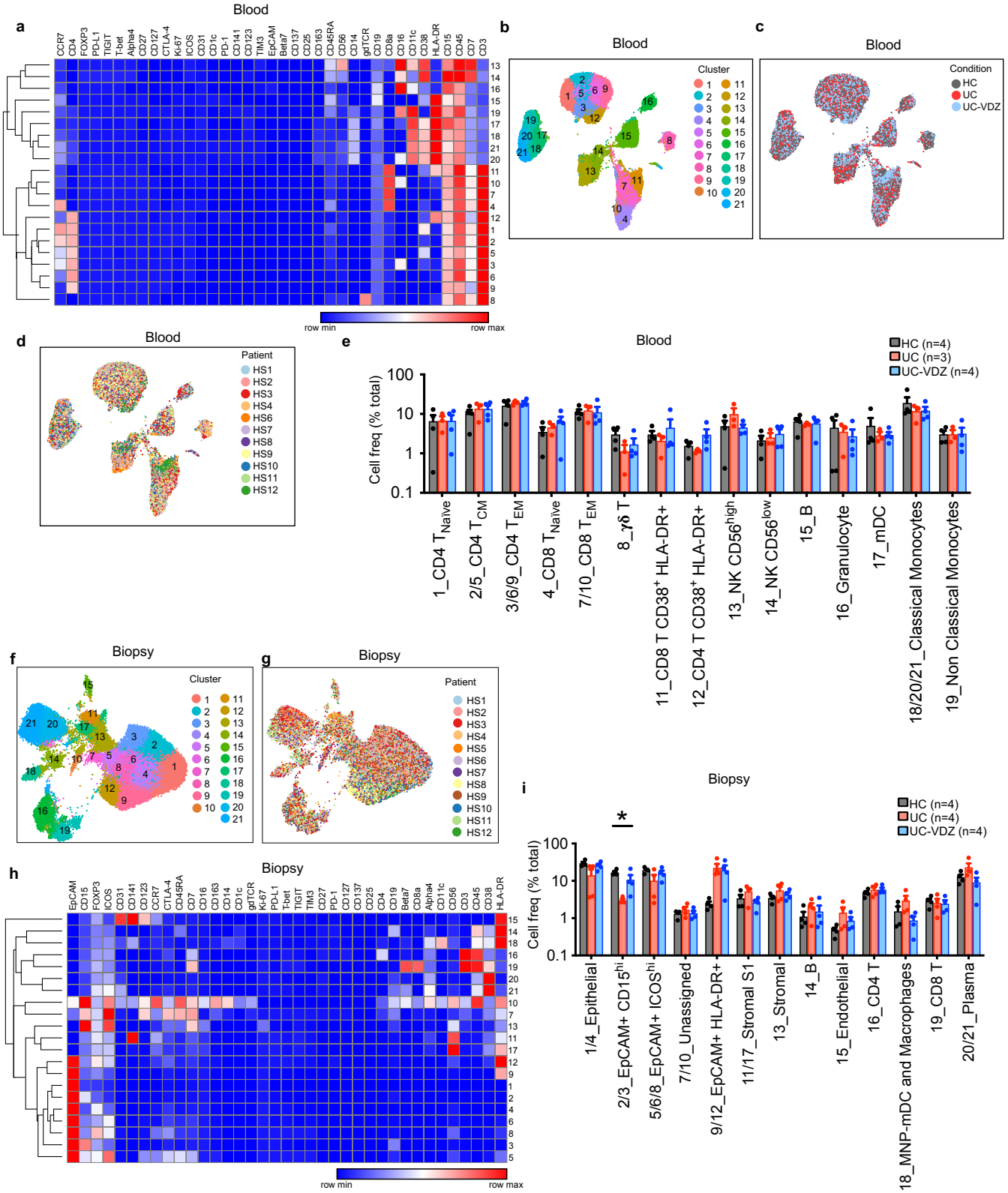

Supplementary Fig. 9| Heatmaps and total frequencies obtained from unsupervised analysis of CyTOF data from blood and biopsies. a,h, Heatmap visualization of mean intensity of each marker for the 21 identified clusters in blood and biopsies, respectively. **b-d,** UMAP visualization of the indicated samples (100,000 out of 1,390,156 live cell events displayed for blood) highlighting (**b**) FlowSOM identified clusters, (**c**) disease and treatment status, and (**d**) patient sample. **e,i,** Cell frequencies for each annotated cell subset per condition for (**e**) blood and (**i**) biopsy samples **(**mean ± SEM; n=number of patients; each dot represents one patient sample). **f,g,** UMAP visualization of the indicated samples (60,000 out of 684,249 live cell events displayed for biopsies) highlighting (**f**) FlowSOM identified clusters, and (**g**) patient sample. One-way ANOVA Kruskal-Wallis test was performed for each cell subset individually in panels (**e**) and (**i**), followed by global FDR correction of all p-values for all cell subsets, with q<0.1 threshold for discovery (*q<0.1, only significant differences are indicated).

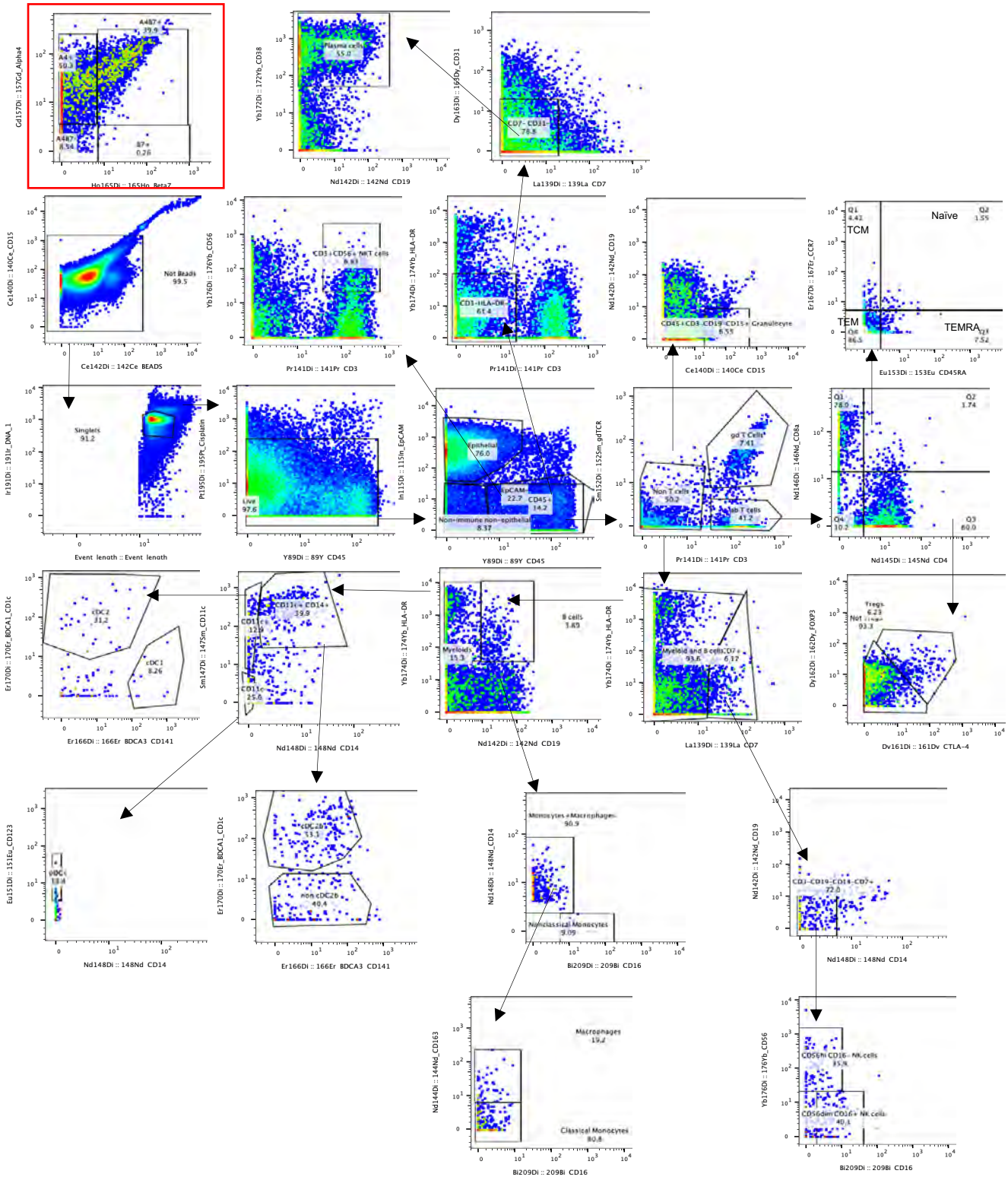

Supplementary Fig. 10| Representative supervised CyTOF gating scheme.

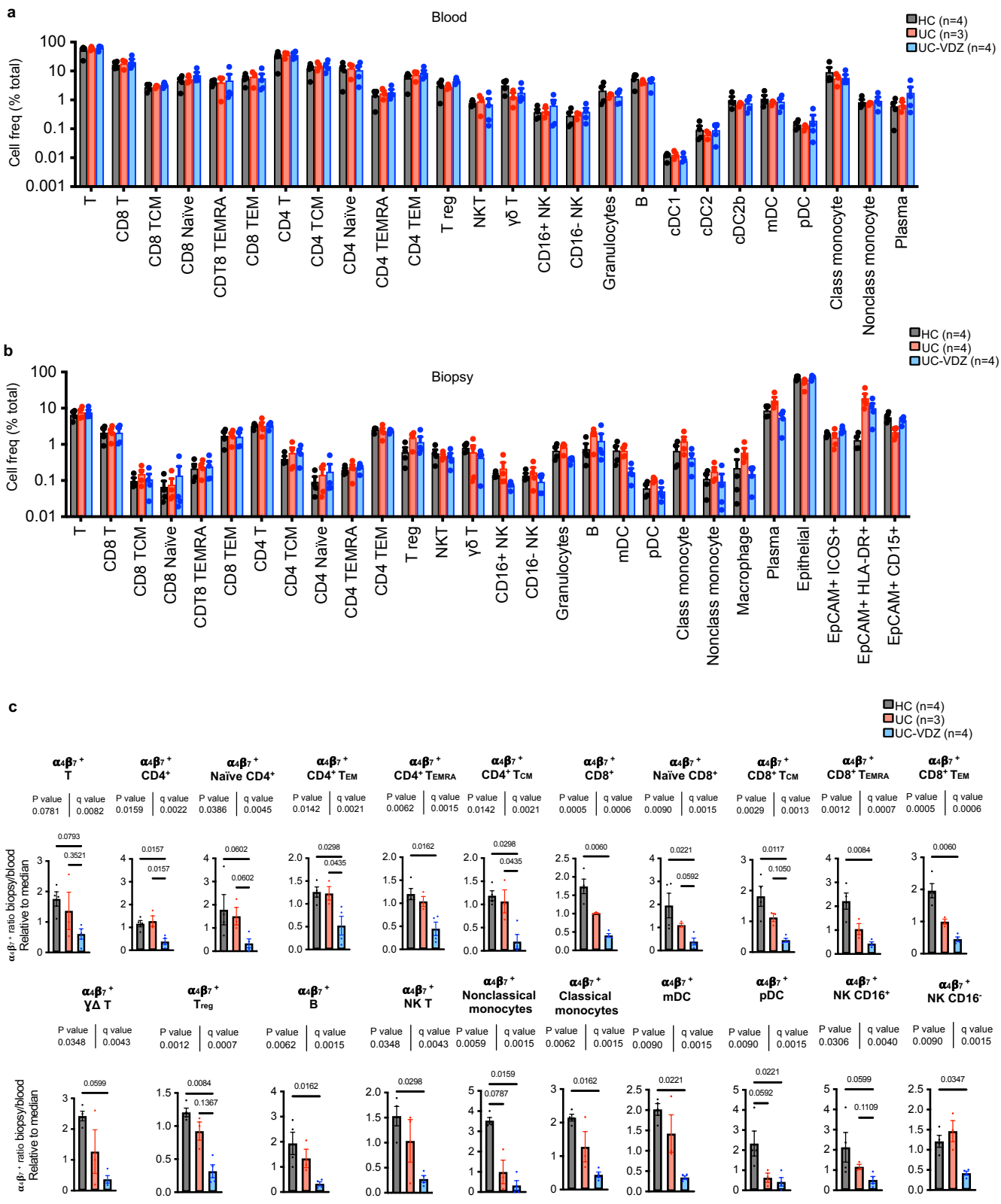

Supplementary Fig. 11| Total frequencies obtained from supervised analysis of CyTOF data from blood and biopsies and significant $\alpha_4\beta_7^+$ cell subsets. a,b, Cell frequencies for each annotated cell subset per condition in blood and biopsy, respectively. **c,** $\alpha_4\beta_7^+$ cell frequency in the biopsy versus blood for the indicated cell subsets relative to the median for each cell subset. For panels **a-b**, mean ± SEM; n=number of patients; each dot represents one patient sample; multiple one-way ANOVA Kruskal-Wallis test with FDR correction; q<0.1 threshold for discovery; individual subsets are shown in (**c**) with exact p-value and q-value; individual inter-column q-values are displayed only for cell subsets with overall FDR corrected q<0.01. Class monocyte-classical monocyte; Nonclass monocyte-nonclassical monocyte; mDC-cDC1,cDC2,cDC2b.

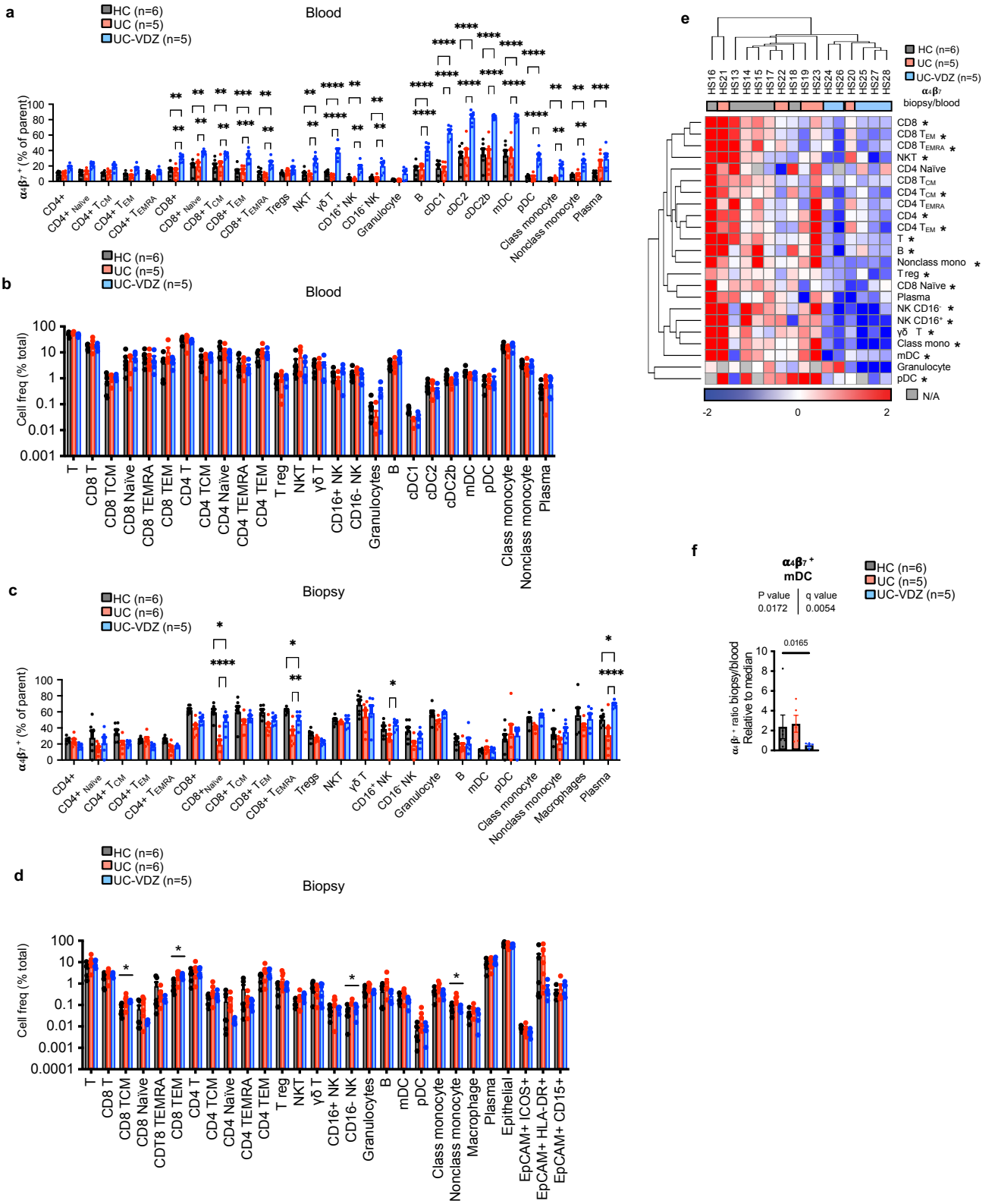

Supplementary Fig. 12| $\alpha_4\beta_7^+$ cell subsets and total frequencies obtained from supervised analysis of CyTOF data from blood and biopsies in a second case control study of patients in near or complete endoscopic remission (HS13-HS30). a,c, Percentage of $\alpha_4\beta_7^+$ cells in each defined cell subset per condition for blood and biopsy samples, respectively (mean ± SEM; n=number of patients; each dot represents one patient sample; two-way ANOVA comparing HC vs UC-VDZ and UC vs UC-VDZ with FDR correction; q<0.1 threshold for discovery; *q<0.05; **q<0.01; ***q<0.001; and ****q<0.0001; only significant differences are indicated. **b,d,** Cell frequencies for each annotated cell subset per condition in blood and biopsy, respectively (mean ± SEM; n=number of patients, multiple one-way ANOVA Kruskal-Wallis test with FDR correction; q<0.1 threshold for discovery). **e,** Heatmap of biopsy/blood ratio of $\alpha_4\beta_7^+$ cells for each cell subset by patient (hierarchically clustered by Euclidian distance, average linkage). **f,** $\alpha_4\beta_7^+$ cell frequency in the biopsy versus blood for mDC relative to the median (mean ± SEM; n=number of patients; each dot represents one patient sample).

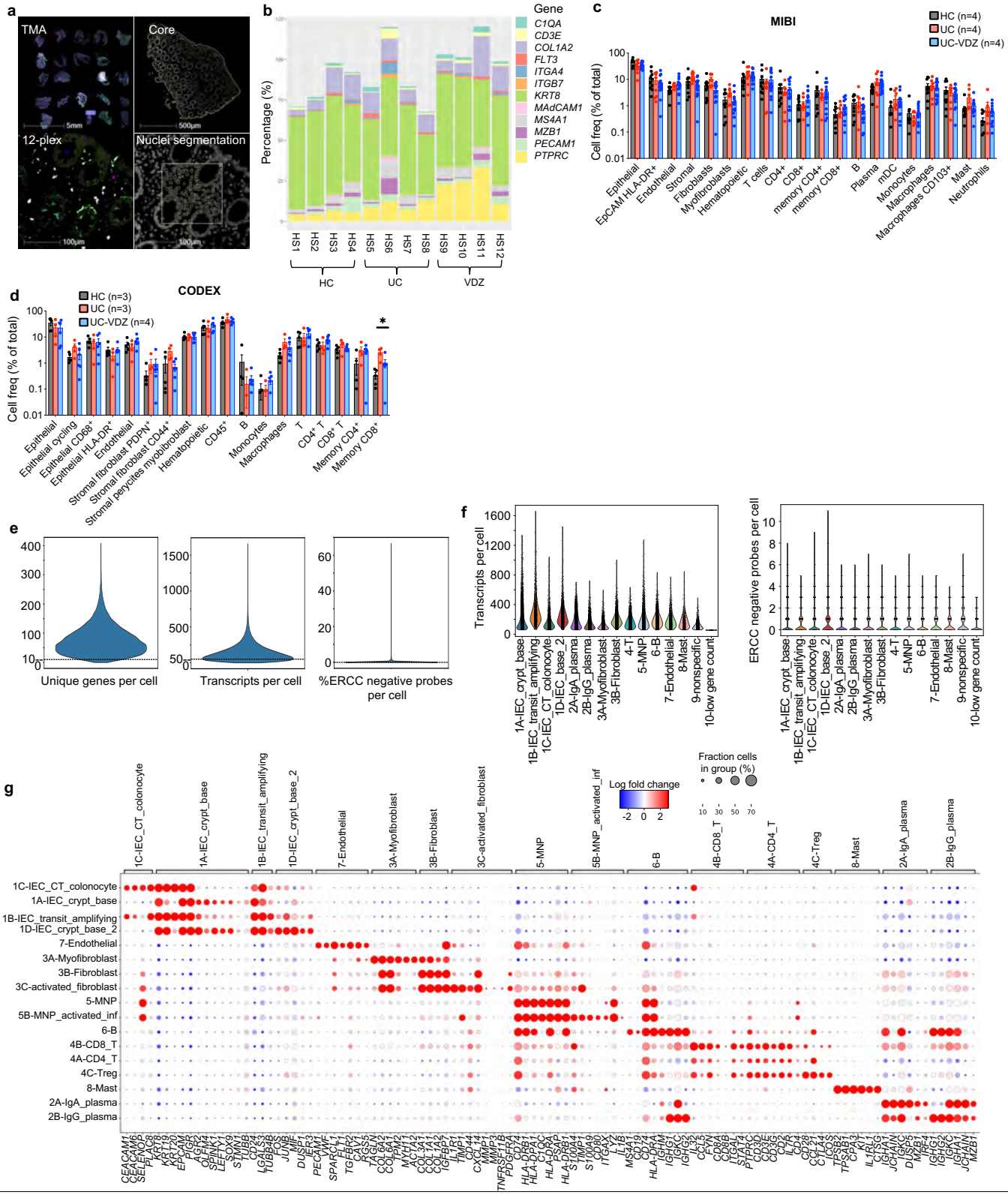

Supplementary Fig.13| Spatial transcriptomics and proteomics on FFPE tissue microarray (TMA). a, Image analysis workflow for 12-plex RNA-ISH assay using HALO, scan of the entire TMA (0.5X), with representative images (4X), representative overlay of the 12 markers (20X), and representative nuclei segmentation and localization of the 12 different markers (20X), which are representative of 19 cores. **b,** Stacked bar plots for cells expressing the indicated gene; values are greater than 100% due to cells co-expressing genes of interest. **c,d,** Cell frequencies as a percent of total for the indicated cell subsets identified by (**c**) MIBI and (**d**) CODEX; multiple one-way ANOVA Kruskal-Wallis test with FDR correction; q<0.1 threshold for discovery; *=q<0.1. **e,** Violin plots showing unique genes, transcripts, and %ERCC negative probes per cell. Cells with <10 unique genes or <50 transcripts per cell were excluded (dashed line). **f**, Transcripts and ERCC negative probes per cell, stratified by coarse annotation. **g,** Dot plot representation of curated landmark genes for annotated subsets. Genes ranked by Wilcoxon rank-sum. ERCC, External RNA Controls Consortium.

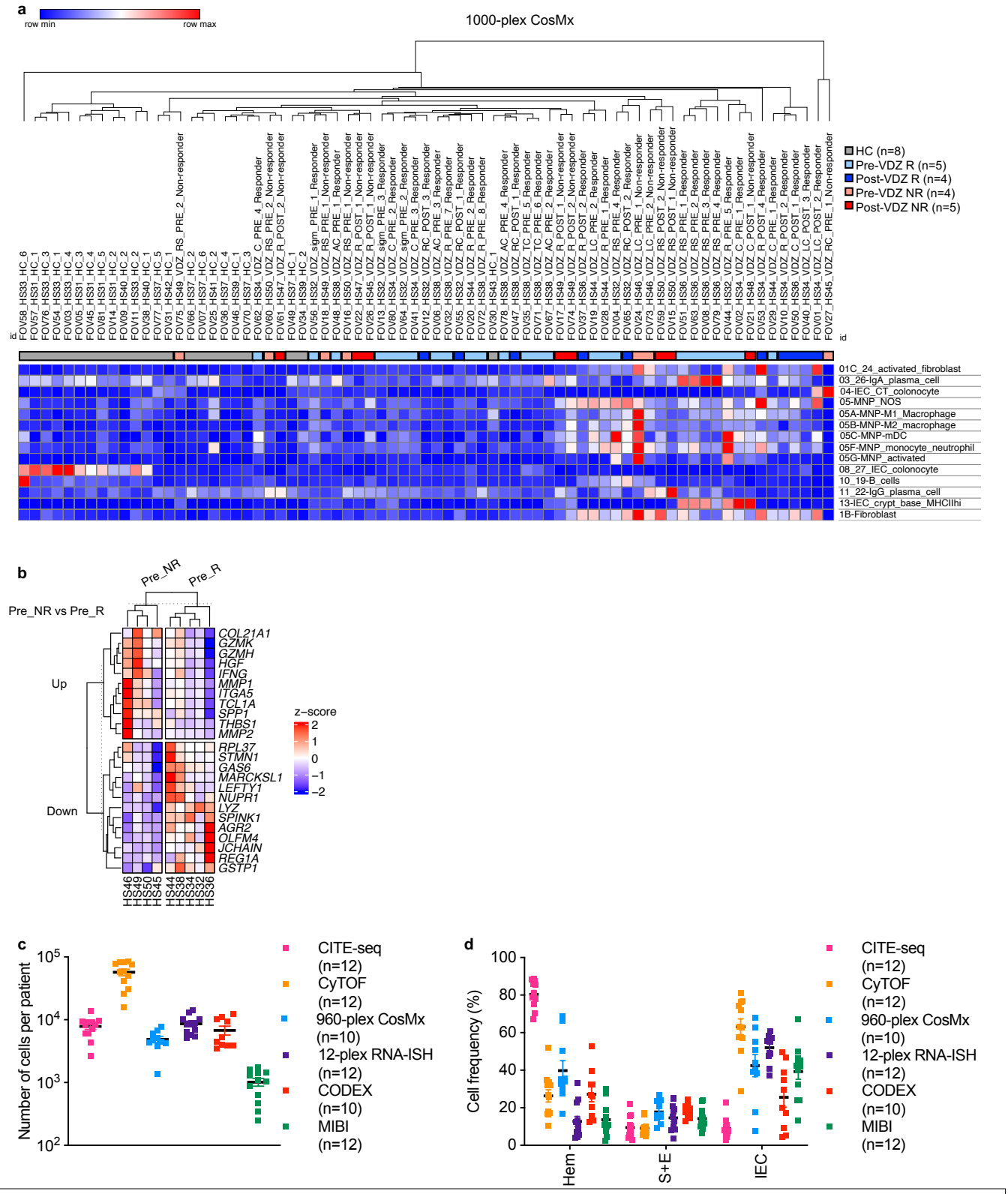

Supplementary Fig.14| CosMx spatial transcriptomic on TMA from retrospective longitudinal study and comparison of total cells analyzed per patient and cell frequency per tissue compartment among study subjects HS1-HS12. a, Heatmap of selected cell subsets by patient fov (hierarchically clustered by Euclidian distance, average linkage, columns color-coded by group). **b.** Heatmap of expression z-scores for the indicated genes in VDZ non-responders (Pre_NR) (Up/Down) relative to responders (Pre_R) before treatment identified by DESeq2. **c,** Total number of cells analyzed per patient using different multi-omic methods. **d,** Cell frequency per patient expressed as percent of total for the indicated cellular compartment among different multi-omic methods. For (**c, d**), mean ± SEM, n=number of patients, each dot represents one patient sample. Hem-hematopoietic; S+E-stromal + endothelial; IEC-intestinal epithelial cell.

Patient ID	Age (y)	Sex	Disease status	UC Medication	Disease duration (y)	Duration VDZ (mo)	Prior anti-TNF exposure	Montreal classification	Mayo Endoscopic subscore	Responder to VDZ
HS1	50-59	M	HC	None	n/a	n/a	No	n/a	0	n/a
HS2	40-49	M	HC	None	n/a	n/a	No	n/a	0	n/a
HS3	20-29	F	HC	None	n/a	n/a	No	n/a	0	n/a
HS4	50-59	F	HC	None	n/a	n/a	No	n/a	0	n/a
HS5	20-29	F	UC	5-ASA	15	n/a	No	E2	2	n/a
HS6	40-49	M	UC	5-ASA	25	n/a	Yes	E3	2	n/a
HS7	60-69	F	UC	5-ASA	7	n/a	No	E2	1	n/a
HS8	50-59	F	UC	5-ASA	5	n/a	No	E1	1	n/a
				Median	11 (7-18)					
HS9	50-59	M	UC	VDZ	25	8	Yes	E2	1	Yes
HS10	30-39	M	UC	VDZ	8	7	No	E2	1	Yes
HS11	20-29	F	UC	VDZ	8	64	Yes	E2	3	No
HS12	50-59	M	UC	VDZ	10	2	Yes	E3	1	Yes
					9 (8-14)					
p-value	ns	ns	p=0.0025	p<0.0001	ns	n/a	ns	ns	p=0.01	
HS13	20-29	M	HC	None	n/a	n/a	No	n/a	0	n/a
HS14	30-39	M	HC	None	n/a	n/a	No	n/a	0	n/a
HS15	20-29	F	HC	None	n/a	n/a	No	n/a	0	n/a
HS16	60-69	F	HC	None	n/a	n/a	No	n/a	0	n/a
HS17	50-59	F	HC	None	n/a	n/a	No	n/a	0	n/a
HS18	40-49	F	HC	None	n/a	n/a	No	n/a	0	n/a
HS19	40-49	M	UC	ADA	27	n/a	Yes	E2	0	n/a
HS20*	30-39	F	UC	ADA	20	n/a	Yes	E2	1-2	n/a
HS21	50-59	M	UC	IFX/MTX	6	n/a	Yes	E3	0	n/a
HS22	30-39	F	UC	5-ASA	6	n/a	No	E3	0	n/a
HS23	40-49	M	UC	IFX/AZA	10	n/a	Yes	E3	1	n/a
HS30	40-49	F	UC	ADA	2	n/a	Yes	E3	0	n/a
					8 (5-22)					
HS24	50-59	M	UC	VDZ	5.5	45	Yes	E2	0	Yes
HS25	60-69	M	UC	VDZ	37	5	No	E3	0	Yes
HS26	30-39	F	UC	VDZ	21	55	Yes	E3	0	Yes
HS27	30-39	F	UC	VDZ	1	6	No	E1	0	Yes
HS28	40-49	M	UC	VDZ	8	45	Yes	E1	0	Yes
					8 (3-29)					
p-value	ns	ns	p=0.0002	p<0.0001	ns	n/a	p=0.0329	ns	ns	
HS31 (HS16)	60-69	F	HC	None	n/a	n/a	No	n/a	0	n/a
HS33 (HS14)	30-39	M	HC	None	n/a	n/a	No	n/a	0	n/a
HS35 (HS15)	20-29	F	HC	None	n/a	n/a	No	n/a	0	n/a
HS37 (HS13)	20-29	M	HC	None	n/a	n/a	No	n/a	0	n/a
HS39	20-29	F	HC	None	n/a	n/a	No	n/a	0	n/a
HS40	60-69	M	HC	None	n/a	n/a	No	n/a	0	n/a
HS41	50-59	M	HC	None	n/a	n/a	No	n/a	0	n/a
HS42	40-49	M	HC	None	n/a	n/a	No	n/a	0	n/a
HS43	50-59	M	HC	None	n/a	n/a	No	n/a	0	n/a
HS32	20-29	F	UC	VDZ	2	4	No	E2	pre 2 ; post 0	Yes
HS34 (HS27)	30-39	F	UC	VDZ	1	6	No	E1	pre 2; post 0	Yes
HS36	40-49	M	UC	VDZ	3	2	Yes	E2	pre 3; post 0	Yes
HS38 (HS9)	50-59	M	UC	VDZ	25	7	Yes	E3	pre 2; post 0	Yes
HS44	30-39	F	UC	VDZ	2	2	No	E1	pre 1	Yes
HS45	40-49	M	UC	VDZ	14	19	Yes	E2	pre 1; post 3	No
HS46	40-49	n/a	UC	VDZ	21	2	Yes	E2	pre 3; post 3	No
HS47	30-39	M	UC	VDZ	11	5	Yes	E2	post 3	No
HS48	70-79	M	UC	VDZ	8	6	Yes	E3	pre 2; post 2	No
HS49	30-39	F	UC	VDZ	2	3	Yes	E2	pre 2; post 3	No
HS50	20-29	M	UC	VDZ	0	5	Yes	E2	pre 2; post 2	No
					3 (2-14)					
p-value	ns	ns	p<0.0001	p<0.0001	n/a	n/a	p=0.0010	ns	pre, ns; post, p=0.0016	

Supplementary Table 1. Baseline demographic and clinical data for study participants. Categorical variables were analyzed by Chi-square test and continuous variables were compared using one-way ANOVA with FDR correction or Mann-Whitney test where appropriate. ns, not significant; n/a, not applicable; pre, pre-VDZ tretament; post, post-VDZ treatment. *HS20 had a short segment of moderate proctitis, otherwise in endoscopic remission with no change in therapy. HS31, HS33, HS35, HS37, HS34, HS38 were additional samples from HS16, HS14, HS15, HS13, HS27, and HS9, respectively. ADA-adalimumab; IFX-infliximab; VDZ-vedolizumab; AZA-azathioprine; 5-ASA-5-aminosalicylic acid.

Patient ID	Disease status	Medication	Biopsy location-severity	Mayo Endoscopic subscore	Geboes grade	Biopsy sample ID	Blood scRNA-seq	Biopsy scRNA-seq	CITE-seq	Blood CyTOF	Biopsy CyTOF	12-plex RNA-ISH	CODEX	MIBI	CosMx SMI 960-plex
HS1	HC	N/A	R-0	0	0.0	HS1-CLR1	Y	Y		Y	Y	Y (1-core)	N/A	N/A	Y (1-FOV)
			L-0		1.1	HS1-CLL1		Y				Y (1-core)	N/A	Y (2-FOV)	Y (2-FOV)
HS2	HC	N/A	R-0	0	1.1	HS2-CLR1	Y	Y		Y	Y	Y (1-core)	Y (1-core)	Y (3-FOV)	Y (1-FOV)
			L-0		1.1	HS2-CLL1		Y				Y (1-core)	Y (1-core)	Y (3-FOV)	Y (1-FOV)
HS3	HC	N/A	R-0	0	0.0	HS3-CLR1	Y	Y		Y	Y	N/A	Y (1-core)	N/A	Y (1-FOV)
			L-0		0.0	HS3-CLL1		Y				Y (1-core)	Y (1-core)	Y (1-FOV)	N/A
HS4	HC	N/A	R-0	0	0.0	HS4-CLR1	Y	Y		Y	Y	Y (1-core)	N/A	N/A	Y (1-FOV)
			L-0		0.0	HS4-CLL1		Y				Y (1-core)	Y (1-core)	Y (1-FOV)	Y (1-FOV)
HS5	UC	5-ASA	R-0	2	0.0	HS5-CLR1	N/A	Y		N/A	Y	Y (1-core)	Y (1-core)	Y (2-FOV)	Y (1-FOV)
			L-2		0.2	HS5-CLL1		Y				Y (1-core)	N/A	Y (1-FOV)	N/A
HS6	UC	5-ASA	R-2	2	2A.2	HS6-CLR1	Y	Y		Y	Y	Y (1-core)	N/A	Y (2-FOV)	N/A
			L-2		3.1	HS6-CLL1		Y				N/A	N/A	N/A	N/A
HS7	UC	5-ASA	R-1	1	1.1	HS7-CLR1	Y	Y		Y	Y	Y (1-core)	Y (1-core)	N/A	Y (1-FOV)
			L-0		0.0	HS7-CLL1		Y				Y (1-core)	Y (1-core)	Y (2-FOV)	Y (1-FOV)
HS8	UC	5-ASA	L-1	1	3.2	HS8-CLL1	Y	Y		Y	Y	Y (1-core)	Y (1-core)	Y (1-FOV)	Y (1-FOV)
HS9	UC	VDZ	R-0	1	0.0	HS9-CLR1	Y	Y		Y	Y	Y (1-core)	Y (1-core)	Y (3-FOV)	N/A
			L-1		0.0	HS9-CLL1		Y				Y (1-core)	Y (1-core)	Y (3-FOV)	N/A
HS10	UC	VDZ	R-0	1	1.1	HS10-CLR1	Y	Y		Y	Y	Y (1-core)	Y (1-core)	Y (1-FOV)	Y (1-FOV)
			L-1		0.1	HS10-CLL1		N/A				N/A	N/A	N/A	Y (1-FOV)
HS11	UC	VDZ	R-0	3	0.1	HS11-CLR1	Y	Y		Y	Y	N/A	N/A	N/A	Y (1-FOV)
			L-3		3.2	HS11-CLL1		Y				Y (1-core)	Y (1-core)	Y (1-FOV)	Y (1-FOV)
HS12	UC	VDZ	R-1	1	1.2	HS12-CLR1	Y	Y		Y	Y	Y (1-core)	Y (1-core)	Y (3-FOV)	N/A
			L-1		1.3	HS12-CLL1		N/A				Y (1-core)	Y (1-core)	Y (3-FOV)	Y (1-FOV)

Supplementary Table 2. Biospecimens analyzed by each multi-omics method. R, right colon; L, left colon; 5-ASA, 5-aminosalicylate; CLR1, right colon biopsy 1; CLL1, left colon biopsy; Y, yes; N/A not applicable. FOV-field of view

Assay type	Target	Ion channel / DNA barcode	Metal / DNA barcode ID	Clone/Probe	Concentration (µg/ml) /Dilution (ratio)	h5ad file symbol	Catalog #	Vendor
CITE-seq (TotalSeq)	CD103 (Integrin αE)	GACCTCATTGTGAAT	A0145	Ber-ACT8	proprietary	CD103	399907	BioLegend
	CD35	ACTTCCGTCGATCTT	A0167	E11	proprietary	CD35	399907	BioLegend
	CD25	TTTGTCCTGTACGCC	A0085	BC96	proprietary	CD25	399907	BioLegend
	CD62L	GTCCCTGCAACTTGA	A0147	DREG-56	proprietary	CD62L	399907	BioLegend
	CD3	CTCATTGTAACTCCT	A0034	UCHT1	proprietary	CD3	399907	BioLegend
	CD33	TAACTCAGGGCCTAT	A0052	P67.6	proprietary	CD33.1	399907	BioLegend
	CD4	TGTTCCCGCTCAACT	A0072	RPA-T4	proprietary	CD4.2	399907	BioLegend
	CD58 (LFA-3)	GTTCCTATGGACGAC	A0174	TS2/9	proprietary	CD58.1	399907	BioLegend
	CD8a	GCTGCGCTTTCCATT	A0080	RPA-T8	proprietary	CD8a	399907	BioLegend
	CD56	TCCTTTCCTGATAGG	A0047	5.1H11	proprietary	CD56--NCAM	399907	BioLegend
	CD11b	GACAAGTGATCTGCA	A0161	ICRF44	proprietary	CD11b	399907	BioLegend
	CD183 (CXCR3)	GCGATGGTAGATTAT	A0140	G025H7	proprietary	CD183--CXCR3	399907	BioLegend
	CD30	TCAGGGTGTGCTGTA	A0028	BY88	proprietary	CD30	399907	BioLegend
	CD336 (NKp44)	GGGCAATTAGCGAGT	A0802	P44-8	proprietary	CD336--NKp44	399907	BioLegend
	CD69	GTCTCTTGGCTTAAA	A0146	FN50	proprietary	CD69.1	399907	BioLegend
	CD335 (NKp46)	ACAATTTGAACAGCG	A0101	9E2	proprietary	CD335--NKp46	399907	BioLegend
	CD49f	TTCCGAGGATGATCT	A0070	GoH3	proprietary	CD49f	399907	BioLegend
	CD161	GTACGCAGTCCTTCT	A0149	HP-3G10	proprietary	CD161	399907	BioLegend
	CD45RO	CTCCGAATCATGTTG	A0087	UCHL1	proprietary	CD45RO	399907	BioLegend
	CD20	TTCTGGGTCCCTAGA	A0100	2H7	proprietary	CD20	399907	BioLegend
	KLRG1 (MAFA)	CTTATTTCCTGCCCT	A0153	SA231A2	proprietary	KLRG1--MAFA	399907	BioLegend
	CD19	CTGGGCAATTACTCG	A0050	HIB19	proprietary	CD19.1	399907	BioLegend
	CD32	GCTTCCGAATTACCG	A0142	FUN-2	proprietary	CD32	399907	BioLegend
	CD276 (B7-H3)	GACTGGGAGGGTATT	A0010	DCN.70	proprietary	CD276--B7-H3	399907	BioLegend
	CD279 (PD-1)	ACAGCGCCGTATTTA	A0088	EH12.2H7	proprietary	CD279--PD-1	399907	BioLegend
	CD197 (CCR7)	AGTTCAGTCAACCGA	A0148	G043H7	proprietary	CD197--CCR7	399907	BioLegend
	CD252 (OX40L)	TTTAGTGATCCGACT	A0021	11C3.1	proprietary	N/A	399907	BioLegend
	CD223 (LAG-3)	CATTTGTCTGCCGGT	A0152	11C3C65	proprietary	CD223--LAG-3	399907	BioLegend
	HLA-DR	AATAGCGAGCAAGTA	A0159	L243	proprietary	HLA-DR	399907	BioLegend
	CD45RA	TCAATCCTTCCGCTT	A0063	HI100	proprietary	CD45RA	399907	BioLegend
	CD196 (CCR6)	GATCCCTTTGTCACT	A0143	G034E3	proprietary	CD196--CCR6	399907	BioLegend
	CD2	TACGATTTGTCAGGG	A0367	TS1/8	proprietary	CD2.1	399907	BioLegend
	CD326 (Ep-CAM)	TTCCGAGCAAGTATC	A0123	9C4	proprietary	CD326--EpCAM	399907	BioLegend
	CD169 (Sialoadhesin, Siglec-1)	TACTCAGCGTGTTTG	A0206	7-239	proprietary	CD169--Sialoadhesin--Siglec-1	399907	BioLegend
	CD41	ACGTTGTGGCCTTGT	A0353	HIP8	proprietary	CD41	399907	BioLegend
	CD49b	GCTTTCTTCAGTATG	A0371	P1E6-C5	proprietary	CD49b	399907	BioLegend
	CD303 (BDCA-2)	GAGATGTCCGAATTT	A0370	201A	proprietary	CD303--BDCA-2	399907	BioLegend
	CD29	GTATTCCCTCAGTCA	A0369	TS2/16	proprietary	CD29	399907	BioLegend
	CD184 (CXCR4)	TCAGGTCCTTTCAAC	A0366	12G5	proprietary	CD184--CXCR4	399907	BioLegend
	CD98	GCACCAACAGCCATT	A0374	MEM-108	proprietary	CD98	399907	BioLegend
	CD124 (IL-4Rα)	CCGTCCTGATAGATG	A0363	G077F6	proprietary	N/A	399907	BioLegend
	CD135 (Flt-3/Flk-2)	CAGTAGATGGAGCAT	A0351	BV10A4H2	proprietary	CD135	399907	BioLegend
	CD370 (CLEC9A/DNGR1)	CTGCATTTCAGTAAG	A0207	8F9	proprietary	CD370--CLEC9A--DNGR1	399907	BioLegend
	CD21	AACCTAGTAGTTCGG	A0181	Bu32	proprietary	CD21	399907	BioLegend
	CD39	TTACCTGGTATCCGT	A0176	A1	proprietary	CD39	399907	BioLegend
	CD141 (Thrombomodulin)	GGATAACCGCGCTTT	A0163	M80	proprietary	CD141--Thrombomodulin	399907	BioLegend
	CD64	AAGTATGCCCTACGA	A0162	10.1	proprietary	CD64	399907	BioLegend
	CD152 (CTLA-4)	ATGGTTCACGTAATC	A0151	BNI3	proprietary	CD152	399907	BioLegend
	CD61	AGGTTGGAGTAGACT	A0372	VI-PL2	proprietary	CD61	399907	BioLegend
	CD163	GCTTCTCCTTCCTTA	A0358	GHI/61	proprietary	CD163.1	399907	BioLegend
	CD357 (GITR)	ACCTTTCGACACTCG	A0360	108-17	proprietary	CD357--GITR	399907	BioLegend
	CD137 (4-1BB)	CAGTAAGTTCGGGAC	A0355	4B4-1	proprietary	CD137	399907	BioLegend
	CD81 (TAPA-1)	GTATCCTTCCTTGGC	A0373	5A6	proprietary	CD81--TAPA-1	399907	BioLegend
	CD366 (Tim-3)	TGTCCTACCCAACTT	A0169	F38-2E2	proprietary	CD366--Tim-3	399907	BioLegend
	CD57 Recombinant	AACTCCCTATGGAGG	A0168	QA17A04	proprietary	CD57	399907	BioLegend
	CD278 (ICOS)	CGCGCACCCATTAAA	A0171	C398.4A	proprietary	CD278--ICOS	399907	BioLegend
	CD95 (Fas)	CCAGCTCATTAGAGC	A0156	DX2	proprietary	CD95--Fas	399907	BioLegend
	CD80	ACGAATCAATCTGTG	A0005	2D10	proprietary	CD80.1	399907	BioLegend
	CD138 (Syndecan-1)	ACTCTTTCGTTTACG	A0055	MI15	proprietary	CD138--Syndecan-1	399907	BioLegend
	CD70	CGCGAACATAAGAAG	A0027	113-16	proprietary	CD70.1	399907	BioLegend
	CD269 (BCMA)	CAGATGATCCACCAT	A0056	19F2	proprietary	CD269--BCMA	399907	BioLegend
	IgM	TAGCGAGCCCGTATA	A0136	MHM-88	proprietary	IgM	399907	BioLegend
	CD59	AATTAGCCGTCGAGA	A0361	p282 (H19)	proprietary	CD59.1	399907	BioLegend
	CD194 (CCR4)	AGCTTACCTGCACGA	A0071	L291H4	proprietary	CD194--CCR4	399907	BioLegend
	CD275 (B7-H2, ICOSL)	GTGCATTCAACAGTA	A0009	2D3	proprietary	CD275--B7-H2--ICOSL	399907	BioLegend
	CD314 (NKG2D)	CGTGTTTGTTCCTCA	A0165	1D11	proprietary	CD314--NKG2D	399907	BioLegend
	CD86	GTCTTTGTCAGTGCA	A0006	IT2.2	proprietary	CD86.1	399907	BioLegend
	Galectin-9	ACTCACTGGAGTCTC	A0016	9M1-3	proprietary	N/A	399907	BioLegend
	CD195 (CCR5)	CCAAAGTAAGAGCCA	A0141	J418F1	proprietary	CD195--CCR5	399907	BioLegend
	CD1c	GAGCTACTTCACTCG	A0160	L161	proprietary	CD1c	399907	BioLegend
	CD28	TGAGAACGACCCTAA	A0386	CD28.2	proprietary	CD28.1	399907	BioLegend
	TSLPR (TSLP-R)	CAGTCCTCTCTGTCA	A0387	1D3	proprietary	TSLPR	399907	BioLegend
	CD38	TGTACCCGCTTGTGA	A0389	HIT2	proprietary	CD38.1	399907	BioLegend
	CD155 (PVR)	ATCACATCGTTGCCA	A0023	SKII.4	proprietary	CD155--PVR	399907	BioLegend
	CD270 (HVEM, TR2)	TGATAGAAACAGACC	A0020	122	proprietary	CD270--HVEM--TR2	399907	BioLegend
	CD178 (Fas-L)	CCGGTCCTCTGTATT	A0177	NOK-1	proprietary	CD178--FasL	399907	BioLegend
	CD127 (IL-7Rα)	GTGTGTTGTCCTATG	A0390	A019D5	proprietary	CD127--IL-7Ra	399907	BioLegend
	CD7	TGGATTCCCGGACTT	A0066	CD7-6B7	proprietary	CD7.1	399907	BioLegend
	CD117 (c-kit)	AGACTAATAGCTGAC	A0061	104D2	proprietary	CD117--c-kit	399907	BioLegend
	CD10	CAGCCATTCATTAGG	A0062	HI10a	proprietary	CD10	399907	BioLegend
	CD40	CTCAGATGGAGTATG	A0031	5C3	proprietary	CD40.1	399907	BioLegend
	CD48	CTACGACGTAGAAGA	A0029	BJ40	proprietary	CD48.1	399907	BioLegend
	CD154	GCTAGATAGATGCAA	A0032	24-31	proprietary	CD154	399907	BioLegend
	CD47	GCATTCTGTCACCTA	A0026	CC2C6	proprietary	CD47.1	399907	BioLegend
	CD112 (Nectin-2)	AACCTTCCGTCTAAG	A0024	TX31	proprietary	CD112--Nectin-2	399907	BioLegend
	CD52	CTTTGTACGAGCAAA	A0033	HI186	proprietary	CD52.1	399907	BioLegend
	CD71	CCGTGTTCCTCATTA	A0394	CY1G4	proprietary	CD71	399907	BioLegend
	CD22	GGGTTGTTGTCTTTG	A0393	S-HCL-1	proprietary	CD22.1	399907	BioLegend
	CD15 (SSEA-1)	TCACCAGTACCTAGT	A0392	W6D3	proprietary	CD15--BEA-1	399907	BioLegend

XCR1	AAGACGCATGTCAAC	A0208	S15046E	proprietary	XCR1.1	399907	BioLegend
CD26	GGTGGCTAGATAATG	A0396	BA5b	proprietary	CD26	399907	BioLegend
B7-H4	TGTATGTCTGCCTTG	A0395	MIH43	proprietary	B7-H4	399907	BioLegend
CD31	ACCTTTATGCCACGG	A0124	WM59	proprietary	CD31	399907	BioLegend
CD14	TCTCAGACCTCCGTA	A0081	M5E2	proprietary	CD14.2	399907	BioLegend
TIGIT (VSTM3)	TTGCTTACCGCCAGA	A0089	A15153G	proprietary	TIGIT--VSTM3	399907	BioLegend
CD294 (CRTH2)	TGTTTACGAGAGCCC	A0102	BM16	proprietary	CD294--CRTH2	399907	BioLegend
CD45	TCCCTTGCGATTTAC	A0048	2D1	proprietary	CD45	399907	BioLegend
CD34	GCAGAAATCTCCCTT	A0054	581	proprietary	CD34.1	399907	BioLegend
CD244 (2B4)	TCGCTTGGATGGTAG	A0189	C1.7	proprietary	CD244--2B4	399907	BioLegend
CD185 (CXCR5)	AATTCAACCGTCGCC	A0144	J252D4	proprietary	CD185--CXCR5	399907	BioLegend
CD18	TATTGGGACACTTCT	A0385	TS1/18	proprietary	CD18	399907	BioLegend
CD119 (IFN-? R ? chain)	TGTGTATTCCCTTGT	A0219	GIR-208	proprietary	CD119--IFN-G-R-A-chain	399907	BioLegend
CD134 (OX40)	AACCCACCGTTGTTA	A0158	Ber-ACT35 (ACT35)	proprietary	CD134--OX40	399907	BioLegend
CD24	AGATTCCTTCGTGTT	A0180	ML5	proprietary	CD24.1	399907	BioLegend
TCR γ/δ	CTTCCGATTCATTCA	A0139	B1	proprietary	TCR-G--TCR-D	399907	BioLegend
CD115 (CSF-1R)	AATCACGGTCCTTGT	A0398	9-4D2-1E4	proprietary	CD115--CSF-1R	399907	BioLegend
CD1d	TCGAGTCGCTTATCA	A0164	51.1	proprietary	CD1d	399907	BioLegend
CD192 (CCR2)	GAGTTCCCTTACCTG	A0242	K036C2	proprietary	CD192--CCR2	399907	BioLegend
CD105	ATCGTCGAGAGCTAG	A0068	43A3	proprietary	CD105	399907	BioLegend
CD144 (VE-Cadherin)	TCCACTCATTCTGTA	A0400	BV9	proprietary	CD144--VE-cadherin	399907	BioLegend
CD193 (CCR3)	ACCAATCCTTTCGTC	A0397	5E8	proprietary	CD193--CCR3	399907	BioLegend
CD55	GCTCATTACCCATTA	A0383	JS11	proprietary	CD55.1	399907	BioLegend
CD79b (Igβ)	ATTCTTCAACCGAAG	A0187	CB3-1	proprietary	CD79b--Ig-B	399907	BioLegend
CD123	CTTCACTCTGTCAGG	A0064	6H6	proprietary	CD123	399907	BioLegend
CD11c	TACGCCTATAACTTG	A0053	S-HCL-3	proprietary	CD11c	399907	BioLegend
CD54	CTGATAGACTTGAGT	A0217	HA58	proprietary	CD54	399907	BioLegend
CD268 (BAFF-R)	CGAAGTCGATCCGTA	A0215	11C1	proprietary	CD268--BAFF-R	399907	BioLegend
TIM-4	CGTCATATAGTATGG	A0428	9F4	proprietary	Tim-4	399907	BioLegend
CD1a	GATCGTGTTGTGTTA	A0402	HI149	proprietary	CD1a	399907	BioLegend
CD301 (CLEC10A)	ACCTAGAAATCAGCA	A0401	H037G3	proprietary	CD301--CLEC10A	399907	BioLegend
CD63	GAGATGTCTGCAACT	A0404	H5C6	proprietary	CD63.1	399907	BioLegend
CD44	AATCCTTCCGAATGT	A0125	BJ18	proprietary	CD44.1	399907	BioLegend
IgD	CAGTCTCCGTAGAGT	A0384	IA6-2	proprietary	IgD	399907	BioLegend
CD72	CAGTCGTGGTAGATA	A0419	3F3	proprietary	CD72.1	399907	BioLegend
CD93	GCGCTACTTCCTTGA	A0446	VIMD2	proprietary	CD93.1	399907	BioLegend
CD85g (ILT7)	TGTCAGTTCCTATGA	A0409	17G10.2	proprietary	CD85g--ILT7	399907	BioLegend
CD172a (SIRPα)	CGTGTTTAACTTGAG	A0408	15-414	proprietary	CD172a--SIRPa	399907	BioLegend
CD284 (TLR4)	GCTTAGCTGTATCCG	A0405	HTA125	proprietary	CD284--TLR4	399907	BioLegend
CD304 (Neuropilin-1)	GGACTAAGTTTCGTT	A0406	12C2	proprietary	CD304--Neuropilin-1	399907	BioLegend
CD36	TTCTTTGCCTTGCCA	A0407	5-271	proprietary	CD36.1	399907	BioLegend
CD102 (ICAM-2)	TGACCTTCCTCTCCT	A0244	CBR-IC2/2	proprietary	CD102	399907	BioLegend
TCR α/β	CGTAACGTAGAGCGA	A0224	IP26	proprietary	TCR-A--TCR-B	399907	BioLegend
CD122 (IL-2R?)	TCATTTCCTCCGATT	A0246	TU27	proprietary	N/A	399907	BioLegend
CD83	CCACTCATTTCCGGT	A0359	HB15e	proprietary	CD83.1	399907	BioLegend
CD267 (TACI)	AGTGATGGAGCGAAC	A0247	1A1	proprietary	CD267--TACI	399907	BioLegend
anti-human IgA	AAGATGTCCGAGCAA	A0186	#N/A	proprietary	N/A	399907	BioLegend
CD107a (LAMP-1)	CAGCCCACTGCAATA	A0155	H4A3	proprietary	CD107a--LAMP-1	399907	BioLegend
CD146	CCTTGGATAACATCA	A0134	P1H12	proprietary	CD146	399907	BioLegend
CD140b (PDGFR?)	CAATGGTTCACTGCC	A0129	18A2	proprietary	CD140b	399907	BioLegend
CD49a	ACTGATGGACTCAGA	A0575	TS2/7	proprietary	CD49a	399907	BioLegend
α	AACTTCTGTGGTAGC	A0584	6B11	proprietary	TCR-V-A-24-J-A-18--iNKT cell	399907	BioLegend
CD9	GAGTCACCAATCTGC	A0579	HI9a	proprietary	CD9.1	399907	BioLegend
TCR Vα7.2	TACGAGCAGTATTCA	A0581	3C10	proprietary	TCR-V-A-7.2	399907	BioLegend
TCR Vγ9	AAGTGATGGTATCTG	A0583	B3	proprietary	TCR-V-G-9	399907	BioLegend
CD49d	CCATTCAACTTCCGG	A0576	9F10	proprietary	CD49d	399907	BioLegend
C5L2	ACAATTTGTCTGCGA	A0572	1D9-M12	proprietary	C5L2	399907	BioLegend
CD338 (ABCG2)	TAAGACTTGGCCGTC	A0569	5D3	proprietary	CD338--ABCG2	399907	BioLegend
CD73 (Ecto-5'-nucleotidase)	CAGTTCCTCAGTTCG	A0577	AD2	proprietary	CD73--Ecto-5-nucleotidase	399907	BioLegend
anti-human CD79a (Ig?)	CTTATCACCCGCTTT	A0578	#N/A	proprietary	N/A	399907	BioLegend
CD158b (KIR2DL2/L3, NKAT2)	GACCCGTAGTTTGAT	A0592	DX27	proprietary	CD158b--KIR2DL2--KIR2DL3--NKAT2	399907	BioLegend
CD226 (DNAM-1)	AGACCAACTCATTCA	A0805	TX25	proprietary	CD226--DNAM-1.1	399907	BioLegend
CD186 (CXCR6)	GACAGTCGATGCAAC	A0804	K041E5	proprietary	CD186--CXCR6	399907	BioLegend
CD158f (KIR2DL5)	AAAGTGATGCCACTG	A0600	UP-R1	proprietary	CD158f--KIR2DL5	399907	BioLegend
CD158e1 (KIR3DL1, NKB1)	GGACGCTTTCCTTGA	A0599	DX9	proprietary	CD158e1--KIR3DL1--NKB1	399907	BioLegend
CD140a (PDGFR?)	ATGCGCCGAGAATTA	A0128	16A1	proprietary	CD140a	399907	BioLegend
CD354 (TREM-1)	TAGCCGTTTCCTTTG	A0586	TREM-26	proprietary	N/A	399907	BioLegend
TCR Vδ2	TCAGTCAGATGGTAT	A0582	B6	proprietary	TCR-V-D-2	399907	BioLegend
CD202b (Tie2/Tek)	CGATCCCTTACCTAT	A0588	33.1 (Ab33)	proprietary	CD202b--Tie2--Tek	399907	BioLegend
CD96 (TACTILE)	TGGCCTATAAATGGT	A0175	NK92.39	proprietary	CD96--TACTILE	399907	BioLegend
CD158 (KIR2DL1/S1/S3/S5)	TATCAACCAACGCTT	A0420	HP-MA4	proprietary	CD158--KIR2DL1--KIR2DS1--KIR2DS3--KIR2DS5	399907	BioLegend
CD337 (NKp30)	AAAGTCACTCTGCCG	A0801	P30-15	proprietary	CD337--NKp30	399907	BioLegend
CD253 (Trail)	GCCATTCCTGCCTAA	A0803	RIK-2	proprietary	CD253--TRAIL	399907	BioLegend
CD319 (CRACC)	AGTATGCCATGTCTT	A0830	162.1	proprietary	CD319--CRACC	399907	BioLegend
CD305 (LAIR1)	ATTTCCATTCCCTGT	A0590	NKTA255	proprietary	CD305--LAIR1	399907	BioLegend
CD325 (N-Cadherin)	CCTTCCCTTTCCTCT	A0433	8C11	proprietary	CD325--N-Cadherin	399907	BioLegend
mast cell tryptase	ACTGATAGACCCGCT	A0580	AA1	proprietary	N/A	399907	BioLegend
CLEC12A	CATTAGAGTCTGCCA	A0853	50C1	proprietary	CD371--CLEC12A	399907	BioLegend
CD90 (Thy1)	GCATTGTACGATTCA	A0060	5E10	proprietary	CD90--Thy1	399907	BioLegend
CD273 (B7-DC, PD-L2)	TCAACGCTTGGCTAG	A0008	24F.10C12	proprietary	CD273--B7-DC--PD-L2	399907	BioLegend
CD272 (BTLA)	GTTATTGGACTAAGG	A0170	MIH26	proprietary	CD272--BTLA	399907	BioLegend
CD5	CATTAACGGGATGCC	A0138	UCHT2	proprietary	CD5.1	399907	BioLegend
CD23	TCTGTATAACCGTCT	A0897	EBVCS-5	proprietary	CD23	399907	BioLegend
CD85j (ILT2)	CCTTGTGAGGCTATG	A0896	GHI/75	proprietary	CD85j--ILT2	399907	BioLegend
CD94	CTTTCCGGTCCTACA	A0867	DX22	proprietary	CD94	399907	BioLegend
CD27	GCACTCCTGCATGTA	A0154	O323	proprietary	CD27.1	399907	BioLegend
CD328 (Siglec-7)	CTTAGCATTTCACTG	A0902	6-434	proprietary	CD328--Siglec-7	399907	BioLegend
CD82	TCCCACTTCCGCTTT	A0920	ASL-24	proprietary	N/A	399907	BioLegend
CD16	AAGTTCACTCTTTGC	A0083	3G8	proprietary	CD16	399907	BioLegend
MERTK	TCCTGCATGTACCCA	A0423	590H11G1E3	proprietary	MERTK.1	399907	BioLegend

	IgG Fc	CTGGAGCGATTAGAA	A0375	M1310G05	proprietary	IgG-Fc	399907	BioLegend
	FcεRIα	CTCGTTTCCGTATCG	A0352	AER-37 (CRA-1)	proprietary	FceRIa	399907	BioLegend
	CD274 (B7-H1, PD-L1)	GTTGTCCGACAATAC	A0007	29E.2A3	proprietary	CD274--B7-H1--PD-L1	399907	BioLegend
	CD254 (TRANCE, RANKL)	TCCGTGTTAGTTTGT	A0356	MIH24	proprietary	CD254--TRANCE--RANKL	399907	BioLegend
	CX3CR1	AGTATCGTCTCTGGG	A0179	K0124E1	proprietary	CX3CR1.1	399907	BioLegend
	CD137L (4-1BB Ligand)	ATTCGCCTTACGCAA	A0022	5F4	proprietary	CD137L--4-1BB-Ligand	399907	BioLegend
	Siglec-8	CTTCTCCTCAGCAAT	A0199	7C9	proprietary	N/A	399907	BioLegend
	CD45	89	Y	HI30	1.5		304002	BioLegend
	EpCAM	115	In	9C4	1.5		324202	BioLegend
	CD7	139	La	M-T701	1.5		555359	BD Bioscience
	CD15	140	Ce	W6D3	1.5		323002	BioLegend
	CD3	141	Pr	UCHT1	0.4		300402	BioLegend
	CD19	142	Nd	HIB19	0.4		302202	BioLegend
	CD163	144	Nd	GHI61	3		333602	BioLegend
	CD4	145	Nd	RPA-T4	0.4		14-0049-82	Thermo
	CD8a	146	Nd	RPA-T8	0.4		301002	BioLegend
	CD11c	147	Sm	BU15	0.4		MA1-82142	Thermo
	CD14	148	Nd	M5E2	1.5		301802	BioLegend
	CD127	149	Sm	A019D5	1.5		351302	BioLegend
	CD123	151	Eu	6H6	0.8		14-1239-82	Thermo
	gdTCR	152	Sm	5A6.E9	0.4		HB-9772	ATCC
	CD45RA	153	Eu	HI100	1.5		304102	BioLegend
	TIM3	154	Sm	F38-2E2	3		345002	BioLegend
	TIGIT	155	Gd	A15153G	1.5		372720	BioLegend
	PD-L1	156	Gd	29E.2A3	1.5		329702	BioLegend
CyTOF	Integrin a4	157	Gd	9F10	1.5		304302	BioLegend
	CD27	158	Gd	O323	0.4		302802	BioLegend
	CD137_4-1BB	159	Tb	4B4-1	1.5		14-9056-82	Thermo
	Tbet	160	Gd	4B10	0.4		14-5825-82	Thermo
	CTLA-4	161	Dy	14D3	0.4		14-1529-82	Thermo
	FOXP3	162	Dy	PCH101	0.8		14-4776-82	Thermo
	CD31	163	Dy	WM59	0.8		303102	BioLegend
	Integrin b7	165	Ho	FIB504	1.5		321202	BioLegend
	CD141_BDCA3	166	Er	M80	0.8		344102	BioLegend
	CCR7	167	Er	GO43H7	1.5		353202	BioLegend
	Ki-67	168	Er	Ki-67	0.8		350502	BioLegend
	CD25	169	Tm	M-A251	0.4		356102	BioLegend
	CD1c_BDCA1	170	Er	L161	0.8		331502	BioLegend
	CD38	172	Yb	HIT2	0.4		303502	BioLegend
	ICOS	173	Yb	C398.4A	0.8		313502	BioLegend
	HLA-DR	174	Yb	L243	1.5		307665	BioLegend
	PD-1	175	Lu	EH12.2H7	1.5		329902	BioLegend
	CD56	176	Yb	NCAM16.2	0.8		559043	BD Bioscience
	CD16	209	Bi	3G8	0.4		302049	BioLegend
	COL1A2	488		432721-T1				ACD bio-techne
	MS4A1	550		426771-T2				ACD bio-techne
	FLT3	650		419491-T3				ACD bio-techne
	ITGα4	488		408591-T4				ACD bio-techne
	MZB1	550		579241-T5				ACD bio-techne
RNA-ISH	*C1QA*	650		485451-T6				ACD bio-techne
	ITGβ7	488		605941-T7				ACD bio-techne
	MAdCAM-1	550		404711-T8				ACD bio-techne
	KRT8	650		310261-T9				ACD bio-techne
	PECAM-1	488		487381-T10				ACD bio-techne
	CD3E	550		553971-T11				ACD bio-techne
	PTPRC	650		601991-T12				ACD bio-techne
	HLA-A	AF750	BX004	EP1395Y	1:200		ab216653	Abcam
	CD34	ATTO550	BX020	QBEND/10	1:150		MA1-10205	Thermofisher
	CD4	Cy5	BX003	EPR6855	1:200		ab133616	Abcam
	CD20	AF750	BX007	L26	1:200		14-0202-82	Thermofisher
	CD14	ATTO550	BX037	EPR3653	1:500		ab133335	Abcam
	CD68	Cy5	BX015	KP1	1:200		MA5-13324	Thermofisher
	Vimentin	AF750	BX022	091D3	1:200		677802	BioLegend
	CD8	ATTO550	BX026	C8/144B	1:200		372908	BioLegend
	CD11c	Cy5	BX024	118/A5	1:200		14-9761-82	Thermofisher
	CD31	AF750	BX001	EP3095	1:100		ab134168	Abcam
	E-Cadherin	ATTO550	BX014	4A2C7	1:300		33-4000	Thermofisher
	CD45	Cy5	BX021	D9M8I	1:300		#13917	CST
	SMA	AF750	BX013	1A4	1:200		ab7817	Abcam
CODEX	CD45RO	ATTO550	BX017	UCHL1	1:200		304202	BioLegend
	CD3e	Cy5	BX045	EP449E	1:200		ab52959	Abcam
	Pan-cytokeratin	AF750	BX019	AE1/AE3	1:200		914204	BioLegend
	CD44	ATTO550	BX005	156-3C11	1:400		#3570	CST
	HLA-DR	Cy5	BX033	EPR3692	1:200		ab92511	Abcam
	Granzyme B	ATTO550	BX041	D6E9W	1:50		#46890	CST
	Collagen IV	Cy5	BX042	EPR209660	1:200		ab214417	Abcam
	Podoplanin	ATTO550	BX023	NC-08	1:200		337002	BioLegend
	FOXP3	AF647	BX031	259D/C7	1:100		560044	BD Pharmigen
	KI67	ATTO550	BX047	B56	1:300		556003	BD Pharmigen
	CD163	AF647	BX016	D6U1J	1:50		#93498	CST
	CD19	ATTO550	BX028	RM332	1:50		31-1219-00	RevMab
	CD11b	Cy5	BX030	EP1345Y	1:50		ab52478	Abcam
	CD21	ATTO550	BX032	EP3093	1:400		ab75985	Abcam
	CD57	AF647	BX049	HNK-1	1:100		359610	BioLegend
	dsDNA	89	Y	3519 DNA	0.2		ab27156	Abcam
	E-Cadherin	113	In	36	0.5		ab287971	Abcam
	Histone H3	115	In	D1H2	1:100		711501-100	Ionpath
	FoxP3-AF488	141	Pr	236A/E7	2		561181	BD Pharmigen
	anti-488	141	Pr	polyclonal	3		#A-11094	Thermofisher
	CD163	142	Nd	EPR14643-36	0.6		ab215976	Abcam
	CD4	143	Nd	EPR6855	1:100		714301-100	Ionpath

	CD11c	144	Nd	EP1347Y	1:100		714401-100	Ionpath
	CD14	145	Nd	D7A2T	0.6		#43878	CST
	CD16	146	Nd	D1N9L	0.6		#72204	CST
	LAG3	147	Sm	17B4	5		NBP1-97657	Novus
	PD-1	148	Nd	D4W2J	1:100		714801-100	Ionpath
	PD-L1	149	Sm	E1L3N	1:100		714902-100	Ionpath
	Granzyme B	150	Nd	D6E9W	1:100		715002-100	Ionpath
	CD56	151	Eu	MRQ-42	1:100		715101-100	Ionpath
	CD31	152	Sm	EP3095	1:100		715201-100	Ionpath
	Ki67	153	Eu	D2H10	0.15		#44092	CST
	CD138	154	Sm	EPR6454	5		ab2261108	Abcam
	CD117	155	Gd	YR145	1:100		715501-100	Ionpath
MIBI	CD68	156	Gd	D4B9C	1:100		715601-100	Ionpath
	CD103	157	Gd	EPR4166(2)	15		ab271889	Abcam
	CD8	158	Gd	C8/144B	1:100		715801-100	Ionpath
	CD3	159	Tb	D7A6E	1:100		715903-100	Ionpath
	Tbet	160	Gd	D6N8B	5		#27112	CST
	CD45RO	161	Dy	UCHL1	1:100		716101-100	ionpath
	TIM3	162	Dy	EPR22241	1:100		716201-100	Ionpath
	Vimentin	163	Dy	D21H3	1:100		716301-100	Ionpath
	CD27	164	Dy	EPR8569	5		ab256583	Abcam
	Pan-Keratin	165	Ho	AE1/AE3	1:100		716501-100	Ionpath
	aSMA	166	Er	SP171	2.5		ab242395	Abcam
	CD20	167	Er	L26	1:100		716701-100	Abcam
	CD11b	168	Er	D6X1N	0.5		ab187537	Abcam
	BDCA3 (CD141)	169	Tm	E7Y9P	10		#34149	CST
	CD21	170	Er	EP3093	1:100		717001-100	Ionpath
	IDO1	171	Yb	EPR20374	1:100		717101-100	Ionpath
	HLA-DR	172	Yb	EPR3692	1:100		717201-100	Ionpath
	EpCAM	173	Yb	D9S3P	0.5		#55725	CST
	CD45	175	Yb	2B11/PD7/26	1:100		717501-100	Ionpath
	HLA Class 1, ABC	176	Yb	EMR8-5	1:100		717602-100	Ionpath
CosMx SMI 960-plex panel	*AATK*							Nanostring
	ABL1							Nanostring
	ABL2							Nanostring
	ACE							Nanostring
	ACE2							Nanostring
	ACKR1							Nanostring
	ACKR3							Nanostring
	ACKR4							Nanostring
	ACTA2							Nanostring
	ACTG2							Nanostring
	ACVR1							Nanostring
	ACVR1B							Nanostring
	ACVR2A							Nanostring
	ACVRL1							Nanostring
	ADGRA2							Nanostring
	ADGRA3							Nanostring
	ADGRB2							Nanostring
	ADGRB3							Nanostring
	ADGRD1							Nanostring
	ADGRE1							Nanostring
	ADGRE2							Nanostring
	ADGRE5							Nanostring
	ADGRF1							Nanostring
	ADGRF3							Nanostring
	ADGRF4							Nanostring
	ADGRF5							Nanostring
	ADGRG1							Nanostring
	ADGRG2							Nanostring
	ADGRG3							Nanostring
	ADGRG5							Nanostring
	ADGRG6							Nanostring
	ADGRL1							Nanostring
	ADGRL2							Nanostring
	ADGRL4							Nanostring
	ADGRV1							Nanostring
	ADIPOQ							Nanostring
	ADIRF							Nanostring
	ADM2							Nanostring
	ADORA2A							Nanostring
	AGR2							Nanostring
	AHI1							Nanostring
	AHR							Nanostring
	AKT1							Nanostring
	ALCAM							Nanostring
	ANGPT1							Nanostring
	ANGPT2							Nanostring
	ANGPT4							Nanostring
	ANGPTL1							Nanostring
	ANXA1							Nanostring
	ANXA2							Nanostring
	ANXA4							Nanostring
	APOA1							Nanostring
	APOB							Nanostring
	APOD							Nanostring
	APP							Nanostring
	AQP3							Nanostring
	AR							Nanostring
	AREG							Nanostring
	ARF1							Nanostring

ARG1	Nanostring
ARHGDIB	Nanostring
ARTN	Nanostring
ATF3	Nanostring
ATG10	Nanostring
ATG12	Nanostring
ATG5	Nanostring
ATM	Nanostring
ATR	Nanostring
AXL	Nanostring
AZGP1	Nanostring
AZU1	Nanostring
B2M	Nanostring
B3GNT7	Nanostring
BAG3	Nanostring
BATF3	Nanostring
BAX	Nanostring
BCL2	Nanostring
BCL2L1	Nanostring
BECN1	Nanostring
BEST1	Nanostring
BGN	Nanostring
BID	Nanostring
BIRC5	Nanostring
BMP1	Nanostring
BMP2	Nanostring
BMP3	Nanostring
BMP4	Nanostring
BMP5	Nanostring
BMP6	Nanostring
BMP7	Nanostring
BMPR1A	Nanostring
BMPR2	Nanostring
BMX	Nanostring
BRCA1	Nanostring
BST1	Nanostring
BST2	Nanostring
BTG1	Nanostring
BTK	Nanostring
C11orf96	Nanostring
C1QA	Nanostring
C1QB	Nanostring
C1QC	Nanostring
C5AR2	Nanostring
C9orf16	Nanostring
CALB1	Nanostring
CALD1	Nanostring
CALM1	Nanostring
CALM2	Nanostring
CALM3	Nanostring
CAMP	Nanostring
CASP3	Nanostring
CASP8	Nanostring
CASR	Nanostring
CAV1	Nanostring
CCL11	Nanostring
CCL13	Nanostring
CCL15	Nanostring
CCL18	Nanostring
CCL19	Nanostring
CCL2	Nanostring
CCL20	Nanostring
CCL21	Nanostring
CCL23	Nanostring
CCL26	Nanostring
CCL28	Nanostring
CCL3	Nanostring
CCL3L3	Nanostring
CCL4	Nanostring
CCL4L2	Nanostring
CCL5	Nanostring
CCL7	Nanostring
CCL8	Nanostring
CCND1	Nanostring
CCR1	Nanostring
CCR10	Nanostring
CCR2	Nanostring
CCR5	Nanostring
CCR7	Nanostring
CCRL2	Nanostring
CD14	Nanostring
CD163	Nanostring
CD164	Nanostring
CD19	Nanostring
CD2	Nanostring
CD209	Nanostring
CD24	Nanostring
CD27	Nanostring
CD274	Nanostring
CD276	Nanostring
CD28	Nanostring

CD300A	Nanostring
CD33	Nanostring
CD34	Nanostring
CD36	Nanostring
CD37	Nanostring
CD38	Nanostring
CD3D	Nanostring
CD3E	Nanostring
CD3G	Nanostring
CD4	Nanostring
CD40	Nanostring
CD40LG	Nanostring
CD44	Nanostring
CD47	Nanostring
CD48	Nanostring
CD52	Nanostring
CD53	Nanostring
CD55	Nanostring
CD58	Nanostring
CD59	Nanostring
CD5L	Nanostring
CD63	Nanostring
CD68	Nanostring
CD69	Nanostring
CD70	Nanostring
CD74	Nanostring
CD79A	Nanostring
CD80	Nanostring
CD81	Nanostring
CD83	Nanostring
CD84	Nanostring
CD86	Nanostring
CD8A	Nanostring
CD8B	Nanostring
CD9	Nanostring
CDH1	Nanostring
CDH11	Nanostring
CDH5	Nanostring
CDKN1A	Nanostring
CDKN3	Nanostring
CEACAM1	Nanostring
CEACAM6	Nanostring
CELSR1	Nanostring
CELSR2	Nanostring
CENPF	Nanostring
CFD	Nanostring
CFLAR	Nanostring
CHEK1	Nanostring
CHEK2	Nanostring
CHGA	Nanostring
CHI3L1	Nanostring
CIDEA	Nanostring
CIITA	Nanostring
CLCF1	Nanostring
CLDN4	Nanostring
CLEC10A	Nanostring
CLEC12A	Nanostring
CLEC14A	Nanostring
CLEC1A	Nanostring
CLEC2B	Nanostring
CLEC2D	Nanostring
CLEC4A	Nanostring
CLEC4D	Nanostring
CLEC4E	Nanostring
CLEC5A	Nanostring
CLEC7A	Nanostring
CLOCK	Nanostring
CLU	Nanostring
CMKLR1	Nanostring
CNTFR	Nanostring
COL11A1	Nanostring
COL12A1	Nanostring
COL14A1	Nanostring
COL15A1	Nanostring
COL16A1	Nanostring
COL17A1	Nanostring
COL18A1	Nanostring
COL1A1	Nanostring
COL1A2	Nanostring
COL21A1	Nanostring
COL27A1	Nanostring
COL3A1	Nanostring
COL4A1	Nanostring
COL4A2	Nanostring
COL4A5	Nanostring
COL5A1	Nanostring
COL5A2	Nanostring
COL5A3	Nanostring
COL6A1	Nanostring
COL6A2	Nanostring
COL6A3	Nanostring

COL8A1	Nanostring
COL9A1	Nanostring
COL9A2	Nanostring
COL9A3	Nanostring
COTL1	Nanostring
CPA3	Nanostring
CPB1	Nanostring
CRIP1	Nanostring
CRP	Nanostring
CRYAB	Nanostring
CSF1	Nanostring
CSF1R	Nanostring
CSF2	Nanostring
CSF2RA	Nanostring
CSF2RB	Nanostring
CSF3	Nanostring
CSF3R	Nanostring
CSHL1	Nanostring
CSK	Nanostring
CST7	Nanostring
CTLA4	Nanostring
CTNNB1	Nanostring
CTSG	Nanostring
CTSW	Nanostring
CUZD1	Nanostring
CX3CL1	Nanostring
CX3CR1	Nanostring
CXCL1	Nanostring
CXCL10	Nanostring
CXCL12	Nanostring
CXCL14	Nanostring
CXCL16	Nanostring
CXCL17	Nanostring
CXCL2	Nanostring
CXCL3	Nanostring
CXCL5	Nanostring
CXCL6	Nanostring
CXCL8	Nanostring
CXCL9	Nanostring
CXCR1	Nanostring
CXCR2	Nanostring
CXCR3	Nanostring
CXCR4	Nanostring
CXCR5	Nanostring
CXCR6	Nanostring
CYP19A1	Nanostring
CYP1B1	Nanostring
CYSTM1	Nanostring
CYTOR	Nanostring
DCN	Nanostring
DDC	Nanostring
DDIT3	Nanostring
DDR1	Nanostring
DDR2	Nanostring
DDX58	Nanostring
DHRS2	Nanostring
DLL1	Nanostring
DMBT1	Nanostring
DNMT1	Nanostring
DNMT3A	Nanostring
DNTT	Nanostring
DPP4	Nanostring
DST	Nanostring
DUSP1	Nanostring
DUSP2	Nanostring
DUSP4	Nanostring
DUSP5	Nanostring
DUSP6	Nanostring
EFNA1	Nanostring
EFNA4	Nanostring
EFNA5	Nanostring
EFNB1	Nanostring
EFNB2	Nanostring
EFNB3	Nanostring
EGF	Nanostring
EGFR	Nanostring
EIF5A	Nanostring
ELANE	Nanostring
EMP3	Nanostring
ENG	Nanostring
ENTPD1	Nanostring
EOMES	Nanostring
EPCAM	Nanostring
EPHA2	Nanostring
EPHA3	Nanostring
EPHA4	Nanostring
EPHA7	Nanostring
EPHB2	Nanostring
EPHB3	Nanostring
EPHB4	Nanostring
EPHB6	Nanostring

EPOR	Nanostring
ERBB2	Nanostring
ERBB3	Nanostring
ESAM	Nanostring
ESR1	Nanostring
ETS1	Nanostring
ETV4	Nanostring
ETV5	Nanostring
EZH2	Nanostring
EZR	Nanostring
FABP4	Nanostring
FABP5	Nanostring
FAS	Nanostring
FASLG	Nanostring
FASN	Nanostring
FCER1G	Nanostring
FCGBP	Nanostring
FCGR3A	Nanostring
FCRLA	Nanostring
FES	Nanostring
FFAR2	Nanostring
FFAR3	Nanostring
FFAR4	Nanostring
FGF1	Nanostring
FGF12	Nanostring
FGF13	Nanostring
FGF18	Nanostring
FGF2	Nanostring
FGF7	Nanostring
FGF9	Nanostring
FGFR1	Nanostring
FGFR2	Nanostring
FGFR3	Nanostring
FGG	Nanostring
FGR	Nanostring
FKBP11	Nanostring
FLT1	Nanostring
FLT3LG	Nanostring
FN1	Nanostring
FOS	Nanostring
FOXF1	Nanostring
FOXP3	Nanostring
FPR1	Nanostring
FYB1	Nanostring
FYN	Nanostring
FZD1	Nanostring
FZD3	Nanostring
FZD4	Nanostring
FZD5	Nanostring
FZD6	Nanostring
FZD7	Nanostring
FZD8	Nanostring
G6PC2	Nanostring
G6PD	Nanostring
GADD45B	Nanostring
GAS6	Nanostring
GATA3	Nanostring
GC	Nanostring
GCG	Nanostring
GDF10	Nanostring
GDF15	Nanostring
GDF3	Nanostring
GDF6	Nanostring
GDF9	Nanostring
GDNF	Nanostring
GLUD1	Nanostring
GLUL	Nanostring
GNLY	Nanostring
GPBAR1	Nanostring
GPER1	Nanostring
GPNMB	Nanostring
GPR183	Nanostring
GPX1	Nanostring
GPX3	Nanostring
GSN	Nanostring
GSTP1	Nanostring
GZMA	Nanostring
GZMB	Nanostring
GZMH	Nanostring
GZMK	Nanostring
H2AZ1	Nanostring
H4C3	Nanostring
HAVCR2	Nanostring
HBA1	Nanostring
HBB	Nanostring
HCAR2	Nanostring
HCAR3	Nanostring
HCK	Nanostring
HCST	Nanostring
HDAC1	Nanostring
HDAC11	Nanostring

HDAC3	Nanostring
HDAC4	Nanostring
HDAC5	Nanostring
HGF	Nanostring
HIF1A	Nanostring
HILPDA	Nanostring
HLA-A	Nanostring
HLA-B	Nanostring
HLA-C	Nanostring
HLA-DPA1	Nanostring
HLA-DPB1	Nanostring
HLA-DQA1	Nanostring
HLA-DQB1	Nanostring
HLA-DRA	Nanostring
HLA-DRB1	Nanostring
HLA-DRB5	Nanostring
HLA-E	Nanostring
HMGB2	Nanostring
HMGN2	Nanostring
HPGDS	Nanostring
HSD17B2	Nanostring
HSD3B2	Nanostring
HSP90AA1	Nanostring
HSP90AB1	Nanostring
HSP90B1	Nanostring
HSPA1A	Nanostring
HSPA1B	Nanostring
HSPB1	Nanostring
HTT	Nanostring
IAPP	Nanostring
ICAM1	Nanostring
ICAM2	Nanostring
ICAM3	Nanostring
ICOS	Nanostring
ICOSLG	Nanostring
IDO1	Nanostring
IER3	Nanostring
IFI27	Nanostring
IFIH1	Nanostring
IFIT1	Nanostring
IFITM1	Nanostring
IFITM3	Nanostring
IFNA1	Nanostring
IFNAR1	Nanostring
IFNAR2	Nanostring
IFNB1	Nanostring
IFNG	Nanostring
IFNGR1	Nanostring
IFNGR2	Nanostring
IFNL2	Nanostring
IFNL3	Nanostring
IGF1	Nanostring
IGF1R	Nanostring
IGF2	Nanostring
IGF2R	Nanostring
IGFBP3	Nanostring
IGFBP5	Nanostring
IGFBP6	Nanostring
IGFBP7	Nanostring
IGHA1	Nanostring
IGHD	Nanostring
IGHG1	Nanostring
IGHG2	Nanostring
IGHM	Nanostring
IGKC	Nanostring
IL10	Nanostring
IL10RA	Nanostring
IL10RB	Nanostring
IL11	Nanostring
IL11RA	Nanostring
IL12A	Nanostring
IL12B	Nanostring
IL12RB1	Nanostring
IL12RB2	Nanostring
IL13RA1	Nanostring
IL15	Nanostring
IL15RA	Nanostring
IL16	Nanostring
IL17A	Nanostring
IL17B	Nanostring
IL17D	Nanostring
IL17RA	Nanostring
IL17RB	Nanostring
IL17RE	Nanostring
IL18	Nanostring
IL18R1	Nanostring
IL1A	Nanostring
IL1B	Nanostring
IL1R1	Nanostring
IL1R2	Nanostring
IL1RAP	Nanostring

IL1RL1	Nanostring
IL1RN	Nanostring
IL2	Nanostring
IL20	Nanostring
IL20RA	Nanostring
IL22RA1	Nanostring
IL23A	Nanostring
IL24	Nanostring
IL27RA	Nanostring
IL2RA	Nanostring
IL2RB	Nanostring
IL2RG	Nanostring
IL32	Nanostring
IL33	Nanostring
IL34	Nanostring
IL36G	Nanostring
IL3RA	Nanostring
IL4R	Nanostring
IL6	Nanostring
IL6R	Nanostring
IL6ST	Nanostring
IL7	Nanostring
IL7R	Nanostring
INHA	Nanostring
INHBA	Nanostring
INHBB	Nanostring
INS	Nanostring
INSR	Nanostring
IRF3	Nanostring
IRF4	Nanostring
ITGA1	Nanostring
ITGA2	Nanostring
ITGA3	Nanostring
ITGA5	Nanostring
ITGA6	Nanostring
ITGA9	Nanostring
ITGAE	Nanostring
ITGAL	Nanostring
ITGAM	Nanostring
ITGAV	Nanostring
ITGAX	Nanostring
ITGB1	Nanostring
ITGB2	Nanostring
ITGB4	Nanostring
ITGB5	Nanostring
ITGB6	Nanostring
ITGB8	Nanostring
ITK	Nanostring
ITM2A	Nanostring
JAG1	Nanostring
JAK1	Nanostring
JAK2	Nanostring
JCHAIN	Nanostring
JUN	Nanostring
JUNB	Nanostring
KDR	Nanostring
KIT	Nanostring
KITLG	Nanostring
KLF2	Nanostring
KLK3	Nanostring
KLRB1	Nanostring
KLRK1	Nanostring
KRAS	Nanostring
KRT1	Nanostring
KRT10	Nanostring
KRT13	Nanostring
KRT14	Nanostring
KRT15	Nanostring
KRT16	Nanostring
KRT17	Nanostring
KRT18	Nanostring
KRT19	Nanostring
KRT20	Nanostring
KRT23	Nanostring
KRT24	Nanostring
KRT4	Nanostring
KRT5	Nanostring
KRT6A	Nanostring
KRT6B	Nanostring
KRT6C	Nanostring
KRT7	Nanostring
KRT8	Nanostring
KRT80	Nanostring
KRT86	Nanostring
LAG3	Nanostring
LAIR1	Nanostring
LAMP2	Nanostring
LAMP3	Nanostring
LCN2	Nanostring
LDLR	Nanostring
LEFTY1	Nanostring

LEFTY2	Nanostring
LEP	Nanostring
LGALS1	Nanostring
LGALS3	Nanostring
LGALS3BP	Nanostring
LGALS9	Nanostring
LIF	Nanostring
LIFR	Nanostring
LINC02446	Nanostring
LMNA	Nanostring
LPAR5	Nanostring
LTB	Nanostring
LTBR	Nanostring
LTF	Nanostring
LUM	Nanostring
LY6D	Nanostring
LY75	Nanostring
LYN	Nanostring
LYZ	Nanostring
MAF	Nanostring
MALAT1	Nanostring
MAML2	Nanostring
MAP1LC3B	Nanostring
MAPK13	Nanostring
MAPK14	Nanostring
MARCO	Nanostring
MECOM	Nanostring
MEG3	Nanostring
MERTK	Nanostring
MET	Nanostring
MGP	Nanostring
MIF	Nanostring
MKI67	Nanostring
MMP1	Nanostring
MMP10	Nanostring
MMP12	Nanostring
MMP14	Nanostring
MMP16	Nanostring
MMP19	Nanostring
MMP2	Nanostring
MMP3	Nanostring
MMP7	Nanostring
MMP8	Nanostring
MMP9	Nanostring
MPO	Nanostring
MRC1	Nanostring
MRC2	Nanostring
MS4A1	Nanostring
MS4A4A	Nanostring
MSMB	Nanostring
MST1R	Nanostring
MT1X	Nanostring
MT2A	Nanostring
MTOR	Nanostring
MTRNR2L1	Nanostring
MX1	Nanostring
MXRA8	Nanostring
MYC	Nanostring
MYH11	Nanostring
MYL9	Nanostring
MZB1	Nanostring
MZT2A	Nanostring
NANOG	Nanostring
NCR1	Nanostring
NDRG1	Nanostring
NEAT1	Nanostring
NFKB1	Nanostring
NFKBIA	Nanostring
NGFR	Nanostring
NKG7	Nanostring
NLRC4	Nanostring
NLRC5	Nanostring
NLRP1	Nanostring
NLRP2	Nanostring
NLRP3	Nanostring
NOD2	Nanostring
NOSIP	Nanostring
NOTCH1	Nanostring
NOTCH2	Nanostring
NOTCH3	Nanostring
NPPB	Nanostring
NPPC	Nanostring
NPR1	Nanostring
NPR2	Nanostring
NPR3	Nanostring
NR1H2	Nanostring
NR1H3	Nanostring
NR1H4	Nanostring
NR3C1	Nanostring
NRG1	Nanostring
NRG4	Nanostring

NRIP3	Nanostring
NRXN1	Nanostring
NRXN3	Nanostring
NTRK2	Nanostring
OAS1	Nanostring
OAS2	Nanostring
OAS3	Nanostring
OASL	Nanostring
OLFM4	Nanostring
OLR1	Nanostring
OSM	Nanostring
OSMR	Nanostring
OXER1	Nanostring
OXGR1	Nanostring
P2RX5	Nanostring
P2RY12	Nanostring
PARP1	Nanostring
PCNA	Nanostring
PDCD1	Nanostring
PDCD1LG2	Nanostring
PDGFA	Nanostring
PDGFB	Nanostring
PDGFC	Nanostring
PDGFD	Nanostring
PDGFRA	Nanostring
PDGFRB	Nanostring
PECAM1	Nanostring
PF4	Nanostring
PGF	Nanostring
PGR	Nanostring
PHLDA2	Nanostring
PIGR	Nanostring
PLA2R1	Nanostring
PLAC8	Nanostring
PNOC	Nanostring
POU5F1	Nanostring
PPARA	Nanostring
PPARD	Nanostring
PPARG	Nanostring
PPBP	Nanostring
PRF1	Nanostring
PROK2	Nanostring
PROKR1	Nanostring
PRSS2	Nanostring
PSAP	Nanostring
PSCA	Nanostring
PTGDR2	Nanostring
PTGDS	Nanostring
PTGES	Nanostring
PTGES2	Nanostring
PTGES3	Nanostring
PTGIS	Nanostring
PTGS1	Nanostring
PTGS2	Nanostring
PTHLH	Nanostring
PTK2	Nanostring
PTK6	Nanostring
PTPRC	Nanostring
PTPRCAP	Nanostring
PTTG1	Nanostring
QRFPR	Nanostring
RAC1	Nanostring
RAC2	Nanostring
RAD51	Nanostring
RAMP1	Nanostring
RAMP2	Nanostring
RAMP3	Nanostring
RARA	Nanostring
RARB	Nanostring
RARG	Nanostring
RARRES1	Nanostring
RARRES2	Nanostring
RB1	Nanostring
RBPJ	Nanostring
REG1A	Nanostring
RELA	Nanostring
RELT	Nanostring
RGCC	Nanostring
RGS1	Nanostring
RGS2	Nanostring
RGS5	Nanostring
RNF43	Nanostring
ROR1	Nanostring
RORA	Nanostring
RPL21	Nanostring
RPL22	Nanostring
RPL32	Nanostring
RPL34	Nanostring
RPL37	Nanostring
RPS4Y1	Nanostring
RSPO1	Nanostring

RSPO2	Nanostring
RSPO3	Nanostring
RUNX3	Nanostring
RXRA	Nanostring
RXRB	Nanostring
RYK	Nanostring
S100A10	Nanostring
S100A2	Nanostring
S100A4	Nanostring
S100A6	Nanostring
S100A8	Nanostring
S100A9	Nanostring
S100B	Nanostring
S100P	Nanostring
SAA1	Nanostring
SAA2	Nanostring
SAT1	Nanostring
SCG5	Nanostring
SCGB3A1	Nanostring
SEC23A	Nanostring
SEC61G	Nanostring
SELENOP	Nanostring
SELL	Nanostring
SELPLG	Nanostring
SERPINA1	Nanostring
SERPINA3	Nanostring
SERPINB5	Nanostring
SERPINH1	Nanostring
SFN	Nanostring
SIGIRR	Nanostring
SLC2A1	Nanostring
SLC2A4	Nanostring
SLC40A1	Nanostring
SLPI	Nanostring
SMAD2	Nanostring
SMAD3	Nanostring
SMAD4	Nanostring
SMARCB1	Nanostring
SMO	Nanostring
SNAI1	Nanostring
SNAI2	Nanostring
SOD1	Nanostring
SOD2	Nanostring
SOSTDC1	Nanostring
SOX2	Nanostring
SOX4	Nanostring
SOX9	Nanostring
SPARCL1	Nanostring
SPINK1	Nanostring
SPOCK2	Nanostring
SPP1	Nanostring
SPRY2	Nanostring
SPRY4	Nanostring
SQSTM1	Nanostring
SRC	Nanostring
SREBF1	Nanostring
SRGN	Nanostring
SST	Nanostring
ST6GAL1	Nanostring
ST6GALNAC3	Nanostring
STAT1	Nanostring
STAT3	Nanostring
STAT4	Nanostring
STAT5A	Nanostring
STAT5B	Nanostring
STAT6	Nanostring
STMN1	Nanostring
SUCNR1	Nanostring
SYK	Nanostring
TACSTD2	Nanostring
TAGLN	Nanostring
TAP1	Nanostring
TAP2	Nanostring
TBX21	Nanostring
TCL1A	Nanostring
TEK	Nanostring
TFEB	Nanostring
TGFB1	Nanostring
TGFB2	Nanostring
TGFB3	Nanostring
TGFBR1	Nanostring
TGFBR2	Nanostring
THBS1	Nanostring
THBS2	Nanostring
TIE1	Nanostring
TIGIT	Nanostring
TIMP1	Nanostring
TLR1	Nanostring
TLR2	Nanostring
TLR3	Nanostring
TLR4	Nanostring

	TLR5	Nanostring
	TLR7	Nanostring
	TLR8	Nanostring
	TM4SF1	Nanostring
	TNF	Nanostring
	TNFAIP6	Nanostring
	TNFRSF10A	Nanostring
	TNFRSF10B	Nanostring
	TNFRSF10D	Nanostring
	TNFRSF11A	Nanostring
	TNFRSF11B	Nanostring
	TNFRSF12A	Nanostring
	TNFRSF13B	Nanostring
	TNFRSF14	Nanostring
	TNFRSF17	Nanostring
	TNFRSF18	Nanostring
	TNFRSF19	Nanostring
	TNFRSF1A	Nanostring
	TNFRSF1B	Nanostring
	TNFRSF21	Nanostring
	TNFRSF4	Nanostring
	TNFRSF9	Nanostring
	TNFSF10	Nanostring
	TNFSF12	Nanostring
	TNFSF13B	Nanostring
	TNFSF14	Nanostring
	TNFSF15	Nanostring
	TNFSF18	Nanostring
	TNFSF4	Nanostring
	TNFSF8	Nanostring
	TNFSF9	Nanostring
	TOP2A	Nanostring
	TOX	Nanostring
	TP53	Nanostring
	TPM1	Nanostring
	TPM2	Nanostring
	TPSAB1	Nanostring
	TPSB2	Nanostring
	TSC22D1	Nanostring
	TSHZ2	Nanostring
	TSLP	Nanostring
	TTR	Nanostring
	TUBB	Nanostring
	TUBB4B	Nanostring
	TWIST1	Nanostring
	TWIST2	Nanostring
	TXK	Nanostring
	TYK2	Nanostring
	TYMS	Nanostring
	TYROBP	Nanostring
	UBE2C	Nanostring
	UCP1	Nanostring
	UPK3A	Nanostring
	VCAM1	Nanostring
	VCAN	Nanostring
	VEGFA	Nanostring
	VEGFB	Nanostring
	VEGFC	Nanostring
	VEGFD	Nanostring
	VHL	Nanostring
	VIM	Nanostring
	VPREB3	Nanostring
	VSIR	Nanostring
	VTN	Nanostring
	VWF	Nanostring
	WIF1	Nanostring
	WNT10B	Nanostring
	WNT11	Nanostring
	WNT2	Nanostring
	WNT2B	Nanostring
	WNT3	Nanostring
	WNT5A	Nanostring
	WNT5B	Nanostring
	WNT7A	Nanostring
	WNT7B	Nanostring
	WNT9A	Nanostring
	XBP1	Nanostring
	XCL1	Nanostring
	XCL2	Nanostring
	YBX3	Nanostring
	YES1	Nanostring
	ZFP36	Nanostring
CosMx SMI 1000-plex panel	*AATK*	Nanostring
	ABL1	Nanostring
	ABL2	Nanostring
	ACACB	Nanostring
	ACE	Nanostring
	ACKR1	Nanostring
	ACKR3	Nanostring
	ACKR4	Nanostring
	ACP5	Nanostring

ACTA2	Nanostring
ACTG2	Nanostring
ACVR1	Nanostring
ACVR1B	Nanostring
ACVR2A	Nanostring
ACVRL1	Nanostring
ADGRA2	Nanostring
ADGRA3	Nanostring
ADGRE2	Nanostring
ADGRE5	Nanostring
ADGRF1	Nanostring
ADGRF3	Nanostring
ADGRF5	Nanostring
ADGRG1	Nanostring
ADGRG3	Nanostring
ADGRG5	Nanostring
ADGRG6	Nanostring
ADGRL1	Nanostring
ADGRL2	Nanostring
ADGRL4	Nanostring
ADGRV1	Nanostring
ADIPOQ	Nanostring
ADIRF	Nanostring
ADM2	Nanostring
AGR2	Nanostring
AHI1	Nanostring
AHR	Nanostring
AIF1	Nanostring
AKT1	Nanostring
ALCAM	Nanostring
ALOX5AP	Nanostring
ANGPT1	Nanostring
ANGPT2	Nanostring
ANGPTL1	Nanostring
ANKRD1	Nanostring
ANXA1	Nanostring
ANXA2	Nanostring
ANXA4	Nanostring
APOA1	Nanostring
APOC1	Nanostring
APOD	Nanostring
APOE	Nanostring
APP	Nanostring
AQP3	Nanostring
AR	Nanostring
AREG	Nanostring
ARF1	Nanostring
ARG1	Nanostring
ARHGDIB	Nanostring
ARID5B	Nanostring
ATF3	Nanostring
ATG10	Nanostring
ATG12	Nanostring
ATG5	Nanostring
ATM	Nanostring
ATP5F1B	Nanostring
ATP5F1E	Nanostring
ATR	Nanostring
AXL	Nanostring
AZGP1	Nanostring
AZU1	Nanostring
B2M	Nanostring
B3GNT7	Nanostring
BAG3	Nanostring
BASP1	Nanostring
BAX	Nanostring
BBLN	Nanostring
BCL2	Nanostring
BCL2L1	Nanostring
BECN1	Nanostring
BEST1	Nanostring
BGN	Nanostring
BID	Nanostring
BIRC3	Nanostring
BIRC5	Nanostring
BMP1	Nanostring
BMP2	Nanostring
BMP3	Nanostring
BMP4	Nanostring
BMP5	Nanostring
BMP7	Nanostring
BMPR1A	Nanostring
BMPR2	Nanostring
BRAF	Nanostring
BRCA1	Nanostring
BST1	Nanostring
BST2	Nanostring
BTF3	Nanostring
BTG1	Nanostring
BTK	Nanostring
C11orf96	Nanostring

C1QA	Nanostring
C1QB	Nanostring
C1QC	Nanostring
C5AR2	Nanostring
CACNA1C	Nanostring
CALB1	Nanostring
CALD1	Nanostring
CALM1	Nanostring
CALM2	Nanostring
CALM3	Nanostring
CAMP	Nanostring
CARMN	Nanostring
CASP3	Nanostring
CASP8	Nanostring
CASR	Nanostring
CAV1	Nanostring
CCDC80	Nanostring
CCL11	Nanostring
CCL13	Nanostring
CCL15	Nanostring
CCL17	Nanostring
CCL18	Nanostring
CCL19	Nanostring
CCL2	Nanostring
CCL20	Nanostring
CCL21	Nanostring
CCL22	Nanostring
CCL26	Nanostring
CCL28	Nanostring
CCL3/L1/L3	Nanostring
CCL4/L1/L2	Nanostring
CCL5	Nanostring
CCL8	Nanostring
CCND1	Nanostring
CCR1	Nanostring
CCR10	Nanostring
CCR2	Nanostring
CCR5	Nanostring
CCR7	Nanostring
CCRL2	Nanostring
CD14	Nanostring
CD163	Nanostring
CD164	Nanostring
CD19	Nanostring
CD1C	Nanostring
CD2	Nanostring
CD209	Nanostring
CD22	Nanostring
CD24	Nanostring
CD27	Nanostring
CD274	Nanostring
CD276	Nanostring
CD28	Nanostring
CD300A	Nanostring
CD33	Nanostring
CD34	Nanostring
CD36	Nanostring
CD37	Nanostring
CD38	Nanostring
CD3D	Nanostring
CD3E	Nanostring
CD3G	Nanostring
CD4	Nanostring
CD40	Nanostring
CD40LG	Nanostring
CD44	Nanostring
CD47	Nanostring
CD48	Nanostring
CD52	Nanostring
CD53	Nanostring
CD55	Nanostring
CD58	Nanostring
CD59	Nanostring
CD5L	Nanostring
CD63	Nanostring
CD68	Nanostring
CD69	Nanostring
CD70	Nanostring
CD74	Nanostring
CD79A	Nanostring
CD80	Nanostring
CD81	Nanostring
CD83	Nanostring
CD84	Nanostring
CD86	Nanostring
CD8A	Nanostring
CD8B	Nanostring
CD9	Nanostring
CD93	Nanostring
CDH1	Nanostring
CDH11	Nanostring

CDH19	Nanostring
CDH5	Nanostring
CDKN1A	Nanostring
CDKN3	Nanostring
CEACAM1	Nanostring
CEACAM6	Nanostring
CELSR1	Nanostring
CELSR2	Nanostring
CENPF	Nanostring
CFD	Nanostring
CFLAR	Nanostring
CHEK1	Nanostring
CHEK2	Nanostring
CHI3L1	Nanostring
CIDEA	Nanostring
CIITA	Nanostring
CLCF1	Nanostring
CLDN4	Nanostring
CLEC10A	Nanostring
CLEC12A	Nanostring
CLEC14A	Nanostring
CLEC1A	Nanostring
CLEC2B	Nanostring
CLEC2D	Nanostring
CLEC4A	Nanostring
CLEC4D	Nanostring
CLEC4E	Nanostring
CLEC5A	Nanostring
CLEC7A	Nanostring
CLOCK	Nanostring
CLU	Nanostring
CMKLR1	Nanostring
CNTFR	Nanostring
COL11A1	Nanostring
COL12A1	Nanostring
COL14A1	Nanostring
COL15A1	Nanostring
COL16A1	Nanostring
COL17A1	Nanostring
COL18A1	Nanostring
COL1A1	Nanostring
COL1A2	Nanostring
COL21A1	Nanostring
COL27A1	Nanostring
COL3A1	Nanostring
COL4A1	Nanostring
COL4A2	Nanostring
COL4A5	Nanostring
COL5A1	Nanostring
COL5A2	Nanostring
COL5A3	Nanostring
COL6A1	Nanostring
COL6A2	Nanostring
COL6A3	Nanostring
COL8A1	Nanostring
COL9A2	Nanostring
COL9A3	Nanostring
COTL1	Nanostring
COX4I2	Nanostring
CPA3	Nanostring
CPB1	Nanostring
CRIP1	Nanostring
CRP	Nanostring
CRYAB	Nanostring
CSF1	Nanostring
CSF1R	Nanostring
CSF2	Nanostring
CSF2RA	Nanostring
CSF2RB	Nanostring
CSF3	Nanostring
CSF3R	Nanostring
CSHL1	Nanostring
CSK	Nanostring
CSPG4	Nanostring
CST7	Nanostring
CSTB	Nanostring
CTLA4	Nanostring
CTNNB1	Nanostring
CTSD	Nanostring
CTSG	Nanostring
CTSW	Nanostring
CUZD1	Nanostring
CX3CL1	Nanostring
CX3CR1	Nanostring
CXCL1/2/3	Nanostring
CXCL10	Nanostring
CXCL12	Nanostring
CXCL13	Nanostring
CXCL14	Nanostring
CXCL16	Nanostring
CXCL17	Nanostring

CXCL5	Nanostring
CXCL8	Nanostring
CXCL9	Nanostring
CXCR1	Nanostring
CXCR2	Nanostring
CXCR3	Nanostring
CXCR4	Nanostring
CXCR5	Nanostring
CXCR6	Nanostring
CYP1B1	Nanostring
CYP2U1	Nanostring
CYSTM1	Nanostring
CYTOR	Nanostring
DCN	Nanostring
DDC	Nanostring
DDIT3	Nanostring
DDR1	Nanostring
DDR2	Nanostring
DDX58	Nanostring
DHRS2	Nanostring
DLL1	Nanostring
DLL4	Nanostring
DMBT1	Nanostring
DNMT1	Nanostring
DNMT3A	Nanostring
DPP4	Nanostring
DPT	Nanostring
DST	Nanostring
DUSP1	Nanostring
DUSP2	Nanostring
DUSP4	Nanostring
DUSP5	Nanostring
DUSP6	Nanostring
EFNA1	Nanostring
EFNA4	Nanostring
EFNA5	Nanostring
EFNB1	Nanostring
EFNB2	Nanostring
EGF	Nanostring
EGFR	Nanostring
EIF5A/L1	Nanostring
ELANE	Nanostring
EMP3	Nanostring
ENG	Nanostring
ENO1	Nanostring
ENTPD1	Nanostring
EOMES	Nanostring
EPCAM	Nanostring
EPHA2	Nanostring
EPHA3	Nanostring
EPHA4	Nanostring
EPHA7	Nanostring
EPHB2	Nanostring
EPHB3	Nanostring
EPHB4	Nanostring
EPHB6	Nanostring
EPOR	Nanostring
ERBB2	Nanostring
ERBB3	Nanostring
ESAM	Nanostring
ESR1	Nanostring
ETS1	Nanostring
ETV4	Nanostring
ETV5	Nanostring
EZH2	Nanostring
EZR	Nanostring
FABP4	Nanostring
FABP5	Nanostring
FAM30A	Nanostring
FAP	Nanostring
FAS	Nanostring
FASLG	Nanostring
FASN	Nanostring
FAU	Nanostring
FCER1G	Nanostring
FCGBP	Nanostring
FCGR3A/B	Nanostring
FCRLA	Nanostring
FES	Nanostring
FFAR2	Nanostring
FFAR3	Nanostring
FFAR4	Nanostring
FGF1	Nanostring
FGF12	Nanostring
FGF13	Nanostring
FGF18	Nanostring
FGF2	Nanostring
FGF7	Nanostring
FGF9	Nanostring
FGFR1	Nanostring
FGFR2	Nanostring

FGFR3	Nanostring
FGG	Nanostring
FGR	Nanostring
FHIT	Nanostring
FKBP11	Nanostring
FKBP5	Nanostring
FLT1	Nanostring
FLT3LG	Nanostring
FN1	Nanostring
FOS	Nanostring
FOXF1	Nanostring
FOXP3	Nanostring
FPR1	Nanostring
FYB1	Nanostring
FYN	Nanostring
FZD1	Nanostring
FZD3	Nanostring
FZD4	Nanostring
FZD5	Nanostring
FZD6	Nanostring
FZD7	Nanostring
FZD8	Nanostring
G0S2	Nanostring
G6PD	Nanostring
GADD45B	Nanostring
GAS6	Nanostring
GATA3	Nanostring
GC	Nanostring
GCG	Nanostring
GDF15	Nanostring
GLUD1	Nanostring
GLUL	Nanostring
GNLY	Nanostring
GPBAR1	Nanostring
GPER1	Nanostring
GPNMB	Nanostring
GPR183	Nanostring
GPX1	Nanostring
GPX3	Nanostring
GSK3B	Nanostring
GSN	Nanostring
GSTP1	Nanostring
GZMA	Nanostring
GZMB	Nanostring
GZMH	Nanostring
GZMK	Nanostring
H2AZ1	Nanostring
H4C3	Nanostring
HAVCR2	Nanostring
HBA1/2	Nanostring
HBB	Nanostring
HCAR2/3	Nanostring
HCK	Nanostring
HCST	Nanostring
HDAC1	Nanostring
HDAC11	Nanostring
HDAC3	Nanostring
HDAC4	Nanostring
HDAC5	Nanostring
HEXB	Nanostring
HEY1	Nanostring
HGF	Nanostring
HIF1A	Nanostring
HILPDA	Nanostring
HLA-DPA1	Nanostring
HLA-DPB1	Nanostring
HLA-DQA1	Nanostring
HLA-DQB1/2	Nanostring
HLA-DRA	Nanostring
HLA-DRB	Nanostring
HMGB2	Nanostring
HMGCS1	Nanostring
HMGN2	Nanostring
HPGDS	Nanostring
HSD17B2	Nanostring
HSP90AA1	Nanostring
HSP90AB1	Nanostring
HSP90B1	Nanostring
HSPA1A/B	Nanostring
HSPB1	Nanostring
HSPG2	Nanostring
HTT	Nanostring
IAPP	Nanostring
ICA1	Nanostring
ICAM1	Nanostring
ICAM2	Nanostring
ICAM3	Nanostring
ICOS	Nanostring
ICOSLG	Nanostring
IDO1	Nanostring
IER3	Nanostring

IFI27	Nanostring
IFI44L	Nanostring
IFI6	Nanostring
IFIH1	Nanostring
IFIT1	Nanostring
IFIT3	Nanostring
IFITM1	Nanostring
IFITM3	Nanostring
IFNA1/13	Nanostring
IFNAR1	Nanostring
IFNAR2	Nanostring
IFNG	Nanostring
IFNGR1	Nanostring
IFNGR2	Nanostring
IFNL2/3	Nanostring
IGF1	Nanostring
IGF1R	Nanostring
IGF2	Nanostring
IGF2R	Nanostring
IGFBP3	Nanostring
IGFBP5	Nanostring
IGFBP6	Nanostring
IGFBP7	Nanostring
IGHA1	Nanostring
IGHD	Nanostring
IGHG1	Nanostring
IGHG2	Nanostring
IGHM	Nanostring
IGKC	Nanostring
IKZF3	Nanostring
IL10	Nanostring
IL10RA	Nanostring
IL10RB	Nanostring
IL11	Nanostring
IL11RA	Nanostring
IL12A	Nanostring
IL12B	Nanostring
IL12RB1	Nanostring
IL12RB2	Nanostring
IL13RA1	Nanostring
IL15	Nanostring
IL15RA	Nanostring
IL16	Nanostring
IL17A	Nanostring
IL17B	Nanostring
IL17D	Nanostring
IL17RA	Nanostring
IL17RB	Nanostring
IL17RE	Nanostring
IL18	Nanostring
IL18R1	Nanostring
IL1A	Nanostring
IL1B	Nanostring
IL1R1	Nanostring
IL1R2	Nanostring
IL1RAP	Nanostring
IL1RL1	Nanostring
IL1RN	Nanostring
IL2	Nanostring
IL20	Nanostring
IL20RA	Nanostring
IL22RA1	Nanostring
IL23A	Nanostring
IL24	Nanostring
IL27RA	Nanostring
IL2RA	Nanostring
IL2RB	Nanostring
IL2RG	Nanostring
IL32	Nanostring
IL33	Nanostring
IL34	Nanostring
IL36G	Nanostring
IL3RA	Nanostring
IL4R	Nanostring
IL6	Nanostring
IL6R	Nanostring
IL6ST	Nanostring
IL7	Nanostring
IL7R	Nanostring
INHA	Nanostring
INHBA	Nanostring
INHBB	Nanostring
INS	Nanostring
INSIG1	Nanostring
INSR	Nanostring
IRF3	Nanostring
IRF4	Nanostring
ISG15	Nanostring
ITGA1	Nanostring
ITGA2	Nanostring
ITGA3	Nanostring

ITGA5	Nanostring
ITGA6	Nanostring
ITGA8	Nanostring
ITGA9	Nanostring
ITGAE	Nanostring
ITGAL	Nanostring
ITGAM	Nanostring
ITGAV	Nanostring
ITGAX	Nanostring
ITGB1	Nanostring
ITGB2	Nanostring
ITGB4	Nanostring
ITGB5	Nanostring
ITGB6	Nanostring
ITGB8	Nanostring
ITK	Nanostring
ITM2A	Nanostring
ITM2B	Nanostring
JAG1	Nanostring
JAK1	Nanostring
JAK2	Nanostring
JCHAIN	Nanostring
JUN	Nanostring
JUNB	Nanostring
KDR	Nanostring
KIT	Nanostring
KITLG	Nanostring
KLF2	Nanostring
KLK3	Nanostring
KLRB1	Nanostring
KLRF1	Nanostring
KLRK1	Nanostring
KRAS	Nanostring
KRT1	Nanostring
KRT10	Nanostring
KRT13	Nanostring
KRT14	Nanostring
KRT15	Nanostring
KRT16	Nanostring
KRT17	Nanostring
KRT18	Nanostring
KRT19	Nanostring
KRT20	Nanostring
KRT23	Nanostring
KRT4	Nanostring
KRT5	Nanostring
KRT6A/B/C	Nanostring
KRT7	Nanostring
KRT8	Nanostring
KRT80	Nanostring
KRT86	Nanostring
LAG3	Nanostring
LAIR1	Nanostring
LAMA4	Nanostring
LAMP2	Nanostring
LAMP3	Nanostring
LCN2	Nanostring
LDB2	Nanostring
LDHA	Nanostring
LDLR	Nanostring
LEFTY1	Nanostring
LEP	Nanostring
LGALS1	Nanostring
LGALS3	Nanostring
LGALS3BP	Nanostring
LGALS9	Nanostring
LGR5	Nanostring
LIF	Nanostring
LIFR	Nanostring
LINC01781	Nanostring
LINC01857	Nanostring
LINC02446	Nanostring
LMNA	Nanostring
LPAR5	Nanostring
LTB	Nanostring
LTBR	Nanostring
LTF	Nanostring
LUM	Nanostring
LY6D	Nanostring
LY75	Nanostring
LYN	Nanostring
LYVE1	Nanostring
LYZ	Nanostring
MAF	Nanostring
MALAT1	Nanostring
MAML2	Nanostring
MAP1LC3B/2	Nanostring
MAP2K1	Nanostring
MAPK13	Nanostring
MAPK14	Nanostring
MARCKSL1	Nanostring

MARCO	Nanostring
MB	Nanostring
MECOM	Nanostring
MEG3	Nanostring
MERTK	Nanostring
MET	Nanostring
MFAP5	Nanostring
MGP	Nanostring
MHC I	Nanostring
MIF	Nanostring
MIR4435-2HG	Nanostring
MKI67	Nanostring
MMP1	Nanostring
MMP12	Nanostring
MMP14	Nanostring
MMP19	Nanostring
MMP2	Nanostring
MMP7	Nanostring
MMP9	Nanostring
MPO	Nanostring
MRC1	Nanostring
MRC2	Nanostring
MS4A1	Nanostring
MS4A4A	Nanostring
MS4A6A	Nanostring
MSMB	Nanostring
MSR1	Nanostring
MST1R	Nanostring
MT1X	Nanostring
MT2A	Nanostring
MTOR	Nanostring
MX1	Nanostring
MXRA8	Nanostring
MYC	Nanostring
MYH11	Nanostring
MYH6	Nanostring
MYL12A	Nanostring
MYL4	Nanostring
MYL7	Nanostring
MYL9	Nanostring
MZB1	Nanostring
MZT2A/B	Nanostring
NACA	Nanostring
NANOG	Nanostring
NCAM1	Nanostring
NCR1	Nanostring
NDRG1	Nanostring
NDUFA4L2	Nanostring
NEAT1	Nanostring
NELL2	Nanostring
NFKB1	Nanostring
NFKBIA	Nanostring
NGFR	Nanostring
NKG7	Nanostring
NLRC4	Nanostring
NLRC5	Nanostring
NLRP1	Nanostring
NLRP2	Nanostring
NLRP3	Nanostring
NOD2	Nanostring
NOSIP	Nanostring
NOTCH1	Nanostring
NOTCH2	Nanostring
NOTCH3	Nanostring
NPPC	Nanostring
NPR1	Nanostring
NPR2	Nanostring
NPR3	Nanostring
NR1H2	Nanostring
NR1H3	Nanostring
NR2F2	Nanostring
NR3C1	Nanostring
NRG1	Nanostring
NRXN1	Nanostring
NRXN3	Nanostring
NTRK2	Nanostring
NUPR1	Nanostring
NUSAP1	Nanostring
OAS1	Nanostring
OAS2	Nanostring
OAS3	Nanostring
OASL	Nanostring
OLFM4	Nanostring
OLR1	Nanostring
OSM	Nanostring
OSMR	Nanostring
P2RX5	Nanostring
PARP1	Nanostring
PCNA	Nanostring
PDCD1	Nanostring
PDCD1LG2	Nanostring

PDGFA	Nanostring
PDGFB	Nanostring
PDGFC	Nanostring
PDGFD	Nanostring
PDGFRA	Nanostring
PDGFRB	Nanostring
PDS5A	Nanostring
PECAM1	Nanostring
PF4/V1	Nanostring
PFN1	Nanostring
PGF	Nanostring
PGK1	Nanostring
PGR	Nanostring
PHLDA2	Nanostring
PIGR	Nanostring
PLAC8	Nanostring
PLAC9	Nanostring
PLCG1	Nanostring
PLD3	Nanostring
PNOC	Nanostring
POU5F1	Nanostring
PPARA	Nanostring
PPARD	Nanostring
PPARG	Nanostring
PPIA	Nanostring
PRF1	Nanostring
PROX1	Nanostring
PRSS2	Nanostring
PRTN3	Nanostring
PSAP	Nanostring
PSCA	Nanostring
PSD3	Nanostring
PTEN	Nanostring
PTGDR2	Nanostring
PTGDS	Nanostring
PTGES	Nanostring
PTGES2	Nanostring
PTGES3	Nanostring
PTGIS	Nanostring
PTGS1	Nanostring
PTGS2	Nanostring
PTK2	Nanostring
PTK6	Nanostring
PTPRC	Nanostring
PTPRCAP	Nanostring
PTTG1	Nanostring
PXDN	Nanostring
QRFPR	Nanostring
RAC1	Nanostring
RAC2	Nanostring
RACK1	Nanostring
RAG1	Nanostring
RAMP1	Nanostring
RAMP2	Nanostring
RAMP3	Nanostring
RARA	Nanostring
RARB	Nanostring
RARG	Nanostring
RARRES1	Nanostring
RARRES2	Nanostring
RB1	Nanostring
RBM47	Nanostring
RBPJ	Nanostring
REG1A	Nanostring
RELA	Nanostring
RELT	Nanostring
RGCC	Nanostring
RGS1	Nanostring
RGS13	Nanostring
RGS2	Nanostring
RGS5	Nanostring
RNF43	Nanostring
ROR1	Nanostring
RORA	Nanostring
RPL21	Nanostring
RPL22	Nanostring
RPL32	Nanostring
RPL34	Nanostring
RPL37	Nanostring
RPS4Y1	Nanostring
RSPO3	Nanostring
RUNX3	Nanostring
RXRA	Nanostring
RXRB	Nanostring
RYK	Nanostring
RYR2	Nanostring
S100A10	Nanostring
S100A2	Nanostring
S100A4	Nanostring
S100A6	Nanostring
S100A8	Nanostring

S100A9	Nanostring
S100B	Nanostring
S100P	Nanostring
SAA1/2	Nanostring
SAT1	Nanostring
SCG5	Nanostring
SCGB3A1	Nanostring
SEC23A	Nanostring
SEC61G	Nanostring
SELENOP	Nanostring
SELL	Nanostring
SELPLG	Nanostring
SERPINA1	Nanostring
SERPINA3	Nanostring
SERPINB5	Nanostring
SERPINH1	Nanostring
SFN	Nanostring
SH3BGRL3	Nanostring
SIGIRR	Nanostring
SLA	Nanostring
SLC2A1	Nanostring
SLC40A1	Nanostring
SLCO2B1	Nanostring
SLPI	Nanostring
SMAD2	Nanostring
SMAD3	Nanostring
SMAD4	Nanostring
SMARCB1	Nanostring
SMO	Nanostring
SNAI1	Nanostring
SNAI2	Nanostring
SOD1	Nanostring
SOD2	Nanostring
SORBS1	Nanostring
SOSTDC1	Nanostring
SOX2	Nanostring
SOX4	Nanostring
SOX9	Nanostring
SPARCL1	Nanostring
SPINK1	Nanostring
SPOCK2	Nanostring
SPP1	Nanostring
SPRY2	Nanostring
SPRY4	Nanostring
SQLE	Nanostring
SQSTM1	Nanostring
SRC	Nanostring
SREBF1	Nanostring
SRGN	Nanostring
SRSF2	Nanostring
SST	Nanostring
ST6GAL1	Nanostring
ST6GALNAC3	Nanostring
STAT1	Nanostring
STAT3	Nanostring
STAT4	Nanostring
STAT5A	Nanostring
STAT5B	Nanostring
STAT6	Nanostring
STMN1	Nanostring
SYK	Nanostring
TACSTD2	Nanostring
TAGLN	Nanostring
TAP1	Nanostring
TAP2	Nanostring
TBX21	Nanostring
TCAP	Nanostring
TCF7	Nanostring
TCL1A	Nanostring
TEK	Nanostring
TFEB	Nanostring
TGFB1	Nanostring
TGFB2	Nanostring
TGFB3	Nanostring
TGFBI	Nanostring
TGFBR1	Nanostring
TGFBR2	Nanostring
THBS1	Nanostring
THBS2	Nanostring
THSD4	Nanostring
TIE1	Nanostring
TIGIT	Nanostring
TIMP1	Nanostring
TLR1	Nanostring
TLR2	Nanostring
TLR3	Nanostring
TLR4	Nanostring
TLR5	Nanostring
TLR7	Nanostring
TLR8	Nanostring
TM4SF1	Nanostring

TNF	Nanostring
TNFAIP6	Nanostring
TNFRSF10A	Nanostring
TNFRSF10B	Nanostring
TNFRSF10D	Nanostring
TNFRSF11A	Nanostring
TNFRSF11B	Nanostring
TNFRSF12A	Nanostring
TNFRSF13B	Nanostring
TNFRSF14	Nanostring
TNFRSF17	Nanostring
TNFRSF18	Nanostring
TNFRSF19	Nanostring
TNFRSF1A	Nanostring
TNFRSF1B	Nanostring
TNFRSF21	Nanostring
TNFRSF4	Nanostring
TNFRSF9	Nanostring
TNFSF10	Nanostring
TNFSF12	Nanostring
TNFSF13B	Nanostring
TNFSF14	Nanostring
TNFSF15	Nanostring
TNFSF4	Nanostring
TNFSF8	Nanostring
TNFSF9	Nanostring
TNNC1	Nanostring
TNNT2	Nanostring
TNXA/B	Nanostring
TOP2A	Nanostring
TOX	Nanostring
TP53	Nanostring
TPI1	Nanostring
TPM1	Nanostring
TPM2	Nanostring
TPSAB1/B2	Nanostring
TPT1	Nanostring
TSC22D1	Nanostring
TSHZ2	Nanostring
TTN	Nanostring
TTR	Nanostring
TUBB	Nanostring
TUBB4B	Nanostring
TWIST1	Nanostring
TWIST2	Nanostring
TXK	Nanostring
TYK2	Nanostring
TYMS	Nanostring
TYROBP	Nanostring
UBA52	Nanostring
UBE2C	Nanostring
UPK3A	Nanostring
VCAM1	Nanostring
VCAN	Nanostring
VEGFA	Nanostring
VEGFB	Nanostring
VEGFC	Nanostring
VEGFD	Nanostring
VHL	Nanostring
VIM	Nanostring
VPREB3	Nanostring
VSIR	Nanostring
VTN	Nanostring
VWA1	Nanostring
VWF	Nanostring
WIF1	Nanostring
WNT10B	Nanostring
WNT11	Nanostring
WNT3	Nanostring
WNT5A	Nanostring
WNT5B	Nanostring
WNT7A	Nanostring
WNT7B	Nanostring
WNT9A	Nanostring
XBP1	Nanostring
XCL1/2	Nanostring
XKR4	Nanostring
YBX3	Nanostring
YES1	Nanostring
ZBTB16	Nanostring
ZFP36	Nanostring

Supplementary Table 3. Antibodies and reagents.

Assay type	Cell subsets	Gating Strategy
CyTOF supervised	Epithelial	EpCAM^{+} CD45^{-}
	EpCAM^{+} CD15^{+}	EpCAM^{+} CD15^{+}
	EpCAM^{+} ICOS^{+}	EpCAM^{+} ICOS^{+}
	T	CD45^{+} EpCAM^{-} CD3^{+} gdTCR^{-}
	gd T	CD45^{+} EpCAM^{-} CD3^{+} gdTCR^{+}
	CD8^{+} T	CD45^{+} EpCAM^{-} CD3^{+} gdTCR^{-} CD4^{-} CD8a^{+}
	Naïve CD8^{+}	CD45^{+} CD3^{+} CD4^{-} CD8a^{+} CD45RA^{+} CCR7^{+}
	CD8$^{+}_{TCM}$	CD45^{+} CD3^{+} CD4^{-} CD8a^{+} CD45RA^{-} CCR7^{+}
	CD8$^{+}_{TEM}$	CD45^{+} CD3^{+} CD4^{-} CD8a^{+} CD45RA^{-} CCR7^{-}
	CD8$^{+}_{TEMRA}$	CD45^{+} CD3^{+} CD4^{-} CD8a^{+} CD45RA^{+} CCR7^{-}
	CD4^{+} T	CD45^{+} EpCAM^{-} CD3^{+} gdTCR^{-} CD4^{+} CD8a^{-}
	Naïve CD4^{+}	CD45^{+} CD3^{+} CD4^{+} CD8a^{-}CD45RA^{+} CCR7^{+}
	CD4$^{+}_{TCM}$	CD45^{+} CD3^{+} CD4^{+} CD8a^{-}CD45RA^{-} CCR7^{+}
	CD4$^{+}_{TEM}$	CD45^{+} CD3^{+} CD4^{+} CD8a^{-} CD45RA^{-} CCR7^{-}
	CD4$^{+}_{TEMRA}$	CD45^{+} CD3^{+} CD4^{+} CD8a^{-}CD45RA^{+} CCR7^{-}
	T_{reg}	CD45^{+} CD3^{+} CD4^{+} CD8a^{-} FOXP3^{+} CTLA-4^{+} CD127^{-}
	NKT	CD45^{+} EpCAM^{-} CD3^{+} CD16^{+} CD56^{+}
	CD16^{-} NK	CD45^{+} EpCAM^{-} CD3^{-} gdTCR^{-} HLA-DR^{+} CD19^{-} CD14^{-} CD7^{+} CD56^{hi} CD16^{-}
	CD16^{+} NK	CD45^{+} EpCAM^{-} CD3^{-} gdTCR^{-} HLA-DR^{+} CD19^{-} CD14^{-} CD7^{+} CD56^{dim} CD16^{+}
	Granulocytes	CD45^{+} CD3^{-} CD19^{-} CD15^{+}
	B	CD45^{+} EpCAM^{-} CD3^{-} gdTCR^{-} HLA-DR^{+} CD7^{-} CD19^{+}
	Plasma	CD45^{+} EpCAM^{-} CD3^{-} HLA-DR^{-} CD7^{-} CD31^{-} CD19^{-} CD38^{+}
	cDC1	CD45^{+} CD3^{-} CD7^{-} HLA-DR^{+} CD19^{-} CD14^{-} CD11c^{+} CD1c^{-} CD141^{+}
	cDC2	CD45^{+} CD3^{-} CD7^{-} HLA-DR^{+} CD19^{-} CD14^{-} CD11c^{+} CD1c^{+} CD141^{-}
	cDC2b	CD45^{+} CD3^{-} CD7^{-} HLA-DR^{+} CD19^{-} CD14^{+} CD11c^{+} CD1c^{+}
	pDC	CD45^{+} CD3^{-} CD7^{-} HLA-DR^{+} CD19^{-} CD14^{-} CD123^{+} CD11c^{-} CD1c^{+}
	Classical Monocytes	CD45^{+} CD3^{-} CD7^{-} HLA-DR^{+} CD19^{-} CD14^{+} CD16^{-} CD163^{-}
	Non-Classical Monocytes	CD45^{+} CD3^{-} CD7^{-} HLA-DR^{+}CD19^{-} CD14^{-} CD16^{+}
	Macrophages	CD45^{+} CD3^{-} CD7^{-}HLA-DR^{+}CD19^{-} CD14^{+} CD16^{-} CD163^{+}
CyTOF unsupervised blood	1_ CD4^{naïve}	CD45^{+} CD3^{+} CD4^{+} CD8a^{-} CD45RA^{+} CCR7^{+}
	2,5_ CD4^{TCM}	CD45^{+} CD3^{+} CD4^{+} CD8a^{-} CD45RA^{-} CCR7^{+}
	3,6,9,_ CD4^{TEM}	CD45^{+} CD3^{+} CD4^{+} CD8a^{-} CD45RA^{-} CCR7^{-}
	4_ CD8^{naïve}	CD45^{+} CD3^{+} CD8a^{+} CD4^{-} CD45RA^{+} CCR7^{+}
	7,10_ CD8^{TEM}	CD45^{+} CD3^{+} CD8a^{+} CD4^{-} CD45RA^{-} CCR7^{-}
	8_gd T	CD45^{+} CD3^{+} gdTCR^{+}
	11_CD8 T CD38^{+} HLA-DR^{+}	CD45^{+} CD8a^{+} HLA-DR^{+} CD38^{+}
	12_CD4 T CD38^{+} HLA-DR^{+}	CD45^{+} CD4^{+} HLA-DR^{+} CD38^{+}
	13_NK CD56^{high}	CD45^{+} CD7^{+} CD56^{hi} CD16^{hi}
	14_NK CD56^{low}	CD45^{+} CD7^{+} CD56^{low} CD16^{low}
	15_B	CD45^{+} HLA-DR^{+} CD7^{-} CD19^{+}
	16_Granulocyte	CD45^{+} CD16^{+} CD15^{+}
	17_mDC	CD45^{+} CD7^{-} HLA-DR^{+} CD14^{low} CD123^{-} CD11c^{+}
	18,20,21_Classical Monocytes	CD45^{+} CD7^{-} HLA-DR^{+} CD14^{+} CD16^{-} CD163^{-}
	19_Non classical Monocytes	CD45^{+} CD7^{-} HLA-DR^{+} CD14^{-} CD16^{+}
CyTOF unsupervised biopsy	1,4_Epithelial	EpCAM^{+}
	2,3_EpCAM^{+} CD15^{high}	EpCAM^{+} CD15^{hi}
	5,6,8_EpCAM^{+} ICOS^{high}	EpCAM^{+} ICOS^{hi}
	9,12_EpCAM^{+} HLA-DR^{+}	EpCAM^{+} HLA-DR^{+}
	11,17_Stromal S1	CD45^{-} CD31^{-} EpCAM^{-} CD56^{+}
	13_Stromal	CD45^{-} CD31^{-} EpCAM^{-}
	14_B	CD45^{+} HLA-DR^{+} CD19^{+}
	15_Endothelial	CD45^{-} HLA-DR^{+} EpCAM^{-} CD31^{+}
	16_CD4 T	CD45^{+} CD3^{+} CD4^{+} CD8a^{-}
	18_MNP-mDC and Macrophages	CD45^{+} CD7^{-} HLA-DR^{+} CD14^{low} CD16^{-} CD11c^{+} CD19^{-} CD163^{+}
	19_CD8 T	CD45^{+} CD3^{+} CD8a^{+} CD4^{-}
	20,21_Plasma	CD45^{+} EpCAM^{-} CD3^{-} HLA-DR^{-} CD7^{-} CD19^{-} CD38^{+}
	Epithelial	E-cadherin^{+} CD45^{-} CD31^{-}
	Epithelial CD68+	E-cadherin^{+} CD68^{+} CD3^{-} CD163^{-}
	Epithelial HLA-DR+	E-cadherin^{+} HLA-DR^{+} CD3^{-} CD163^{-}

CODEX supervised	Epithelial cycling	E-cadherin^{+} Ki67^{+}
	Endothelial	CD31^{+} E-cadherin^{-} CD45^{-}
	Stromal fibroblast CD44^{+}	Vimentin^{+} CD44^{+} CD45^{-} CD31^{-} CD20^{-} CD14^{-} CD3^{-} E-cadherin^{-} PDPN^{-}
	Stromal pericytes myofibroblats	Vimentin^{+} SMA^{+} Collagen IV^{+}
	Stromal fibroblast PDPN^{+}	Vimentin^{+} PDPN^{+} CD45^{-} CD31^{-} CD20^{-} CD14^{-} CD3^{-} E-cadherin^{-} CD44^{-}
	Hematopoietic	CD45^{+} E-cadherin^{-} CD31^{-}
	CD45^{+}	CD45+
	Monocyte	CD45^{+} HLA-DR^{+} CD3^{-} CD163^{-} CD20^{-} CD14^{+} CD68^{+}
	Macrophages	CD45^{+} HLA-DR^{+} CD3^{-} CD163^{+}
	B	CD45^{+} HLA-DR^{+} CD20^{+} CD3^{-} E-cadherin^{-} CD163^{-}
	T	CD45^{+} CD3^{+} E-cadherin^{-}
	CD4^{+} T	CD45^{+} CD3^{+} CD4^{+} CD8^{-}
	CD8^{+} T	CD45^{+} CD3^{+} CD4^{-} CD8^{+}
	Memory CD4^{+} T	CD45^{+} CD8^{-} CD3^{+} CD4^{+} CD45RO^{+}
	Memory CD8^{+} T	CD45^{+} CD4^{-} CD3^{+} CD8^{+} CD45RO^{+}
CODEX unsupervised	1_B	CD45^{+} HLA-DR^{+} CD19^{+} CD20^{+}
	2_Endothelial	E-cadherin- CD45^{-} CD31^{+}
	3_Epithelial	E-cadherin^{+} PCK^{+} CD45^{-} CD31^{-}
	4_Epithelial CD68^{+}	E-cadherin^{+} PCK^{+} CD68^{+}
	5_Epithelial cycling	E-cadherin^{+} PCK+ Ki67+
	6_Macrophages	CD45^{+} HLA-DR^{+} CD163^{+}
	7_Memory T	CD45^{+} CD3^{+} CD45RO^{+}
	8_Stromal fibroblast CD44^{+}	Vimentin^{+} CD44^{+} CD45^{-} CD3^{-} E-cadherin^{-}
	9_Stromal pericytes myofibroblast	Vimentin^{+} SMA^{+} Collagen IV^{+}
	10_Stromal fibroblast PDPN^{+}	Vimentin^{+} PDPN^{+} CD45^{-} CD3^{-} E-cadherin^{-}
	11_T CD45RO^{-}	CD45^{+} CD3^{+} CD45RO^{-}
MIBI supervised	Hematopoietic	CD45^{+} EpCAM^{-} CD31^{-}
	Epithelial	EpCAM^{+} CD45^{-} CD31^{-}
	Epithelial HLA-DR+	EpCAM^{+} HLA-DR^{+}
	Endothelial	CD31^{+} EpCAM^{-} CD45^{-}
	Stromal	Vimentin^{+} EpCAM^{-} CD45^{-} CD31^{-}
	T	CD45^{+} CD3^{+}
	CD4^{+} T	CD45^{+} CD3^{+} CD4^{+} CD8a^{-}
	CD8^{+} T	CD45^{+} CD3^{+} CD4^{-} CD8a^{+}
	Memory CD4^{+} T	CD45^{+} CD8^{-} CD3^{+} CD4^{+} CD45RO^{+}
	Memory CD8^{+} T	CD45^{+} CD4^{-} CD3^{+} CD8^{+} CD45RO^{+}
	Neutrophils	CD45^{+} EpCAM^{-} CD3^{-} CD20^{-} CD16^{+} CD56^{-} HLA-DR^{-}
	B	CD45^{+} CD3^{-} HLA-DR^{+} CD20^{+}
	Plasma	CD45^{+} CD3^{-} CD20^{-} CD138^{+}
	mDC	EpCAM^{-} CD45^{+} CD3^{-} CD20^{-} CD11c^{+}
	Mast	EpCAM^{-} CD45^{+} CD3^{-} CD20^{-} CD117^{+}
	Monocytes	HLA-DR^{+} CD163^{-} CD3^{-} CD20^{-} CD14^{+} CD68^{+}
	Macrophages	CD163^{+} CD68^{+} CD3^{-}
	Macrophages CD103^{+}	CD163^{+} CD3^{-} CD68^{+} CD103^{+}
	Fibroblasts	CD45^{-} EpCAM^{-} CD31^{-} Vimentin^{+} CD56^{-}
	Myofibroblasts	CD45^{-} EpCAM^{-} CD31^{-} Vimentin^{+} SMA^{+} CD56^{-}

Supplementary Table 4. Cell subset phenotypes for supervised and unsupervised analyses for each multi-omics method.

Cell type	Gene list	Numeric ID
MNP-pDC	*HLA-DRA*	8118548
	CD74	8115147
	HLA-DRB1	8125445
	CST3	8065403
	LYZ	7957023
	HLA-DPA1	8125556
	GZMB	7978366
	ITM2C	8048995
	SEC61B	8156838
	IRF1	8114010
	LILRA4	8039246
	APP	8069644
	C12orf75	7958253
	PPP1R14B	7949060
	JCHAIN	8100827
	TCF4	8023415
	UGCG	8157216
	ALOX5AP	7968344
	SERPINF1	8003667
	CCDC50	8084818
MNP-Monocytes	*HLA-DRA*	8118548
	CD74	8115147
	HLA-DRB1	8125445
	CST3	8065403
	LYZ	7957023
	HLA-DPA1	8125556
	S100A9	7905571
	S100A8	7920244
	TIMP1	8167185
	FCN1	8165011
	SERPINA1	7981068
	S100A4	7920271
	LILRA5	8039236
	S100A6	7920258
	TYMP	8077103
	VCAN	8106743
	SOD2	8130556
	CD44	7939341
	CD14	8114612
	EREG	8095728
	TSPO	8073612
MNP-Macrophage	*HLA-DRA*	8118548
	CD74	8115147
	HLA-DRB1	8125445
	CST3	8065403
	LYZ	7957023
	HLA-DPA1	8125556
	C1QA	7898793
	FTL	8030171
	C1QC	7898799
	C1QB	7898805
	ITM2B	7969003
	NPC2	7980146
	SLC40A1	8057677
	CCL3	8014369
	MS4A7	7940259
	CTSS	7919800
	FCGRT	8030374
	CCL4	8006602
MNP-mDC	*HLA-DRA*	8118548
	CD74	8115147
	HLA-DRB1	8125445
	CST3	8065403
	LYZ	7957023
	HLA-DPA1	8125556
	BASP1	8104601
	SLC38A1	7962516
	LTB	8124950
	CST7	8061416
	CD1C	7906348
	ACAP1	8004331
	DAPP1	8096602
	STK17A	8132503
	ADAM8	7937150
	FCER1A	7906443
	RHOF	7967202
	FSCN1	8131339
	ICAM3	8033987
	CD86	7896700
	CXCR4	8055465
	COL6A2	8069301
	CXCL14	8114249
	CALD1	8136347
	COL3A1	8046922

Stromal-Activated Fibroblast	*IGFBP7*	8100541
	C11orf96	7939492
	TIMP1	8167185
	MMP3	7951284
	MMP1	7951271
	AREG	8095736
	TMEM158	8086530
	TNFRSF11B	8152512
	ACSL4	8174474
	PLAU	7928429
	HGF	8140556
	STC1	8149825
	GJA1	8121749
	CD82	7939546
	ISG20	7985777
	NRG1	8145766
Stromal S2	*COL6A2*	8069301
	CXCL14	8114249
	CALD1	8136347
	COL3A1	8046922
	IGFBP7	8100541
	C11orf96	7939492
	F3	7917875
	POSTN	7971077
	ENHO	8160816
	PDGFRA	8095080
	SOX6	7946757
	PLAT	8150509
	NSG1	8093839
	HSD17B2	7997491
	DDHD1	7979223
	PDGFD	7951351
	AGT	7924987
	WNT5B	7953012
Endothelial	*IGFBP7*	8100541
	PLVAP	8035297
	SPARCL1	8101659
	IFITM3	7945371
	IGFBP4	8007100
	CAV1	8135594
	CCL21	8160889
	TFF3	8070567
	TFP1	8057599
	NUPR1	8000574
	MMRN1	8096415
	PROX1	7909681
	LYVE1	7946579
	AKAP12	8122807
	TBX1	8071276
	FABP4	8151532
	PPFIBP1	7954559
	RBP1	8091078
	EFEMP1	8052355
	NR2F1	8106923
	ACKR1	7906435
	NPC2	7980146
	CPE	8098204
	CLU	8149927
	MADCAM1	8023941
	DUSP23	7906469
	IL1R1	8043995
	ZNF385D	8085774
	KCTD12	7972055
	IL33	8154295
	ADGRG6	8122365
	LPCAT4	7987230
	SELP	7922200
	CTNNAL1	8163063
	TLL1	8098214
	GSN	8157582
	SLC9A3R2	7992463
	NOTCH4	8125383
	RGCC	7968789
	A2M	7960947
	MGLL	8090433
	VAMP5	8043203
	FLT1	7970763
	TSC22D1	7971350
	RBP7	7897522
	ADGRF5	8126798
	ADGRL4	7917182
	SRGN	7927964
	IL7R	8104901
	CD3E	7944179
	ARL4C	8059854
	KLRB1	7961059

CD4 T	*SPOCK2*	7934215
	KLF2	8026564
	SELL	7896687
	LEF1	8102232
	CCR7	8015031
	C1orf162	7903980
	LYPD3	8037301
	ACTN1	7979824
	TRABD2A	8053379
	GCNT4	8112668
	SLC40A1	8057677
	FHIT	8088458
	FAM117B	8047565
	S100A4	7920271
	JUN	7916609
	CCL5	8014316
	TNFAIP3	8122265
	ANXA1	8155849
	ANKRD28	8085628
	ID2	8040103
	EGR1	8108370
	GPR65	7976080
	LGALS3	7974461
	HOPX	8100507
T reg	*IL7R*	8104901
	CD3E	7944179
	ARL4C	8059854
	KLRB1	7961059
	SPOCK2	7934215
	CTLA4	8047692
	TIGIT	8081799
	MAF	8002969
	ARID5B	7927732
	BATF	7975793
	TBC1D4	7972021
	PHACTR2	8122426
	RNF19A	8152041
	TNFRSF4	7911413
	UCP2	7950307
	ICA1	8138202
	TNFRSF1B	7896721
	TNFRSF18	7911403
	DUSP4	8150076
	TOX2	8062782
Cytotoxic lymphocyte	*CCL5*	8014316
	NKG7	8038809
	GZMA	8105340
	IL32	7992828
	CCL4	8006602
	CD7	8019478
	GZMK	8105331
	ITGB2	8070826
	GZMH	7978360
	KLF2	8026564
	KLRG1	7953835
	KLRB1	7961059
	SPRY1	8097282
	CMC1	8078312
	SH2D1A	8169792
	HCST	8028104
	SH3BGRL3	7899153
	KLRD1	7953949
	CD3E	7944179
	CD3D	7952056
	CD69	7896693
	CD3G	7944185
	CD8A	8053584
B	*CD74*	8115147
	HLA-DRA	8118548
	MS4A1	7940287
	HLA-DRB1	8125445
	HLA-DPA1	8125556
	CD79A	8029136
	IGHM	7896697
	TCL1A	7981183
	FCER2	8033420
	YBX3	7961230
	KLF4	8163002
	KLF6	7931810
	GPR183	7972557
	TNFSF9	8025053
	CD27	7953333
	LDLRAD4	8020308
	ACTG1	8019183
	GAPDH	7953385
	BASP1	8104601

	PFN1	8011759
	HMGN1	8070389
	YBX1	7900585
	LCP1	7971461
	SLC25A5	8169640
	ARPC1B	8134552
	ANP32B	8156750
	ACTR3	8044686
	MARCKSL1	7914525
Plasma	*JCHAIN*	8100827
	MZB1	8114511
	SSR4	8170775
	CD79A	8029136
	IGHM	7896697
	CD44	7939341
	CD9	7953291
	CD48	7921667
	THY1	7952268
	LAG3	7953418
Epithelial	*LGALS4*	8036591
	PIGR	7923929
	KRT8	7963567
	C15orf48	7983478
	SH2D6	8043157
	TRPM5	7945742
	TLE4	8156060
	FABP1	8053654
	AQP8	7994252
	SLC26A3	8142171
	GUCA2A	7915404
	CEACAM7	8037053
	SLC26A2	8109194
	OTOP2	8009705
	BEST4	7915598
	CA4	8008900
	OLFM4	7969288
	LEFTY1	7924663
	PTGDR	7974363
	UBE2C	8063043
	HMGN2	7899187
	TOP2A	8014974
	HMGB2	8103728
	TUBA1B	7963046
Neutrophil	*S100A8*	7920244
	S100A9	7905571
	FCGR3A	7921868
	FCGR3B	7921873
	IL1R2	8043981
	GCA	8046003
	CSF3R	7914950
	S100P	8093950
	BASP1	8104601
	FPR1	8038899
	IFITM2	7937330
	ELANE	8024956
Pre-VDZ response signature	*GAS6*	7970329
	LEFTY1	7924663
	STMN1	7913864
	RPL37	8111814
	MARCKSL1	7914525
	NUPR1	8000574
	GSTP1	7941936
	LYZ	7957023
	SPINK1	8114964
	AGR2	8138381
	OLFM4	7969288
	JCHAIN	8100827
	REG1A	8042986
Pre-VDZ non-response signature	*MMP2*	7995681
	THBS1	7982597
	MMP1	7951271
	TCL1A	7981183
	COL21A1	8127201
	SPP1	8096301
	ITGA5	7963786
	HGF	8140556
	GZMK	8105331
	GZMH	7978360
	IFNG	7964787

Supplementary Table 5. Cell subset-specific gene signatures used for Gene Set Enrichment Analysis (GSEA). Numeric ID, Affymetrix numeric probe identifier corresponding to each gene.

Assay type	Patient ID	Specimen/imaged	Number of cells	% of hematopoietic	% of Stromal and Endothelial	% IEC	Multi-omic method
CITE-seq	HS1	Blood	899				single cell transcriptomic and proteomic
	HS2	Blood	3120				
	HS3	Blood	1699				
	HS4	Blood	1761				
	HS5	N/A	N/A				
	HS6	Blood	3474				
	HS7	Blood	2356				
	HS8	Blood	1111				
	HS9	Blood	1473				
	HS10	Blood	1669				
	HS11	Blood	1003				
	HS12	Blood	1565				
	HS1	Biopsy	9572	87.4	3.9	7.7	
	HS2	Biopsy	2648	85.7	5.4	8.3	
	HS3	Biopsy	8256	88.6	7.4	2.8	
	HS4	Biopsy	13662	77.8	10.5	10.7	
	HS5	Biopsy	6103	75.2	15.9	7.8	
	HS6	Biopsy	9036	70.2	22.2	6.3	
	HS7	Biopsy	9548	88.2	3.0	7.9	
	HS8	Biopsy	6076	79.1	15.8	4.3	
	HS9	Biopsy	4393	67.4	8.7	23.0	
	HS10	Biopsy	9192	80.6	5.7	13.3	
	HS11	Biopsy	7072	86.1	5.2	6.1	
	HS12	Biopsy	8342	78.9	10.8	9.6	
CyTOF	HS1	Blood	57374				single cell proteomic
	HS2	Blood	136673				
	HS3	Blood	167045				
	HS4	Blood	151381				
	HS5	N/A	N/A				
	HS6	Blood	75079				
	HS7	Blood	162640				
	HS8	Blood	121482				
	HS9	Blood	139270				
	HS10	Blood	85768				
	HS11	Blood	176299				
	HS12	Blood	117145				
	HS1	Biopsy	82382	16.6	6.1	76.4	
	HS2	Biopsy	83878	17.1	4.7	76.7	
	HS3	Biopsy	82480	32.0	8.9	57.7	
	HS4	Biopsy	57637	25.7	9.7	63.2	
	HS5	Biopsy	50659	26.7	9.4	62.9	
	HS6	Biopsy	30428	52.1	17.3	28.7	
	HS7	Biopsy	59387	34.6	5.6	57.2	
	HS8	Biopsy	41843	31.9	16.4	50.3	
	HS9	Biopsy	78302	18.0	7.0	74.1	
	HS10	Biopsy	25923	10.6	6.6	80.9	
	HS11	Biopsy	75650	33.8	7.4	57.7	
	HS12	Biopsy	15680	16.8	10.0	71.8	
Multiplexed RNA-ISH	HS1	Core	8816	4.2	3.8	57.0	FFPE spatial transcriptomic
	HS2	Core	10198	4.3	8.1	58.2	
	HS3	Core	6314	6.5	19.0	61.0	
	HS4	Core	5091	5.5	24.9	47.5	
	HS5	Core	8490	8.8	15.4	49.4	
	HS6	Core	8868	12.4	18.0	48.9	
	HS7	Core	5779	7.2	10.3	55.4	
	HS8	Core	5365	13.1	13.0	37.1	
	HS9	Core	10212	22.9	8.7	57.9	
	HS10	Core	6975	24.5	8.4	55.3	
	HS11	Core	13223	33.2	25.1	41.0	
	HS12	Core	14161	10.6	20.8	55.0	
CosMx SMI 960-plex	HS1	FOV	5131	30.6	14.3	55.2	FFPE spatial transcriptomic
	HS2	FOV	6021	27.7	9.4	62.9	
	HS3	FOV	1353	50.2	11.2	38.6	
	HS4	FOV	4262	16.9	15.1	68.0	
	HS5	FOV	3774	32.8	16.4	50.8	
	HS6	FOV	N/A				
	HS7	FOV	4451	35.1	20.8	44.1	
	HS8	FOV	4888	68.7	23.6	7.7	
	HS9	FOV	N/A				
	HS10	FOV	7765	35.7	24.0	40.3	
	HS11	FOV	6819	66.2	16.1	17.8	
	HS12	FOV	4319	33.9	27.0	39.1	
CODEX	HS1	Core	N/A				FFPE spatial proteomic
	HS2	Core	10302	12.6	15.5	49.6	
	HS3	Core	3987	32.5	17.4	29.6	
	HS4	Core	3868	25.9	17.6	17.4	
	HS5	Core	3451	20.5	13.0	47.0	
	HS6	Core	N/A				
	HS7	Core	4487	13.2	19.8	20.1	
	HS8	Core	5214	39.5	20.7	5.2	
	HS9	Core	3937	15.6	14.3	38.9	
	HS10	Core	11201	26.8	24.6	34.7	
	HS11	Core	12286	52.9	16.4	4.5	
	HS12	Core	9351	32.5	21.7	9.2	
MIBI	HS1	FOV	893	10.7	23.6	41.9	FFPE spatial proteomic
	HS2	FOV	1455	14.4	10.3	45.4	
	HS3	FOV	1295	7.6	6.4	50.1	
	HS4	FOV	250	2.4	8.8	67.2	
	HS5	FOV	636	10.2	18.4	43.4	
	HS6	FOV	1630	29.9	16.0	13.4	
	HS7	FOV	349	11.0	24.2	42.5	
	HS8	FOV	473	18.8	14.8	23.9	
	HS9	FOV	1090	11.4	12.1	40.2	
	HS10	FOV	1041	4.3	10.2	46.5	
	HS11	FOV	1732	27.7	11.8	24.2	
	HS12	FOV	1401	15.3	14.6	32.4	

Supplementary Table 6. Cell counts and percentages of hematopoietic, stromal and endothelial, and intestinal epithelial cell (IEC) subsets for each patient biospecimen and multi-omic method.

Gene	per FOV				FOVs as replicates				Biopsies as replicates				Include in
upregulated	baseMean	log2FoldChange	p-value	padj	baseMean	log2FoldChange	p-value	padj	baseMean	log2FoldChange	p-value	padj	gene set
KRT20	526.97688	1.04072071	0.06350846	0.41395902	1053.37471	1.829395189	0.01106976	0.29072685	1259.97142	1.759530615	0.03333355	0.58904936	
MMP2	214.781871	0.779233372	8.81E-05	0.00881248	408.395547	0.650608071	0.02130012	0.40684052	489.294934	0.704799783	0.04645766	0.64526877	Yes
CLDN4	759.82305	0.745929417	0.02768877	0.31826169	1483.20505	1.290087005	0.00365172	0.20246759	1776.28492	1.241179209	0.02295442	0.54436599	
TIMP1	276.204316	0.737634615	0.01112788	0.20232501	508.769011	0.667081209	0.12191453	0.76158335	602.95769	0.541749624	0.25696256	0.82642476	
PLAC8	935.934625	0.720560727	0.06581948	0.41395902	1848.43313	1.347448175	0.00690973	0.27583642	2314.7905	1.208635846	0.03799885	0.62106315	
THBS1	344.101653	0.672537259	0.00119803	0.04991792	647.142023	0.611143584	0.02401064	0.40684052	750.480415	0.745730473	0.00962025	0.40743756	Yes
JUN	453.634985	0.660664794	0.00672182	0.16894968	870.901615	0.956538051	0.00759029	0.28460002	1009.87437	1.096086482	NA	NA	
CEACAM1	294.859297	0.64336382	0.03858965	0.35695204	557.851558	1.107380773	0.00344384	0.20217367	673.708459	1.040242363	0.0190342	0.48659234	
MALAT1	5162.4939	0.636166653	0.19155692	0.58401499	10254.0368	1.040230675	0.08184969	0.69225416	12095.2239	1.062920598	0.11062494	0.73528713	
COL3A1	392.521296	0.633436878	0.0630143	0.41395902	739.85146	0.541377924	0.22738874	0.84271262	860.298456	0.433934687	0.42279269	0.95203628	
MMP1	207.858993	0.618646275	1.89E-07	0.00011484	385.571488	0.550571237	0.00041056	0.14987715	466.18652	0.56304112	0.00336529	0.23712057	Yes
FOS	352.469296	0.606341877	0.05283546	0.4033241	643.747795	0.869332204	0.05856023	0.60978778	714.941229	0.965660035	0.06011965	0.7039651	
SOD2	296.546792	0.598764496	0.01659691	0.26344298	564.82725	0.538386908	0.11886782	0.76044926	676.89997	0.477775366	0.20524567	0.79313927	
NEAT1	866.390363	0.572790109	0.122019	0.48996338	1726.88505	1.120800306	0.01984024	0.40684052	2078.89566	1.00077444	0.06888335	0.71379068	
MT2A	934.428365	0.571389758	0.00954193	0.19083854	1775.58372	0.495068787	0.09284265	0.70715244	2111.81567	0.565782914	0.11290352	0.74055794	
SQSTM1	474.161774	0.512804338	0.00661297	0.16894968	930.493327	0.848882786	0.00154193	0.15418283	1115.58897	0.813626862	0.01383623	0.47568006	
MMP9	255.898007	0.511030856	0.00172926	0.06404677	487.427814	0.380037984	0.06231327	0.61346199	583.529078	0.426210316	0.06352648	0.7039651	
ATF3	246.586056	0.505668525	0.00875501	0.18140874	459.530162	0.74200607	0.00798477	0.28460002	544.420923	0.785730082	0.01587284	0.48605613	
DUSP1	372.731731	0.486584761	0.00782812	0.18140874	678.460406	0.675381703	0.00409368	0.20427463	798.90527	0.704769132	0.00981204	0.40743756	
EZR	464.523069	0.436439785	0.13530634	0.50487439	906.187312	0.834827562	0.01687739	0.374303	1086.54509	0.747947535	0.07461127	0.71379068	
KRT16	609.755295	0.425423051	0.05657241	0.40890046	975.556748	0.445061083	0.14559645	0.78606569	1220.06216	0.428064554	0.22402087	0.80631339	
CDKN1A	378.607985	0.411588752	0.04890184	0.39601595	709.030108	0.777604211	0.00430737	0.20470263	865.725998	0.677779355	0.03367684	0.58904936	
CCL18	181.931178	0.399177236	0.00096405	0.04191509	333.952038	0.355215006	0.02214067	0.40684052	402.185354	0.365597111	0.05635691	0.70234803	
CRIP1	579.174589	0.377509857	0.06923619	0.41774829	1180.98787	0.665194598	0.04315395	0.55932003	1378.27245	0.741358386	0.06495967	0.7039651	
OAS1	262.689164	0.372964912	0.07135545	0.41825833	483.452543	0.728088809	0.00948109	0.29072685	588.271886	0.683797817	0.04216207	0.63067923	
CCL21	283.216261	0.34774063	0.11548864	0.48534695	543.974464	0.124593639	0.67556408	0.97295876	619.389899	0.311076366	0.18767891	0.79313927	
TCL1A	161.962139	0.324429339	4.83E-05	0.00604232	297.745557	0.286217762	0.00128782	0.15418283	358.914476	0.313275735	0.00066112	0.13182804	Yes
FKBP5	156.655595	0.319563737	0.01196562	0.20630378	288.313877	0.24083704	0.16907511	0.80350933	338.101572	0.241524611	0.21504822	0.80164351	
CXCL13	261.757772	0.304432077	0.02551588	0.31291833	486.537263	0.20020022	0.20258663	0.81386279	586.178145	0.259310993	0.15162784	0.77280279	
MYL12A	504.843393	0.303773039	0.22682194	0.61367037	993.525404	0.720716688	0.03159557	0.47063252	1160.67198	0.666088033	0.09287529	0.7263558	
OASL	258.014594	0.298766106	0.00554993	0.1541648	474.548174	0.456788851	0.00318848	0.20217367	577.31661	0.465282666	0.01485569	0.47777821	
ZFP36	466.041918	0.29221624	0.13335282	0.50487439	831.650665	0.475025375	0.05956942	0.60978778	988.611548	0.478474463	0.10912591	0.73528713	
RSPO3	65.2895623	0.290966063	0.04109392	0.35695204	122.094016	0.257943678	0.11869048	0.76044926	143.914325	0.308995191	0.09961188	0.7263558	
COL21A1	96.5411045	0.290774928	0.00083991	0.03999577	178.277478	0.319372181	0.00147965	0.15418283	213.722185	0.33860771	0.0022411	0.22083429	Yes
ARHGDIB	205.966227	0.287861641	0.04096562	0.35695204	382.444048	0.257510969	0.10132545	0.70715244	455.340504	0.218177936	0.16459059	0.78052343	
COL1A1	623.954591	0.284562889	0.33760458	0.71526394	1151.76314	0.251325271	0.49427984	0.95529411	1379.01178	0.06702276	0.88072016	0.97848848	
IL4R	220.007153	0.280776618	0.01092497	0.20231429	416.543543	0.348377681	0.01407256	0.32991373	495.252051	0.385286083	0.01478337	0.47777821	
SPP1	193.795024	0.274902042	0.00265226	0.08037161	352.005521	0.319550212	0.0020901	0.17382665	424.562732	0.317695632	0.00524	0.26121389	Yes
ITGA5	182.035166	0.273837899	0.00211066	0.07278133	340.852052	0.226084173	0.04506812	0.56934157	402.26067	0.25635497	0.03038689	0.5716175	Yes
IER3	401.465412	0.267372809	0.08111706	0.43161934	733.389792	0.512339802	0.01421472	0.32991373	878.336888	0.438805495	0.08685337	0.72408968	
KLF2	409.778611	0.259101857	0.03253334	0.338889	753.184873	0.297889683	0.02445935	0.40684052	892.492339	0.283721192	0.04879193	0.65261317	
CD163	117.519516	0.257539282	0.03652784	0.35695204	215.741815	0.235189381	0.10572635	0.72768895	256.577475	0.22120639	0.20230369	0.79313927	
CD52	178.342569	0.249309495	0.03080577	0.33484528	329.444325	0.171281424	0.22098906	0.84271262	388.811356	0.214139449	0.15035973	0.77280279	
VEGFC	116.304572	0.241700243	0.04845146	0.39601595	219.034269	0.196831987	0.19780647	0.81386279	263.045931	0.244462294	0.15182682	0.77280279	
MARCO	125.215062	0.23998011	0.00838667	0.18140874	231.83625	0.232269458	0.0238297	0.40684052	281.024054	0.265672579	0.02692013	0.55278634	
CCL3/L1/L3	418.653572	0.239374684	0.03389583	0.34587584	767.44468	0.262720995	0.08733366	0.69678309	930.295985	0.232282368	0.20422157	0.79313927	
CD22	92.3974621	0.23741245	0.07935439	0.43161934	171.503826	0.177683837	0.24582977	0.85483662	206.285795	0.191005006	0.25886286	0.82719957	
CHI3L1	218.435892	0.236505611	0.17854785	0.56041039	403.415375	0.233093136	0.33684141	0.92608189	491.699117	0.171029084	0.54958045	0.96029886	
HGF	128.808174	0.236183406	0.00028303	0.01818949	238.968156	0.247246483	0.00108059	0.15418283	287.728884	0.252449156	0.00200411	0.22083429	Yes
GZMK	177.279418	0.233999116	0.00092078	0.0418538	330.256396	0.246065621	0.00333458	0.20217367	397.674623	0.260074683	0.00454881	0.25195327	Yes
GZMH	181.54976	0.233366814	0.00033614	0.01977282	332.248125	0.215417286	0.00533193	0.23074301	398.359545	0.237092767	0.00374203	0.23712057	Yes
CSTB	349.213445	0.231526772	0.28965551	0.6758503	695.910767	0.618706889	0.04965394	0.5944744	812.204594	0.635499632	0.09632235	0.7263558	
KRT8	3308.93852	0.230305325	0.56872815	0.89607096	6431.03228	0.685827652	0.16679337	0.80350933	7524.25128	0.606972503	0.30805751	0.87752381	
COL6A3	260.388401	0.228403251	0.17222085	0.55376478	480.886454	0.1757595	0.33575148	0.9256353	565.933646	0.133127424	0.53617699	0.95668154	
IGHG1	11861.3389	0.227212704	0.72987109	0.94788453	21515.2779	0.226515772	0.81470406	0.98267871	28446.8984	-0.222486389	0.83419359	0.97848848	
P2RX5	212.30091	0.225002807	0.03911167	0.35695204	387.684989	0.186952907	0.16030126	0.80350933	470.149445	0.158137544	0.30897581	0.87763215	
MS4A1	141.663715	0.224287822	0.11323991	0.48187198	266.691471	0.145828457	0.37003973	0.93483037	317.340453	0.200614537	0.28703487	0.84792809	
ADGRL2	156.091385	0.222648518	0.06134205	0.41301069	289.506618	0.260626292	0.01292383	0.32244956	347.203971	0.279900004	0.02292565	0.54436599	
FGR	135.270051	0.218239284	0.01179528	0.20630378	248.924379	0.197430655	0.03606925	0.52169727	297.93001	0.218763278	0.04238266	0.63067923	
MMP14	223.439612	0.215868778	0.0230019	0.31251486	412.802454	0.170848858	0.14136747	0.78606569	486.266457	0.166358881	0.22042274	0.80164351	
LINC01781	161.499891	0.213090821	0.05752892	0.41092087	300.553731	0.33227904	0.01079723	0.29072685	360.094115	0.332373888	0.027883	0.5539472	
IFNG	132.922106	0.209627524	0.00083159	0.03999577	239.056038	0.201291538	0.01056766	0.29072685	287.138969	0.19944648	0.01204569	0.46190573	Yes
downregulated	baseMean	log2FoldChange	p-value	padj	baseMean	log2FoldChange	p-value	padj	baseMean	log2FoldChange	p-value	padj	
GAS6	221.185196	-0.422669228	4.1694E-05	0.00604232	398.898573	-0.433875128	0.00046858	0.14987715	459.862459	-0.4628411	0.00114575	0.1903854	Yes
RACK1	395.864527	-0.425699582	0.01391385	0.23582791	762.497029	-0.417365445	0.07758377	0.67046604	841.084843	-0.4667354	0.06624517	0.71017669	
LEFTY1	350.783571	-0.432882828	0.00076319	0.03999577	639.63574	-0.453902055	0.00477864	0.21677649	737.521281	-0.4766157	0.00854651	0.38731238	Yes
IFITM1	567.786594	-0.440511233	0.01166314	0.20630378	1027.34029	-0.393607065	0.09681441	0.70715244	1201.7823	-0.4863162	0.07691141	0.71664179	
SOD1	404.63738	-0.450326937	0.05683716	0.40890046	746.774687	-0.079510578	0.80252197	0.98267871	896.877388	-0.3422656	0.36383608	0.91987571	
STMN1	224.277107	-0.463971741	0.00222845	0.0742816	435.776705	-0.625848399	0.00387591	0.20358727	482.73007	-0.5502268	0.00380535	0.23712057	Yes
TAGLN	400.794087	-0.465372414	0.06054485	0.41301069	815.102372	-0.744071978	0.05150451	0.5944744	825.899445	-0.5244593	0.10191485	0.7263558	
ACTA2	208.410846	-0.467436601	0.0273665	0.31821516	409.307163	-0.674494762	0.02808689	0.45181565	422.322919	-0.4852252	0.04974784	0.65261317	
MZB1	457.395572	-0.469900866	0.11222921	0.48187198	787.510698	-0.391960885	0.30378442	0.90750876	951.358379	-0.6931322	0.07390732	0.71379068	
ENO1	674.764242	-0.47779548	0.03666936	0.35695204	1303.79448	-0.317671337	0.33289831	0.92286809	1509.60236	-0.4546723	0.25412041	0.8224827	
RPL37	1164.07257	-0.486565076	0.00184741	0.06597882	2254.52979	-0.567664791	0.00935087	0.29072685	2504.86947	-0.57782	0.01712215	0.48605613	Yes
CD24	893.47863	-0.496530225	0.09146679	0.44070361	1667.75422	-0.146530844	0.70889992	0.97295876	1924.15652	-0.2239604	0.62216763	0.96787016	
SERPINA1	316.905262	-0.505236225	0.02617137	0.31291833	572.590806	-0.337715433	0.27135833	0.87980019	665.767487	-0.5111801	0.06039109	0.7039651	
MARCKSL1	507.135416	-0.514949839	7.0838E-05	0.00787092	977.42141	-0.564491512	0.00078801	0.15418283	1092.40002	-0.5396293	0.00287948	0.22083429	Yes
CD74	1049.66347	-0.534416692	0.14557251	0.51682078	2047.43748	-0.634548304	0.18115517	0.80963857	2307.09604	-0.7836118	0.14481695	0.77280279	
NUPR1	414.135769	-0.542692124	0.00019168	0.0159736	750.641452	-0.496580349	0.00554893	0.23074301	864.005331	-0.529875	0.01254247	0.46314239	Yes
B3GNT7	326.536483	-0.560074569	0.0087201	0.18140874	631.550734	-0.67283412	0.02007386	0.40684052	674.458565	-0.5700646	0.04341242	0.63587154	
HSP90B1	244.268644	-0.5730694	0.01920323	0.28240045	455.244785	-0.546593252	0.07392523	0.6587266	506.42238	-0.6716737	0.02833632	0.5539472	
MIF	573.764636	-0.580882137	0.00731452	0.17415516	1081.86355	-0.6188022	0.0299933	0.45353505	1224.95284	-0.7397064	0.02508609	0.54779261	
GSTP1	401.351548	-0.593350286	0.00029103	0.01818949	753.491949	-0.491038079	0.02191854	0.40684052	845.178733	-0.5512753	0.02716803	0.55278634	Yes
XBP1	577.23872	-0.641598281	0.02444558	0.31251486	1025.23707	-0.56662493	0.14501216	0.78606569	1230.1811	-0.8573794	0.04169768	0.63067923	
TPM1	494.150118	-0.71891683	0.00028995	0.01818949	960.663094	-0.59210089	0.03973153	0.53583874	1046.16519	-0.5607185	0.08082574	0.72407637	
CXCL14	507.92397	-0.732029017	0.00987198	0.19266287	943.741862	-0.853766756	0.00842687	0.29000056	989.277974	-0.7483399	0.01755067	0.48605613	
FCGBP	583.972558	-0.766128118	0.02660682	0.31302146	1046.67936	-0.311774044	0.45566901	0.94573569	1176.92456	-0.5233057	0.26835162	0.84091614	
DMBT1	364.246918	-0.97960325	0.00128207	0.05128285	610.525892	-0.770871177	0.06588797	0.61971043	753.707716	-1.1509374	0.01302456	0.46376738	
LYZ	569.374814	-1.037726899	0.0003767	0.020928	1056.66259	-1.028751814	0.0023336	0.17914868	1186.49451	-1.1332978	0.00175111	0.22083429	Yes
IGKC	11391.2045	-1.081614737	0.04945073	0.39601595	19778.4443	-0.977617238	0.19049449	0.81386279	24238.2781	-1.4487737	0.07588948	0.71379068	
LCN2	373.12094	-1.118920726	0.00888903	0.18140874	613.075854	-0.902177296	0.12686875	0.76475159	774.995768	-1.4393452	0.02527428	0.54779261	
SPINK1	305.115064	-1.143197997	2.7571E-05	0.00551416	543.240618	-0.942639545	0.00792159	0.28460002	626.056659	-1.2421363	0.00186529	0.22083429	Yes
PIGR	2000.98599	-1.20820319	0.01495401	0.2451477	4094.95998	-0.793324568	0.20071777	0.81386279	4303.68823	-0.8914037	0.2312494	0.81018631	
AGR2	642.44532	-1.469522932	0.00010943	0.00994812	1253.02418	-1.492627964	0.00161069	0.15418283	1286.01099	-1.5726278	0.00282642	0.22083429	Yes
OLFM4	500.656969	-1.828631209	4.2451E-06	0.00141503	848.632798	-1.572535026	0.00330047	0.22017367	1024.66082	-2.0813306	0.0000552	0.02749459	Yes
IGHA1	19640.0736	-2.007187077	0.00024446	0.01818949	32960.2753	-1.838110589	0.01014572	0.29072685	39977.4172	-2.2911562	0.00415302	0.24356234	Yes
JCHAIN	1575.31083	-2.26824587	2.4837E-05	0.00551416	2810.2006	-2.161967137	0.00060071	0.14987715	3124.38258	-2.5234216	0.00024797	0.08240874	Yes
REG1A	807.633311	-2.727471055	2.8969E-07	0.00014484	1095.12586	-2.38186226	0.00169941	0.15418283	1327.72378	-2.9479076	0.00000482	0.0048067	Yes

Supplementary Table 7. Pseudobulk DE gene analysis of CosMx data comparing baseline biopsies prior to VDZ therapy in non-responders versus responders. In addition to q<0.1 after FDR-correction for all FOVs, DEseq2 comparisons were made treating FOVs and biopsies as replicates, with an unadjusted p<0.05 as an additional threshold for including in the gene sets.